AD-781 997

INVESTIGATION OF THE FEASIBILITY OF A MAGNETO-HYDRODYNAMIC LASER

UNITED AIRCRAFT RESEARCH LABORATORIES

PREPARED FOR
NAVAL ORDNANCE LABORATORY
ADVANCED RESEARCH PROJECTS AGENCY

31 MAY 1974

DISTRIBUTED BY:

NTIS
National Technical Information Service
U. S. DEPARTMENT OF COMMERCE

Unclassified

SECURITY CLASSIFICATION OF THIS PAGE (When Date Entered)

AD 781 997

REPORT DOCUMENTATION PAGE

READ INSTRUCTIONS BEFORE COMPLETING FORM

1. REPORT NUMBER: N-921308-4

2. GOVT ACCESSION NO.

3. RECIPIENT'S CATALOG NUMBER

4. TITLE (and Subtitle): INVESTIGATION OF THE FEASIBILITY OF A MAGNETOHYDRODYNAMIC LASER

5. TYPE OF REPORT & PERIOD COVERED: Final Report, June 3, 1971 to April 30, 1974

6. PERFORMING ORG. REPORT NUMBER

7. AUTHOR(s): Robert H. Bullis, Peter O. Erlandsen, Thomas L. Churchill, Elliot R. Schulman, William L. Nighan

8. CONTRACT OR GRANT NUMBER(s): N60921-71-C-0279

9. PERFORMING ORGANIZATION NAME AND ADDRESS: United Aircraft Corporation Research Laboratories, 400 Main Street, East Hartford, Connecticut 06108

10. PROGRAM ELEMENT, PROJECT, TASK AREA & WORK UNIT NUMBERS: ARPA Order Number 2032

11. CONTROLLING OFFICE NAME AND ADDRESS: Supply Officer, Code 313, U. S. Naval Ordnance Laboratories, White Oak, Silver Springs, Maryland 20910

12. REPORT DATE: May 31, 1974

13. NUMBER OF PAGES

14. MONITORING AGENCY NAME & ADDRESS (if different from Controlling Office): Commander Naval Ordnance Laboratories, White Oak, Silver Springs, Maryland 20910, Code 313

15. SECURITY CLASS. (of this report): Unclassified

15a. DECLASSIFICATION/DOWNGRADING SCHEDULE

16. DISTRIBUTION STATEMENT (of this Report)

Approved for Public Release; Distribution Unlimited.

17. DISTRIBUTION STATEMENT (of the abstract entered in Block 20, if different from Report)

SAME

18. SUPPLEMENTARY NOTES

NONE

19. KEY WORDS (Continue on reverse side if necessary and identify by block number)

Magnetohydrodynamic Laser (MHDL)
Molecular Lasers
Carbon Dioxide Lasers
Nonequilibrium Magnetohydrodynamics
High Power Lasers
Supersonic Plasmas
Plasma Physics

Reproduced by NATIONAL TECHNICAL INFORMATION SERVICE U S Department of Commerce Springfield VA 22151

20. ABSTRACT (Continue on reverse side if necessary and identify by block number)

This investigation is directed towards the evaluation of the feasibility of a magnetohydrodynamic laser concept (MHDL) employing nonequilibrium electron kinetics to provide efficient energy transfer in a molecular laser system. To achieve this goal comprehensive modeling of the MHD plasma which has been based upon a detailed knowledge of electron and heavy particle kinetics has been developed. Experimental investigations conducted on small scale laminated and solid wall generator configurations have confirmed theoretical modeling predictions and indicate the potential attractiveness of the MHDL concept for

DD FORM 1 JAN 73 1473 EDITION OF 1 NOV 65 IS OBSOLETE

Unclassified

SECURITY CLASSIFICATION OF THIS PAGE (When Data Entered)

high power laser applications. Major emphasis in this report has been placed on the additional experimental information obtained from small scale generator tests as well as experimental results obtained in a generator configuration suitable for optical power extraction investigations.

N-921308-4

INVESTIGATION OF THE FEASIBILITY OF A MAGNETOHYDRODYNAMIC LASER

Final Report

June 3, 1971 - April 30, 1974

May 31, 1974

Sponsored by

The Advanced Research Projects Agency
and
The U. S. Naval Ordnance Laboratory
under
Contract N60921-71-C-0279

R. H. Bullis
Principal Investigator
(203) 565-7046

Project Scientists

T. L. Churchill
W. L. Nighan
P. O. Erlandsen
E. R. Schulman

DISTRIBUTION STATEMENT A
Approved for public release;
Distribution unlimited

UNITED AIRCRAFT RESEARCH LABORATORIES
East Hartford, Connecticut 06108

ib

Investigation of The Feasibility Of A Magnetohydrodynamic Laser

TABLE OF CONTENTS

I. SUMMARY

Under joint ARPA and Navy sponsorship the United Aircraft Research Laboratories under Contract N-60921-71-C-0279 has conducted a series of analytical and experimental investigations to establish the feasibility of the magnetohydrodynamic laser concept for high power laser applications. The work conducted under Contract N-60921-71-C-0279 represents an extension of the investigations of the MHDL concept initiated under Contract N-60921-71-C-0213, and was embarked upon because of the promising results obtained from this initial work. Under the initial program, a self-consistent theoretical model of the nonequilibrium MHD expansion including all the key collisional interactions and the effects on the medium of power extraction was developed. From this modeling the most favorable conditions for production of a population inversion in a nonequilibrium MHD plasma medium to which small quantities of CO_2 are added were established. Supporting these theoretical studies small scale experiments were used, where possible, to verify the qualitative trends predicted from the modeling. Based on the findings of these investigations, an experiment was constructed to evaluate in detail the MHDL concept.

In order to obtain a meaningful experimental evaluation it is deemed critically important to establish experimental operating times on the order of several seconds so that all the commonly encountered MHD boundary layer heating and electrode interaction phenomena are developed to the same extent as would be encountered in an operating high power MHD laser device. Under this program, the experimental capabilities were developed to operate a nonequilibrium MHD system at stagnation temperatures up to 2800°K and pressures of 20 atm. The high temperature-high pressure experimental capability developed under this program still far exceeds any other MHD experimental capability presently in existence. Tests with this system conducted on a 20 cm optical path length laminated generator-cavity configuration have confirmed the major predictions of the theoretical modeling. The most important of these predictions which has been confirmed through controlled experimentation has been the observation of ignition of the MHD medium without the use of a preionizer in the presence of CO_2 concentrations determined from theoretical and analytical modeling studies to be sufficient to produce attractive high power MHD laser performance.

Under the present contract major emphasis has been placed on the development of a generator-laser cavity configuration having a high degree of medium uniformity and in obtaining power extraction measurements with this configuration. A high degree of medium uniformity has been achieved through the use of a smooth wall generator configuration which is electrically conducting in both the Hall field and transverse current flow directions. Based on the significant improvements in medium uniformity achieved with this configuration power extraction tests were conducted on a smooth wall generator configuration having a 55 cm optical path length. These tests, despite the fact that all the optical systems in the generator-laser cavity performed as expected did not result in extraction of optical power from the medium. To establish the potential source of difficulty, gain measurements on the medium in the 55 cm generator-laser configuration were conducted. Contrary to the earlier results obtained with the 20 cm optical path length configuration significant absorption rather than gain was detected. This occurred despite the fact that increased magnetic field intensities were employed which allowed ignition to be achieved in the MHDL medium at significantly higher CO_2 concentra-

tions. High speed motion pictures and visible laser medium quality measurements indicated a strong attenuation was being produced due to the presence of small concentrations of particles being introduced into the flow from the decomposition of the insulating material in the high temperature-high pressure heat source used in the experiments. This problem which was not present in earlier measurements on the 20 cm optical path length generator configurations in which positive gain signals were detected is not an inherent drawback of the MHDL concept, but rather a correctible difficulty with the experimental apparatus that has arisen due to the large number of tests conducted with the system. In addition, further simulation measurements conducted with an electron beam sustained plasma, in which the drift field of the sustainer was operated at levels corresponding to typical MHD conditions, confirmed the presence of gain in the medium at levels theoretically predicted by MHD modeling programs. More importantly, the observed dependence of gain on electron density and electron energy for the range of conditions tested was also found to be in good agreement with the predictions of the MHD modeling program. In addition to these results from supporting experiments, the vast change in the operating characteristics of the large scale generator configuration (55 cm optical path length) with regard to mass flow, test times, etc. has revealed several factors which now allow a more definitive interpretation to be made of earlier gain measurements. In particular, it is no longer felt that there is any ambiguity associated with the earlier gain measurements due to the findings of the more recent tests obtained with the large scale (55 cm) generator configuration. Based on these results, and a clear understanding of the factors which caused the failure of the power extraction measurements it is strongly recommended that an additional series of the power extractions tests be conducted after the problems associated with the insulating material of the high temperature-high pressure heat source are corrected. This recommendation is based on the fact that no inherent basic limitations can be found with the MHDL concept which would preclude achieving the performance predicted from modeling studies after significant experimental testing and critical evaluation of results. Further, power extraction testing is also being recommended because of the overall potential of the MHDL concept for many high power laser applications.

II. INTRODUCTION

The United Aircraft Research Laboratories has conducted a series of analytical and experimental investigations to establish the feasibility of a magnetohydrodynamic laser employing nonequilibrium electron kinetics in order to provide efficient energy transfer in a molecular laser system. The concept under investigation is illustrated in Fig. 1. The MHDL concept involves conversion of thermal energy to electrical energy in a nonequilibrium MHD generator, short circuited to provide maximum electron energy dissipation in the gas. The energetic electrons, in turn provide efficient excitation of the asymmetric stretch mode of CO_2. This concept is based on the fact that the cross section for direct electron excitation of the asymmetric stretch level of CO_2 shown in Fig. 2 as determined by Andrick, Danner and Ehrhardt (Ref. 1) is large compared to that for excitation of the symmetric stretch level in the 0.2 to 0.3 eV range typical of nonequilibrium MHD generator operating conditions. Further, when the cross sections for direct electron excitation of the bending and asymmetric stretch modes of CO_2 are weighted by the energy exchange associated with these collisions, namely 0.083 and 0.29 eV, respectively, the electron energy transfer collision frequency to the asymmetric stretch level dominates over that for collisions to the bending mode for electron temperatures in excess of approximately 2500°K as shown in Fig. 3. Detailed calculations, as described in Ref. 2 which also appear as Appendix I of this report, show that significant optical energy at 10.6 μm may be extracted from an optical cavity located in the MHD generator section. In addition, the MHDL concept, which requires no external source of electrical power, takes advantage of the naturally high level of internal dissipation of power commonly encountered with nonequilibrium MHD devices. The ability to internally dissipate on the order of 20 to 30 per cent of the thermal power available when combined with the calculated electrical-optical conversion efficiency for this system which is estimated to be between 15 to 20 per cent promises overall MHDL thermal to optical conversion efficiencies of approximately 3 to 6 per cent. Moreover, by not extracting the electrical power from the nonequilibrium MHDL medium, but rather, by direct pumping of CO_2 in a short circuited generator configuration it is possible to circumvent the electrode boundary layer interaction problem which has plagued the performance of nonequilibrium MHD power generators for years.

Initial program efforts under Contract N-60921-70-C-0213 were directed toward the development of analytical and experimental techniques needed for evaluating the feasibility of the MHDL concept. The results of these investigations which will be summarized in Section III indicate that it is possible to produce ignition in a nonequilibrium MHD generator in the presence of a sufficient concentration of CO_2 to produce attractive MHD laser performance. In addition, a strong dependence of generator performance on CO_2 concentration, as predicted from the theoretical modeling studies, has been experimentally observed in these investigations. Lastly, gain measurements although not interpretable in an entirely unambiguous fashion at the time these measurements were initially obtained on a small scale laminated generator configuration indicated positive results. Subsequent measurements on a large scale 55 cm optical power extraction configuration conducted under Contract N-60921-71-C-0279 in which test times and mass flow rates were significantly different than in the small scale tests have revealed that prior difficulties in interpreting the gain measurements in a completely unambiguous fashion have been due to timing sequence errors rather than any inherent difficulties in the measurements.

The objectives of the present MHD investigations conducted under Contract

N-60921-71-C-0279 have been to demonstrate MHDL concept feasibility by conducting a series of power extraction tests on an MHD generator-laser cavity configuration designed to optimize MHDL performance. In order to achieve as close to optimum performance as possible, considerable emphasis under the present investigations was devoted to the development of a generator-cavity configuration which would yield high medium uniformity. To this end, a smooth walled generator configuration with a 20 cm optical path length was developed in which both the transverse current and Hall fields are electrically shorted. While shorting the generator in the Hall field direction as well as the transverse current direction results in a small loss in generator performance, this loss is more than compensated for by the significant improvement in aerodynamic performance and medium uniformity which results.

As a consequence of the very promising results obtained from small scale smooth walled generator testing a 55 cm optical path length generator-laser cavity configuration was constructed and utilized in optical power extraction tests. In addition, in these tests the magnetic field capability of the experiment was increased from 2.2 to 3.3 Tesla to increase the operating CO_2 concentrations at which ignition could be achieved. Lastly, boundary layer injection was employed in the supersonic diffuser section of this larger configuration to improve the aerodynamic performance of the system under high generator loading conditions. Despite the fact that the generator operated as predicted with the onset of ignition occurring at higher CO_2 concentrations, and with the optical power extraction system operating well within desired limits, no optical power was extracted from the medium. From subsequent tests conducted on the generator medium, it was found from gain measurements at 10.6 μm and medium uniformity measurements obtained with a HeNe laser system that the insulating material surrounding the high temperature-high pressure bed used as a thermal energy source in these experiments was introducing small concentrations of particles ($n \sim 10^4/cm^3$) into the flow medium of the generator. The presence of these particles was found to be sufficient to produce significant absorption in the medium at both 10.6μm and at visible wavelengths. This effect which was not present in the earlier series of measurements on both the laminated and solid wall 20 cm optical path length generator configurations resulted from a decomposition of insulating material produced by the extended number of tests (on the order of several hundred) that have been conducted with this experimental system.

An additional series of experiments conducted with the 55 cm system, as will be described in Section III, definitively established that decomposition of the insulating material was the cause of the strong absorption in the medium observed in the most recent optical power extraction experiments. Because it has been found that it is not possible to completely eliminate this problem with the present experimental configuration without repair of the insulating material it has not been possible to confirm the feasibility of the MHDL concept by extracting power from the MHDL medium in the 55 cm generator-laser configuration. However, the additional understanding of the nonequilibrium generator performance attained with tests on the 55 cm configuration has served to strengthen the interpretation that can be placed on earlier gain measurements. Furthermore, analysis of all the more recently available data for low energy electron-CO_2 collisional processes by Lowke, Phelps and Irwin (Ref. 3) essentially confirms the vibrational excitation cross section data of Fig. 2. Further, a more direct measurement obtained by Bulos and Phelps (Ref. 4) suggests that if anything the excitation to the asymmetric stretch level of CO_2 is more favorable at low energies than would be predicted by the data of Fig. 2. In simulation measurements of MHDL medium conducted with an e-beam sustained discharge, as described in Section III, the

measured gain levels and trends with the electron temperature and electron density follow closely the theoretical modeling predictions further supporting MHDL concept feasibility.

Based on the large amount of experimental information on MHD generator performance characteristics with CO_2 added to the medium, and the results of several supporting simulation experiments, as well as a recent critical review of the entire concept there appears to be no inherent fundamental factors which will limit the feasibility of the concept. Therefore, despite the failure to extract optical power from the most recent series of tests, because of difficulties associated with the supporting experimental apparatus, it is felt that the MHDL concept holds sufficient promise for high power laser applications to strongly recommend an additional series of experiments to demonstrate concept feasibility.

III DISCUSSION OF RESULTS

A. Theoretical Modeling

Under the initial investigations on the MHDL concept conducted under Contract N-60921-70-C-0213 an analytical model of a one dimensional nonequilibrium magnetohydrodynamic expansion was developed for the purpose of establishing and evaluating conditions favorable for the development of an efficient high power MHD laser using CO_2 as the active medium. Quantitative analysis of the MHDL concept illustrated in Fig. 1 requires a coupled formulation of electron and molecular kinetic processes and the fluid mechanics of the magnetohydrodynamic expansion. Illustrated in Fig. 4 are the key features of the internally self-consistent analytical model which was developed to treat the above outlined processes in detail. The individual elements of this modeling procedure which were first described in Ref. 2, for the sake of clarity and consistency of presentation, are attached as Appendix I to this report.

The coupled set of MHDI equations developed in Ref. 2 forms the basis for a numerical computer analysis. For a specified set of initial conditions the governing differential equations are integrated along the channel to provide a streamline history of medium properties. The initial conditions are adjusted to correspond to various physical situations. For example, one computational procedure relies on specification of the gas conditions in the stagnation region and subsequently traces the fluid properties through the nozzle and generator sections. Joule dissipation in the supersonic MHD generator region provides an elevated electron temperature and subsequent additional ionization of the seed. Of major importance in this modeling has been the molecular quenching channel for vibrationally excited CO_2. Earlier calculations of similar processes in vibrationally excited nitrogen by Fisher and Smith (Ref. 5) suggested that this process can significantly influence the population of the asymmetric stretch level of CO_2 in the MHDL medium. Subsequent direct measurements by Benson, Benard and Walker (Ref. 6), however, have shown this loss channel not to be of major importance for typical MHDL medium conditions.

One of the most critical parameters in MHDL operation is the maintenance of the electron density at the proper level. The importance of maintaining the electron density at an optimum level is illustrated by the predicted variations of gain and saturation intensity obtained from the MHDL modeling analysis shown in Fig. 5. Presented in this figure is the dependence of CO_2 vibrational temperatures (vibrational populations), small signal gain and small signal gain-saturation intensity product on electron density for typical MHDL operating conditions. The electron temperature and gas translational temperature in this example were held constant for the purpose of illustration. For generator channel pressures on the order of 0.1 atm and electron density values below 10^{11} cm^{-3} the asymmetric stretch level temperature in $CO_2(T_{001})$ is elevated only slightly above the gas translational temperature and the small signal gain as a consequence is relatively small for the conditions considered in Fig. 5. However, as the electron density increases into the 10^{12} to 10^{13} cm^{-3} range the small signal gain rises and exhibits a maximum of approximately 0.2 per cent cm^{-1}. This condition results because of the efficient electron pumping of the CO_2 asymmetric stretch level and because selective relaxation of the symmetric stretch level (T_{100}) of the CO_2 system occurs due to the high helium concentration in the medium. As the electron density is increased beyond the 10^{13} cm^{-3} range, the He in the mixture can no longer relax the symmetric stretch level of CO_2 at a rate commensurate with the rate at which it is being pumped by electron collisional processes. As a consequence, it is no longer possible to maintain the symmetric stretch level temperature near the gas translational tempera-

ture. Once a significant population of the lower laser level of the CO_2 system occurs a corresponding decrease in overall gain results. For electron densities in excess of approximately 5×10^{14} cm^{-3} the pumping of the lower laser level is so significant that the gain is effectively zero for the conditions typical of the MHDL operating environment.

Efficient MHD conversion of flow kinetic energy to electrical energy is the second most important consideration that enters into the design of an optimum MHDL configuration, if a system with reasonable overall conversion efficiency of thermal energy to optical energy is to be developed. To achieve sufficient electrical conductivity in the MHDL medium to produce attractive MHD performance, electron densities in the range of $3\text{-}5 \times 10^{13}$ cm^{-3} are required. In this range, as indicated in Fig. 5, the gain has dropped to approximately one half its peak level. Although this gain level is only on the order of .05 to 0.15 per cent cm^{-1} for reasonable generator-laser cavity configurations it should be possible to achieve conditions optimal for optical power extraction. The second important point to be noted is that even though the gain is lower in this electron density regime the gain-saturation intensity product actually peaks in this region which suggests the maximum optical power output will be achieved from a nonequilibrium MHD generator which is operating in its most efficient range.

From the initial phases of the program predictions of the theoretical modeling of the MHDL laser conditions indicated that several factors associated with the development of the plasma in the generator-laser cavity are crucial to the development of optimal performance with high thermal-to-optical conversion efficiency. As would be expected, and has been experienced in other MHD devices, the aerodynamics associated with the expansion of the flow through the power extraction region of the generator are critical to the performance of the system. Nonuniformities in the flow field impact several key generator and laser performance parameters. Specifically, the static temperature and pressure must be maintained uniform across the generator-cavity to maintain a uniform gain profile across the medium. Furthermore, nonuniformities in the flow field produce nonuniformities in the MHD interaction. As a consequence, these potential nonuniformities in the flow field can result in strong aerodynamic effects such as the development of shocks through the laser cavity region which are highly undesirable for high power laser applications. Lastly, channel wall roughness plays an important role in influencing not only the aerodynamic performance of the generator-laser channel, but it also influences plasma arc phenomenon at the electrodes and in the channel boundary layers. As will be shown in Section III-B of this report, channel wall roughness actually produces enhancements in arc phenomenon which allow gross heating to occur at electrode surfaces. This heating of the electrode surface results in a runaway phenomenon in which a region of high electrical conductivity is produced that then propagates out into the flow field of the generator. As a consequence, a strong MHD interaction is produced and a runaway effect occurs which results in choking and overall deterioration of the flow properties of the medium.

A second major area of prime importance in employing a nonequilibrium generator for laser applications is the influence that preionization has on the overall medium uniformity. Prior results obtained from MHD generator testing indicated that the use of an upstream preionizer to enhance the electrical conductivity of the medium to levels satisfactory for production of efficient conversion of thermal to electrical energy usually results in also producing a high degree of nonuniformity in the medium. Therefore, in the experiments to be described it was decided based on theoretical modeling predictions not to employ preionization, but rather, to rely on a "boot strap" type of ionization phenomena

which is only dependent on the plasma conditions at the throat of the MHD nozzle.

In addition to the factors described above which can influence generator performance, it was expected that the introduction of molecular species such as CO_2 to the MHD medium could also result in the development of additional non-uniformities in the medium unless the dispersal of the CO_2 was highly uniform. This occurs because the electron coupling to the vibrational levels in CO_2 is so highly efficient in comparison to the other collisional processes which are taking place in the generator medium. An additional consideration was also potential cesium-CO_2 chemical reactions. To prevent the formation of undesirable cesium-CO_2 compounds the injection techniques employed in the measurements that will be described in the subsequent sections were designed to produce uniform dispersal of CO_2, and also, to minimize the interaction time between the cesium and CO_2 as it passed through the generator-laser cavity region. Also, as pointed out in the previous paragraphs, the various deactivation processes associated with cesium and CO_2 vibrationally excited states as well as CO_2 deactivation of cesium excited states, was given careful consideration prior to embarking on any experimental measurements. As indicated in Appendix I these interaction channels have been considered in detail in the MHD modeling analysis employed under this program. In addition to the supporting experimental information that is available on these reactions, probably the most direct confirmation that it is possible to achieve MHDL operating conditions in which these processes do not grossly influence performance is the fact that as described in the experimental section of this report ignition in the MHDL medium was achieved without having to resort to the use of preionization. Furthermore, this ignition occurred in the presence of CO_2 at the concentrations predicted from the theoretical modeling studies.

1. Supporting Experimental Confirmation of Concept Feasibility

In order to confirm the predictions of the MHDL modeling studies, three different supporting experiments were conducted. Initially, tests were conducted on the MIT nonequilibrium MHD generator (Ref. 7) to confirm that it was possible to add a significant molecular loading to a nonequilibrium MHD generator medium without extinguishing the plasma. Results of these investigations, which were conducted in CO rather than CO_2, indicated that it was possible to maintain ignition of the plasma in the presence of significant loadings of CO while producing an elevation in the vibrational population. Direct measurements of CO vibrational populations in these experiments were made using a radiometer. With this technique it was also possible to determine the change in the vibrational population of the CO system under various generator operating conditions. As predicted by the MHD modeling results, it was found that indeed it was possible to pump CO to levels corresponding very closely to vibrational temperatures that were near or equal to the electron temperature in the nonequilibrium MHD plasma medium. Due to the MIT MHD facility limitations on magnetic field intensity and operating Mach number, CO with a lower electron energy exchange collision frequency than CO_2 was employed in these experiments.

Also, to confirm the predictions of the MHDL modeling, namely that direct pumping of CO_2 with low energy electrons typical of those encountered in nonequilibrium generators is feasible, experiments were conducted in a fast flowing gas mixing-type discharge as depicted in Fig. 6. In this system typical laser mixtures to be investigated were passed through a fast flow (~100m/sec) coaxial type discharge configuration. Just upstream of the entrance port of the gases to the laser discharge region cesium was injected with a vapor boiler configuration as shown in Fig. 6. With this type of discharge

configuration, it was possible to decrease the E/n ratio, i.e. the characteristic electron energy by approximately 60 per cent while increasing the measured overall gain of the system by as much as 30 per cent. These results tend to substantiate the fact that it was possible to operate a laser discharge on ionization processes other than those directly associated with ionization of the N_2, CO_2, He and also, while lowering the characteristic electron energy produce significant direct vibrational pumping of the upper CO_2 laser level. When consideration is given to both the N_2 as well as the CO_2 vibrational excitation cross sections, as shown in Fig. 2, it is realized that what is happening in this experiment is that direct electron pumping of the CO_2 upper laser level dominates the collisional processes at lower energies. This set of measurements also served to confirm that it was possible to introduce cesium into an active discharge with CO_2 and prevent significant reaction of the cesium and CO_2 from occurring within the discharge residence times investigated. Furthermore, since residence times in this experiment were much longer than those encountered in the typical MHDL configurations this experimental information also tended to support the modeling results which indicated that significant chemical reactions between the cesium and CO_2 could be prevented by the proper design of the cesium and CO_2 injector systems.

Lastly, information supporting the feasibility of the MHDL concept has become available from tests conducted with a transverse laser discharge configuration employing e-beam augmentation of the ionization process. In this experiment it is possible to achieve operating conditions which closely approximate the MHDL environment, i.e. gas temperatures and densities, and characteristic electron energies. In particular, as shown in Fig. 7, operating pressures in the system were 50 Torr with 0.5 Torr CO_2 and 49.5 Torr of He which is representative of the actual operating conditions investigated in MHDL tests. Shown in Fig. 7 is the measured dependence of gain on electron density and electron temperature. As can be seen from this figure, the trend is quite consistent with the theoretical predictions of the MHDL modeling studies.

2. Detailed Predictions of MHDL Performance

Employing the MHDL model developed as described in previous sections and Appendix I, it is possible to predict the detailed properties of the MHDL plasma as a function of position downstream from the throat of the generator nozzle. Presented in Figs. 8 thru 11 are the results of a detailed computation of plasma properties as a function of position for operating conditions which are typical of the type of operation achieved in the experimental phase of the program. Shown in Fig. 8 is a calculated spatial response of key characteristic temperatures associated with the MHDL plasma medium. As the high temperature-high pressure plasma is expanded from the throat of the nozzle a reduction of all key temperatures in the system is experienced. However, Joule dissipation in the supersonic portion of the MHD generator region provides a rapid elevation of the electron temperature as can be seen in Fig. 8. As a consequence of the high degree of coupling between the electron gas and the asymmetric stretch level of CO_2 the population, and therefore, the temperature of the asymmetric stretch level gradually increases and approaches the electron temperature. In contrast the temperature of the symmetric stretch level which is the lower laser level remains closely coupled to the gas temperature. This is both a consequence of the electron pumping conditions existing in this region of the generator as well as due to the effectiveness of He relaxation processes. If reference is made to Fig. 9 it can be seen that in response to the rapid electron temperature rise the electron density also increases in the downstream direction. However due to the finite kinetics associated with this system the increase in the electron density is less rapid than the

response of the electron temperature. At the 30 cm point for the conditions investigated a rapid rise in electron density occurs and a near runaway condition results. To prevent the electron density from increasing beyond optimal values required to achieve reasonable gain in the system an optical cavity is clamped at the 30 cm point and optical power is extracted. As a consequence of extraction of power from the system the electron temperature drops and the electron density runaway situation is prevented. It is important to note that the runaway electron density condition must be prevented if medium uniformity is to be achieved and choking of the flow in the generator channel is to be prevented. As shown in Fig. 8, in response to the extraction of optical power, both the electron temperature and also, the temperature associated with the vibrational population of the upper laser level decreases. Correspondingly, the population of the lower laser level increases and as can be seen in Fig. 8, the temperature associated with the vibrational population of this level rises above the gas translational temperature of the system even for the extremely high He loadings considered. For the conditions depicted in Figs. 8 and 9 the total cumulative optical power that can be extracted from the system is significant as shown in Fig. 10. Presented in Fig. 10 is the optical power available for extraction as a function of the position and the specific optical power that can be achieved. From this data it can be seen that even in the small experimental generator-laser cavity configurations under investigation, the MHD type device is predicted to be able to achieve significant optical power outputs at impressive specific optical powers. Lastly, and most importantly, if consideration is given to the fractional power transfer which is occurring in this type of system as depicted in Fig. 11, it can be seen that the overall conversion of electrical to optical power achieved results in an efficiency of approximately 20 per cent which compares quite favorably with the conversion of electrical to optical power in conventional electric discharge type lasers. Also shown in Fig. 11 is the fractional power transfer to the upper laser level as well as to the other combined levels of the CO_2 system and the losses associated with other collisional channels found to be of importance from MHD modeling studies. It should be emphasized that the attractive feature of the MHDL concept is that it is possible to directly pump the CO_2 upper laser level with low energy electrons typical of those obtainable in nonequilibrium MHD devices. Moreover, the highly efficient nature of this pumping process permits conversion efficiencies of electrical-to-optical power on the order of 20 per cent to be achieved.

B. Experimental Results

Under Contract N-60921-70-C-0213 initial measurements were carried out with a laminated generator configuration which was composed of alternate copper bus bars which served to short out the transverse current flow and insulating segments which were used to electrically isolate the bus bars so that measurements of the Hall field developed in the generator could be obtained. In the initial phase of the program this configuration was thought to be the optimum from the standpoint of producing maximum dissipation in the plasma while maintaining medium uniformity. However, as will be shown in subsequent paragraphs a more optimum generator configuration was developed as a result of small scale testing under Contract N-60921-71-C-0279 which insured that optimum medium uniformity could be achieved for optical power extraction tests. This generator configuration was a solid copper wall generator in which both the transverse current and the Hall field were shorted. With this configuration studies have been conducted which show a high degree of medium uniformity is achieved. Lastly, the third configuration upon which optical power extraction tests were conducted under Contract N-60921-71-C-0279 was a 55 cm solid wall configuration. Since there was a wide variation in the

mass flows associated with the small scale generators which had 20 cm optical path lengths and the 55 cm optical path length solid wall configuration, a significant range of test parameters was spanned in these investigations. In addition to the optical power extraction tests, the magnetic fields employed in the experiment were increased from 2.2 Tesla to 3.3 Tesla in an endeavor to enhance the CO_2 loading, and thereby, the gain that could be achieved in the optical medium.

Depicted schematically in Fig. 12 is the experimental configuration employed in these investigations. A graphite core high temperature heater bed was used to provide He mass flows in the range from 0.8 to 2.5 lbs. per second at the throat of the generator-laser cavity. The helium gas flow was heated by passing through a multi-passage graphite core which was operated in the range from 2,000 to 2,800°K. Prior to introduction of this high temperature flow of He into the generator-laser cavity cesium was injected into the flow by a positive displacement injection system. Complete mixing was achieved in a mixing plenum specifically designed to optimize the uniformity of cesium in the flow. This was achieved by flash evaporation of the cesium upon injection into the high temperature bed and through the use of a long mixing region which extended upstream of the throat of the nozzle as shown in Fig. 12. Immediately adjacent to the throat of the nozzle, CO_2 was injected into the flow stream through a multiplicity of small fine nozzles. By locating the injection point for the CO_2 in the region immediately adjacent to the nozzle it was possible to minimize the interaction between the cesium in the flow stream and the CO_2 to reduce chemistry effects.

In order to adequately analyze the properties of the MHDL plasma for the purpose of obtaining valid comparisons with the MHD modeling predictions, several different diagnostic approaches were employed. All diagnostic information was obtained on a time resolved basis so that from one experimental test run a wealth of information over a wide range of test parameters could be obtained. The properties of the flow field were determined from detailed static pressure maps of the aerodynamic performance of the generator. The relative location of these static pressure taps in the generator-cavity is shown schematically in Fig. 12. In addition to the use of static and total pressure measurements, measurements were also made of medium uniformity by observing the deflection of a HeNe beam which was passed through the generator-laser cavity region at a point located 10 cm downstream from the throat of the nozzle. The properties of the plasma produced within the generator were determined by several independent measurements. The measurements included direct determination of the transverse current and Hall field in the laminated generator configurations as depicted schematically in Fig. 13. By employing a segmented bus bar it was possible to determine the current flowing in the segment. In addition, measurements of the potential developed on selected electrodes in the downstream flow direction provided an estimate of the Hall field that was produced in the generator. From these measurements it was possible to infer the electron density and electron temperature. Secondly, measurements of the two body cesium recombination continuum at four selected wave lengths at the 10 cm diagnostic port allowed direct determination of the electron density and temperature and provided a cross check on the electron density estimates inferred from the transverse current and Hall field measurements. In this manner, two independent techniques were employed to determine electron densities as a function of the CO_2 concentrations and various other generator operating parameters. To analyze the bulk medium uniformity both low and high speed motion pictures were employed at diagnostic ports located in the downstream region near the exit plane of the generator. As shown schematically in Fig. 12 the viewing angle for the motion picture information was such that it was possible to view a large bulk of the plasma near the 10 cm diagnostic port as well as the electrodes and sidewalls

of the generator-laser cavity in this region. Optical measurements of the laser properties of the MHD plasma were obtained by using a CO_2 probe laser located at the 10 cm point, and in the larger 55 cm generator configuration optical power extraction measurements were conducted in this region of the generator-laser cavity. With these diagnostic techniques, it was possible to obtain a rather comprehensive assessment of the characteristics of the nonequilibrium MHDL plasma.

Initial experimental measurements of the properties of the MHDL plasma were obtained with a laminated copper and supermica generator as shown in Fig. 14. This configuration was designed with bus bars employed for electrically shorting the transverse current. Also, as shown in Fig. 14, selected bus bars were split and electrically isolated so that measurements could be made of the transverse current which was flowing in these segments. The diagnostic port shown in Fig. 14 was located approximately 10 cm from the throat of the nozzle. This generator configuration was also carefully instrumented with numerous static pressure taps to determine the overall aerodynamic performance of the generator-laser cavity configuration under various CO_2 loadings. The hypo-tubing employed for the static pressure measurements is shown attached to the nozzle which is located directly in the center of the photograph in Fig. 14. The overall dimensions of this channel were 20 x 20 cm. Tests under Contract N-60921-71-C-0213 were limited exclusively to investigations of this configuration. Under the follow-on efforts under Contract N-60921-71-C-0279 an improved version of this laminated generator with vastly improved diagnostics was employed to determine the precise characteristics of the MHDL plasma. These tests were conducted with magnetic field intensities of up to 2.2 Tesla and are described in the following paragraphs.

Depicted in Fig. 15 is the predicted electron density variation that would be expected to be obtained with the generator configuration shown in Fig. 14. Operating conditions for these tests were stagnation temperatures of 2400°K and stagnation pressures of 19.7 atm with an applied magnetic field of 2.2 Tesla. As indicated previously, the diagnostic port for determination of electron densities and temperatures from two body recombination continuum measurements was located at a point 10 cm downstream from the throat of the nozzle. Therefore, attention should be focused on the predicted electron density variation with CO_2 concentration that occurs at this point. As can be seen in Fig. 15, an extreme sensitivity of generator performance to CO_2 concentration is predicted from the theoretical modeling studies for concentrations ranging from 0.5 to 1.25 per cent. For concentrations below approximately 0.6 per cent a rapid increase in the electron density to levels in excess of 10^{14} cm^{-3} occurs. Under this condition, such a high electrical conductivity is produced in the plasma that the MHD interaction is enhanced to the point that the flow chokes and it is not possible to maintain optimum test conditions. In contrast, as the CO_2 concentration is increased the electron density level which is achieved at the 10 cm point decreases in a rather abrupt fashion. With concentrations of 1.25 per cent CO_2 the electron density is frozen at the value achieved as a result of the expansion through the nozzle. Presented in Fig. 16 are the experimental results obtained for the generator conditions depicted in Fig. 15. As can be seen from this data which was obtained from two body recombination continuum measurements it appears possible to achieve ignition in the generator at electron densities of approximately 8×10^{12} cm^{-3} and CO_2 concentrations of approximately 0.68 per cent. As the CO_2 concentration is decreased the electron density rises as predicted by the modeling data of Fig. 15 up to density levels of approximately 5×10^{14} cm^{-3}. At this point, as mentioned previously, pressure rises occur in the generator channel so that it is no longer possible to maintain optimum conditions for the production of a highly uniform plasma and the flow becomes choked thereby limiting further enhancement of the MHD interaction. The important point to note in this data is that it is possible to achieve ignition with significant CO_2 loadings without having to resort to preionization and to maintain this ignition in the proper electron density operating range for efficient thermal-to-electrical conversion efficiency in the generator medium. In addition,

these conditions, as suggested from the electron density data also pass through the optimum region for achieving gain in the MHDL medium. Depicted in Fig. 17 are the theoretical predictions of the electron temperature variation with CO_2 concentration for the same test conditions as described in Figs. 15 and 16. Again, as predicted theoretically there is a sensitivity of the electron temperature to CO_2 concentration. At the 10 cm point for concentrations of CO_2 ranging from 0.6 per cent to 1.25 per cent the electron temperature varies between 1500 and 3000°K. A direct measurement of the value of the electron temperature obtained from two body recombination continuum measurements is indicated in Fig. 18 for these test conditions. As shown in this figure, ignition occurs at a CO_2 concentration of approximately 0.68 per cent and the electron temperature increases from 2000 to 3500°K as the CO_2 concentration is reduced from this level. Because an absolute rather than a relative measurement of the recombination continuum at four selected wave lengths is required in this measurement the electron temperature data exhibits a greater amount of scatter than that experienced in the density measurements. Despite this scatter there is a definitive trend established with varying CO_2 concentration. Furthermore, it should be noted that the data both from the electron density and electron temperature measurements succinctly points out the strong sensitivity of MHD performance to CO_2 concentration. In addition, this data indicates as predicted, it is possible to achieve optimum plasma medium conditions required to produce a population inversion in the CO_2 in the working medium of the generator.

As mentioned previously, one of the diagnostics included at the 10 cm location was a direct measurement of gain. Because of the rather hostile environment the MHD experiment represents, considerable development had to be carried out to insure that it was possible to obtain meaningful gain measurements. In particular, techniques had to be developed to insure that the optical properties of the windows which are used to isolate the laser channel from the atmospheric pressure environment surrounding the experiment could be maintained throughout the course of an experimental test which was on the order of 15 to 20 seconds in duration. In addition, techniques for shielding the windows from the flow field and the cesium seed contained in the flow field also had to be developed in order to insure unambiguous gain measurements. Shown in Fig. 19 is a typical small signal gain measurement obtained with the laminated generator configuration. In order to conduct this measurement, a small portion of the main laser probe beam was split off and sent to a reference signal detector so that it would be possible to monitor laser probe beam stability throughout the course of an experimental test. In addition, in order to lengthen as much as possible, the signal path length a multipass configuration was employed in these investigations in which the beam traversed from the probe laser through the MHD generator laser channel to a corner cube and returned back through the plasma to a signal detector. With this configuration two salt flat windows were employed to isolate the MHDL plasma from the surrounding environment. However, it was found in the course of the experimental investigation, that the complete isolation of the salt flats from the cesium environment was not possible unless shutters were employed on the windows to protect them from the high pressure pulses associated with the start-up and shut-down phases of the experimental sequence. At these times in the experimental sequence cesium contact with the windows occurred because the generator channel was operating subsonically at above atmospheric pressure. However, as indicated, the use of shutters on both windows served to minimize the problem of cesium contamination at least in the initial portion of the experimental run.

Depicted in Fig. 19 is the data obtained from a typical small signal gain measurement. The CO_2 probe laser beam level prior to the start-up of a test is shown on the far side of the figure. At this point the shutters are closed across

both windows and the blow-down procedure is initiated. Upon successfully establishing supersonic aerodynamic performance in the generator section it is possible to then open the shutters and measure the properties of the MHDL medium. The sequence employed to achieve these conditions was to mix CO_2 with the He but not introduce the cesium into the system prior to the establishment of supersonic flow in the laser channel. By this technique it was possible to preclude the deposition of cesium and its subsequent attack on the salt windows used in the optical train. Upon injection of cesium into the already established supersonic He-CO_2 flow, ignition occurred in the generator. The timing sequence associated with this procedure is depicted on the lower portion of Fig. 19. As can be seen from the timing sequence indicated in this figure prior to introduction of cesium into the channel the probe laser signal level was comparable to the signal level measured prior to the start of the run. Upon introduction of cesium ignition occurs and a positive increase in the overall signal level of the probe laser beam is detected indicating gain. It is also important to note that the output signal level of the probe laser as indicated by the reference signal level on the top portion of this figure did not change during this period. Therefore, any changes in detected beam intensity could only be produced by changes occurring in the measurement arm of the optical system further reenforcing the interpretation that positive gain was present in the medium. From the time that the cesium is introduced into the MHD channel until the first CO_2 off signal, the CO_2 is ramped in a continuous fashion to smaller CO_2 concentrations. Therefore, as shown in the experimental data, maximum gain occurs at the higher CO_2 concentrations and gradually the overall measured gain decreases with decreasing CO_2 concentration. Upon removing the CO_2 completely from the flow a runaway situation as described previously occurs in the generator in which an above atmospheric pressure plasma is produced. This results in severe degradation of the salt windows due to cesium attack, and also produces a deflection of the CO_2 laser beam because of the aerodynamic nonuniformities that are produced under these operating conditions. Upon reintroduction of CO_2 into the system an increase in signal level is experienced. However, interpretation of CO_2 probe signal levels once Cs attack of the salt windows occurs is not possible. By comparing the measured probe signal level after the end of the experimental test with the measured probe signal level prior to the test and noting the variation in the reference signal levels both before and after it can definitively be established that Cs attack on the salt windows is responsible for the decrease in signal level in the later portions of the experimental measurements. Therefore, the most important aspect of the gain data obtained in Fig. 19 is the information contained from the time the shutter is opened with He and CO_2 only in the supersonic flow to the point at which the CO_2 is first removed from the flow stream. Earlier interpretations of this type of gain information were somewhat ambiguous in that the timing mark for the introduction of cesium into the laser channel did not precisely correspond to the point at which ignition and an increase in gain was observed. However, subsequent experiments in the large scale 55 cm optical path length generator configuration have shown that the cesium actually enters the flow field prior to the timing signal due to flash boiling in the injection tube. Gain values established from these measurements range from 0.05 to 0.15 per cent cm^{-1}.

Based on the above measurements, it would appear optimum conditions have been achieved in the MHDL laminated generator configuration to provide a medium suitable for optical power extraction measurements. However, high speed motion pictures of the properties of the flow in the generator-laser cavity revealed a high degree of nonuniformity as shown in Fig. 20. In particular a highly structured plasma was observed in the motion pictures with arc spots present on the walls of the generator. Furthermore, the location of the arc spots appeared to be relatively fixed. This data tended to suggest that the plasma medium in the generator was highly

nonuniform with electron pumping occurring only in selected regions. While this condition could produce relatively uniform gain because of the wide range of electron densities over which gain can be achieved in the MHDL medium as shown in Fig. 5 it would not be expected that the same would be true for the saturation intensity of the medium. Again, based on the data contained in Fig. 5 it would be expected that the regions in which the electron densities were low, saturation intensities would be correspondingly low. As a consequence, it would not be expected that high optical beam quality could be achieved with this medium.

Careful examination of the high speed motion pictures revealed that the arc spots were attached at the electrode walls. In particular, this attachment appeared to occur in regions where small amounts of the insulating material immediately adjacent to a shorting segment were missing due to ablation. As a consequence, in this region a recirculation zone of hot gas was produced which enhanced the electron emission processes at the electrode surface and forced the formation of a large arc channel which extended out into the bulk of the plasma medium. Further examination of the laminated generator configuration revealed that ablation was taking place on all insulator surfaces because of the inability of these surfaces to remove heat. As a consequence the surface conditions along the wall of the laser channel were quite rough. This situation is not uncommon in MHD power generating configurations. An analysis of the fluid dynamics of the situation indicated that the type of roughness that was being encountered especially after prolonged periods of operation suggested that the velocity profile as shown in Fig. 21 was quite nonuniform across the channel. More importantly, the nonuniform velocity profile of the type indicated for a wall roughness of 0.1 inch resulted in regions immediately adjacent to the wall where the gas temperature was significantly higher than the centerline temperature of the channel. As a consequence the medium in this region could actually become absorbing. Also, as indicated in the data contained in Fig. 21, it is possible to achieve a relatively uniform velocity profile, and therefore, temperature profile by resorting to a smooth wall generator configuration. To do so, however, requires not only shorting the transverse current flow, but also, the Hall field. To understand why it is possible to achieve optimum MHDL performance in this type of completely shorted generator configuration consideration has to be given to the expression for the Joule heating in a nonequilibrium magneto-plasma which has been developed in detail in (Ref. 2).

$$\bar{J}\cdot\bar{E} = \sigma_{eff} U^2 B^2 \frac{1+\beta_{app}^2}{1+\beta_{eff}^2}$$

where

$$\beta_{eff} \equiv \frac{E_{\perp J}}{E_{\parallel J}} \qquad (2)$$

and

$$\beta_{app} \equiv \frac{E_H}{UB} \qquad (3)$$

In a laminated generator configuration it has been established experimentally that β_{eff} is approximately 1 and β_{app} is approximately 0.4. Therefore the term

$$\frac{1+\beta_{app}^2}{1+\beta_{eff}^2} = \frac{1.16}{2} \qquad (4)$$

for the laminated generator without the Hall field shorted. With shorting of the Hall field i.e. $E_H=0, \beta_{app}=0$ and

$$\frac{1+\beta_{app}^2}{1+\beta_{eff}^2} = \frac{1.0}{2} \qquad (5)$$

Thus, it would be anticipated that a small penalty would be incurred by operation of the generator with the Hall field shorted, as well as the transverse current. Experimental confirmation of these modeling predictions has been obtained with the laminated generator configuration shown in Fig. 14 by placing shorting busses in the flow direction to completely short out the Hall field. The variation in plasma performance was determined by measuring the electron density achieved for a specific CO_2 loading as presented in Fig. 22. As can be seen a comparison of a shorted and nonshorted Hall field generator operation results in approximately a 25 to 50 per cent variation in electron density. This slight degradation in generator performance with the Hall field completely shorted was deemed not to be of sufficient significance to prevent pursuing small scale tests of a solid copper wall configuration to determine the actual improvements that can be achieved in medium uniformity.

To evaluate smooth wall generator performance characteristics a small scale 20 cm optical path length solid copper walled generator-laser cavity configuration was constructed and tested. As shown in Fig. 23 this small scale generator configuration was instrumented with a myriad of pressure taps and diagnostics ports to insure that detailed experimental information on the properties of the plasma medium could be obtained. Aside from the removal of the insulating segments in this solid wall configuration the overall geometrical configuration and size of the generator precisely approximated that of the laminated configuration. The most important result obtained from tests on this generator configuration in addition to determination of the plasma properties, which were in good agreement with the earlier results obtained in the laminated generator with the Hall field shorted, was the fact that the medium uniformity was significantly improved. High speed motion pictures, a frame of which is shown in Fig. 24, indicated a relatively high degree of uniformity was achieved in this medium and also that arc spots along the walls of the generator channel were minimized in size and did not attach to localized areas to promote the formation of larger arc channels. Based on these quite promising results, the power extraction phase of the program was embarked upon with a solid wall generator configuration with an optical path length of 55 cm. The schematic of this experimental configuration is shown in Fig. 25. In addition to employing a completely solid copper wall generator configuration the 55 cm optical power extraction generator-laser cavity was equipped with 5 diagnostic ports spaced in the flow direction. A supersonic diffuser was employed on this configuration with boundary layer injection, as well as the subsonic diffuser in order to improve the overall aerodynamic performance of the laser channel. In addition, the magnetic field intensity was increased from 2.2 to 3.3 Tesla for the purpose of increasing the CO_2 concentrations that could be introduced into the medium while still maintaining plasma ignition. Shown in Fig. 26 is a picture of the two segmented portions of the generator-optical cavity along with the location of the diagnostic ports. As with other generator configurations this configuration was well instrumented so that both the aerodynamic performance as well as the plasma characteristics of the medium could be measured. The overall simplicity of this type of MHDL configuration and an appreciation for the

relative simplicity of the other components of the system can be obtained from the pictures of Figs. 26-28. Shown in Fig. 27 is the CO_2 injection system and the subsonic and supersonic diffuser configuration employed in these measurements is shown in Fig. 28. It is important to note that the CO_2 injector system was designed so that a variable position injector tube could be employed. It was also possible to change the diameter of the injection holes in the injector so that the penetration of CO_2 into the flow stream could either be enhanced or reduced depending on experimental results.

The initial phase of experimental investigations conducted with this large scale generator were directed toward establishing the operating characteristics of the system with a 2.5-fold increase in mass flow which was required for operation of the 55 cm configuration over the 20 cm configuration. In addition to this, complete diagnostics of the plasma medium were carried out to insure that performance obtained on the small scale laminated and solid wall (20 cm) generator configurations was being reproduced with the larger scale generator configuration. One of the more apparent, gratifying results obtained with this larger generator was that it was possible with the increases in applied magnetic field to operate at higher CO_2 concentrations. In the course of the experiments the full extent to which the CO_2 loading could be increased was not completely investigated. However, ignition at significant electron densities occurred at CO_2 concentrations greater than 0.75 per cent in all tests conducted.

Optical power extraction measurements were conducted with this system by placing an optical cavity at the diagnostic port located 10 cm from the throat of the nozzle. This location was picked because a majority of the information obtained on both small generators as well as the earlier phases of the experimental testing on the 55 cm generator-laser cavity configuration was obtained at this location. The optical cavity for these tests was comprised of a mirror system in which the mirror located on the top of the generator was partially transmitting so that power could be extracted from the system rather than measuring power deposition into the mirrors. The generator configuration with the optical cavity in place and with additional diagnostics which were located downstream of the optical cavity ports is shown in Fig. 29. In these tests mirror reflectivities were measured directly before conducting the experimental measurements and immediately upon completion of the experimental MHD test the mirrors were removed and reflectivity was again checked. To insure mirror alignment was being maintained throughout the course of the test, HeNe lasers were reflected onto the back surface of each mirror and the location of the retrospots reflected from these surfaces was monitored on TV cameras to insure that no misalignments were occurring within the optical cavity. The bench for the optical cavity was the pole face of the magnet. In the series of tests conducted in an attempt to extract optical power, it was found that no power could be detected even though detector sensitivities were on the order of one mW. In addition, with the proper shuttering and protection devices on the mirrors themselves, it was possible to maintain degradations in mirror reflectivity well below those required to insure that total cavity losses were less than the total gain predicted.

In an endeavor to determine the cause of the difficulty in the power extraction measurements the optical cavity on the system was removed and the system was again set up to conduct 10.6 μm gain measurements as well as to conduct measurements of the optical properties of medium with a HeNe beam. The diagnostic configurations employed in these measurements are shown in Figs. 30 and 31. In addition in these measurements the gain path for the 10.6μm beam was carefully shielded with He filled propagation tubes to insure that any environmental problems

associated with changes in the ambient environment in the MHD test cell would not influence the determination of the gain characteristics. Quite contrary to the results that had been obtained earlier and as shown in Fig. 19, gain measurements on a large scale generator indicated that complete attentuation of the 10.6μm beam was occurring at the time determined to be the optimum for the establishment of gain in the system. A typical 10.6μm transmission measurement is shown in Fig. 32. In contrast to the results presented in Fig. 19 it can be seen that complete attenuation of the beam occurs. Post-run window calibrations as shown in this figure indicate that this degradation is not due to either misalignment of the diagnostic laser system itself or due to window degradation problems. Visible laser propagation through the medium indicated that the visible laser beam was not deflected from its original position but exhibited similar near total attenuations as shown in Fig. 32 for the 10.6μm beam. After careful consideration of the various possibilities which can be producing this gross attenuation it was found a small amount of decomposition of the insulating material of the high temperature-high pressure bed used as a thermal source in these experiments (Fig. 12) was responsible for producing this attenuation. Micron size particle densities on the order of 10^4 cm^{-3} were found to be sufficient to produce the attenuations typical of the data of Fig. 32. Several additional experiments were conducted in addition to the measurements presented in Fig. 32 in an attempt to establish the actual mechanism for the introduction of small micron sized particles in the channel flow. It was found that the outer insulating blankets of the high temperature bed were gradually decomposing and this decomposition which was produced by the large number of hours that this experiment has been operated at elevated temperatures resulted in this decomposition. Attempts were made to remove this material through various processes such as changing test operating sequence or by introducing other chemical species to combust these particles in the throat of the nozzle. Although these attempts were partially successful, it was not possible to completely achieve a uniform clean flow as had been done in earlier measurements. After careful review of the entire problem associated with the decomposition of the insulating blankets on the high temperature-high pressure bed it was found that the most expedient way to eliminate this problem, which is an artifact of the experimental configuration employed in these tests and would not be an inherent problem in an operational MHD laser configuration, was to remove the existing insulating material and replace it with a higher temperature graphite type insulation. In addition, it is recommended that modifications be made to the flow paths through the high temperature-high pressure bed to insure that it is not possible in future experiments to allow any of the gas flow which passes through the generator-laser cavity configuration to come in contact with this insulating material in the bed. These modifications while being rather minor in nature do, however, require a general rebuild of the outer insulating material on the high temperature-high pressure vessel. As a consequence further testing has been terminated until these repairs can be made.

C. Summary of Results

In the series of tests conducted with three different generator-laser cavity configurations under Contract N-60921-70-C-0213 and N-60921-71-C-0279 it has been established that it is possible to achieve thermal ignition without the use of preionization in a nonequilibrium MHD generator configuration suitable for high power laser application. Indicated in Table I is a comparison of the properties theoretically predicted and experimentally observed from these experiments.

TABLE I

MHDL PERFORMANCE CHARACTERISTICS

B = 3.3 TESLA

T_{STAG} = 2400°K

THEORY PREDICTS THE ONSET OF IGNITION WITHOUT PREIONIZATION FOR THE FOLLOWING CONDITIONS

CO_2 CONCENTRATIONS	0.5 - 1.0%
J	1 - 10 amp/cm^2
E_{HALL}	1 - 5 KV/m
n_e	$\geq 5 \times 10^{13}$
T_e	≥2200°K
GAIN	0.1 - 0.2% cm^{-1}

IGNITION OBSERVED EXPERIMENTALLY WITHOUT PREIONIZATION FOR FOLLOWING CONDITIONS

CO_2 CONCENTRATIONS	0.75% AND GREATER
J	10 - 50 amps/cm^2
E_{HALL}	3.5 - 5kV/m
n_e	1×10^{13} - 4×10^{14}/cm^3
T_e	1800°K - 3800°K
GAIN	0.1 - 0.2% cm^{-1}

As can be seen from this data, the modeling of the MHDL system accurately reflects the actual conditions which have been achieved experimentally. With the exception of the extraction of optical power all properties of the MHD plasma either meet or exceed theoretical predictions. In addition, it appears perfectly feasible to achieve operating conditions in the generator portion of the system which allow efficient conversion of thermal energy to electrical energy. This suggests that the overall conversion efficiency from thermal-to-optical energy for an MHD laser as as predicted by the theoretical modeling is in the range of between 3-6 per cent. More importantly, the experimental results and technology which have been developed under this program have resulted in the production of a highly uniform plasma which does not require the use of a preionizer, and therefore, additional electrical energy input to achieve desired operating conditions. As a consequence, the overall MHD configuration for high power laser applications based on this data would appear to be a relatively simple, compact system with minimum requirements for auxiliary power sources.

IV. CONSIDERATIONS PERTAINING TO THE USE OF OTHER GASES IN THE MHDL MEDIUM

Consideration has also been given to the operation of the MHDL device on molecular species other than CO_2. Potentially a large group of other species based on existing collisional information can be pumped by low energy electron collisional processes. Specifically, gases such as N_2O, CO, HCl, HBr, HF and DF are possible molecular species which can be pumped with the high electron pumping rates typical of the MHD environment. The key in determining which of these species would be the most optimum to produce other wavelength operation with an MHDL system is crucially dependent on the electron pumping mechanism. For efficient operation of the MHD generator high thermal-to-electrical conversion efficiencies only occur for electron densities of 10^{13} cm^{-3} and above. As a consequence, the vibrational distribution is therefore determined by electron-molecule pumping times and is not influenced by anharmonic pumping effects. As a consequence of these considerations it appears that N_2O based on the collisional information that is available would be pumped as effectively as CO_2 and would produce attractive performance. The output of this system would be at 10.8 μm rather than 10.6 μm. Furthermore, the use of HCl and HBr as an alternate molecular species appears to be quite attractive for MHD applications because of the fact that vibrational temperature distributions of 2500°K produce population inversions in these two species. This vibrational temperature corresponds closely to the electron temperatures that can be achieved with nonequilibrium MHD generators. In these systems V-T relaxation rates are much less favorable than other diatomic species but the high pumping rates of the MHDL configuration make operation with these species quite attractive. It should be recognized that one drawback to this type of operation is the relatively fast chemistry associated with cesium-HCl or HBr type interactions which would require a completely different configuration for injection of HCl into the medium to prevent chemical reactions from influencing performance. However, in favor of operation with HCl is the fact that this material can be introduced in the form of hydrochloric acid rather than hydrogen and chlorine which from a logistics point of view has many attractive features.

Consideration has also been given to the use of CO in the MHD device. Unfortunately, because anharmonic pumping will not be effective in an MHDL device and because of the fact that vibrational populations corresponding to vibrational temperatures of 5000°K are required to achieve gain, CO does not appear to be an attractive alternate candidate for use in MHDL systems. Lastly, consideration has been given to operation with HF and DF. In this case extremely rapid vibrational-translational rates tend to suggest that operations with these species would not be as attractive as with HCl and HBr. However, preliminary experimental data from pulsed electric discharge laser work tends to suggest that it is possible to pump both of these species under electric discharge conditions, and therefore, it is suspected that if a true direct electron pumping is being achieved in an HF or DF electric discharge laser configuration it would be possible to pump these species in an MHD configuration which operates at much higher electron densities to achieve similar type performance.

V. RECOMMENDATIONS

Based on the experimental data that has been presented in the preceeding sections of this final report and the overall evaluation of the predicted and experimentally observed operational characteristics that have been obtained from the MHD generator testing it appears that the collisional processes which serve to govern the performance of MHD lasers are well understood. As a result of these findings it appears feasible to achieve population inversions in the MHDL medium and to produce an operating laser system which has the potential for achieving high specific powers and attractive overall thermal-to-optical conversion efficiencies. Unfortunately due to failure of the insulating material of the high temperature-high pressure bed used in these experiments, attempts to extract optical power have not been successful to date. However, since the failure to extract optical power is not a fundamental difficulty associated with the concept, but rather a specific problem peculiar to the heat source employed in the measurements it is recommended that a further series of power extraction tests be conducted. These tests should be conducted with the experimental configurations which are presently available in United Aircraft Research Laboratories since the problems associated with high temperature-high pressure heat source have been corrected. This recommendation is also being made on the basis of the fact that considerable effort and resources have been expended on this program and significant progress has been made in establishing the precise properties of the plasma that can be produced in the rather complex MHDL environment. In addition, this recommendation to conduct a further set of power extraction tests is being made because of the potential of this approach for high power laser applications coupled with its relative simplicity.

REFERENCES

1. A. Andrick, D. Danner, and H. Ehrhardt, Phys. Letters 29A, 346(1969).

2. W. L. Nighan, T. Brown, and R. J. Hall, "Laser Excitation Using a Non-Equilibrium MHD Generator," Presented At The AIAA Ninth Aerospace Sciences Meeting, New York, New York, January 25-27, 1971, Paper 71-67.

3. J. J. Lowke, A. V. Phelps and B. W. Irwin, J. Appl. Phys. 44, 4664 (1973)

4. B. R. Bulos, A. V. Phelps, "Electron Excitation of the 001 Level of CO_2 and the Vibrational Levels of N_2," Proceedings of the 26th Annual Gaseous Electronics Conference held October 16-19, 1973 in Madison, Wisconsin.

5. E. R. Fisher and C. K. Smith, Chem. Phys. Letters 6, 438(1970).

6. R. C. Benson, D. J. Benard, R. E. Walker, "Vibrational Relaxation of N_2 and CO_2(001) by Alkali Metal Atoms," To Be Published J. Chem. Phys.

7. Initial studies in 1968 to establish the plasma properties of an MHD medium to which molecular gases were added were conducted on the non-equilibrium MHD generator in the Department of Aeronautics and Astronautics at the Massachusetts Institute of Technology.
J. L. Kerrebrock, J. S. Draper, "Nonequilibrium MHD Generators with Molecular Gases," Presented to AIAA Eight Aerospace Science Meeting, New York, January 19-21, 1970, AIAA Paper No. 70-41.

LIST OF FIGURES

LIST OF FIGURES (CON'T)

FIG. 1

LASER EXCITATION USING SHORT–CIRCUITED MHD GENERATOR

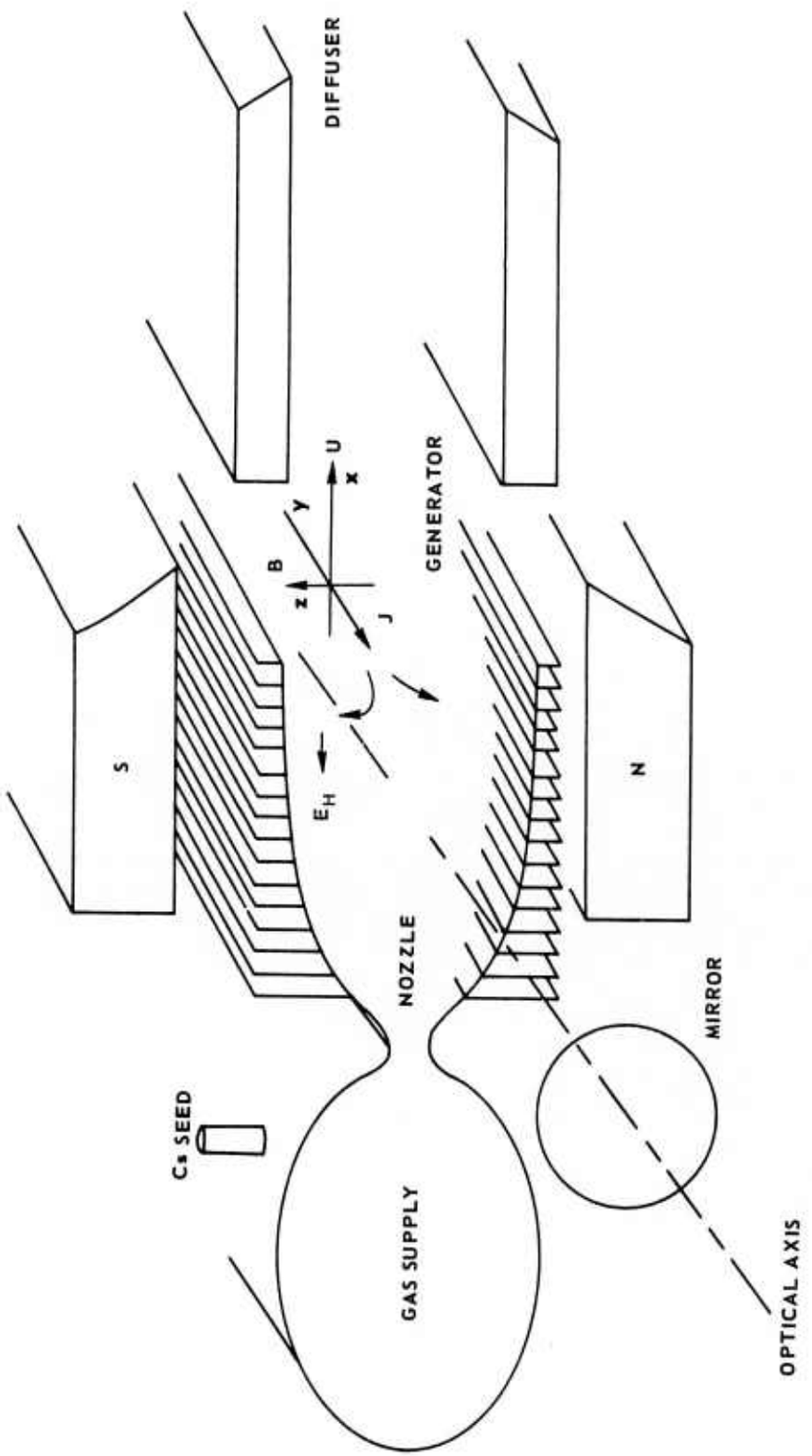

FIG. 2

ELECTRON CROSS SECTIONS FOR VIBRATIONAL EXCITATION OF CO_2 AND N_2

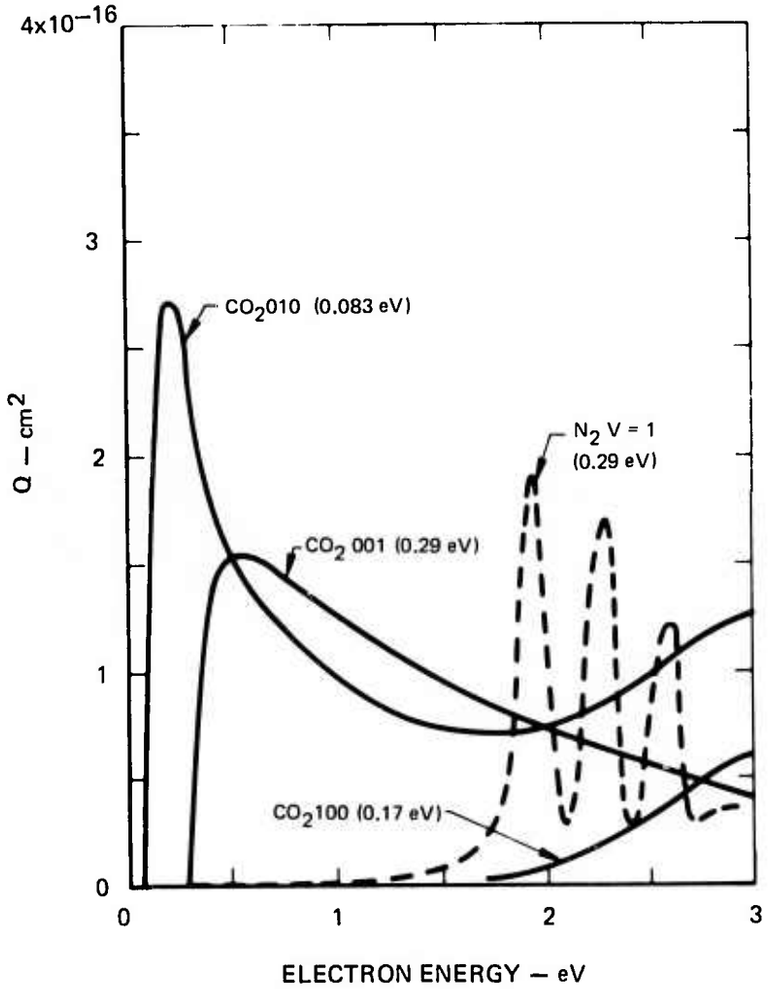

FIG. 3

ELECTRON ENERGY TRANSFER COLLISION FREQUENCY IN CO_2

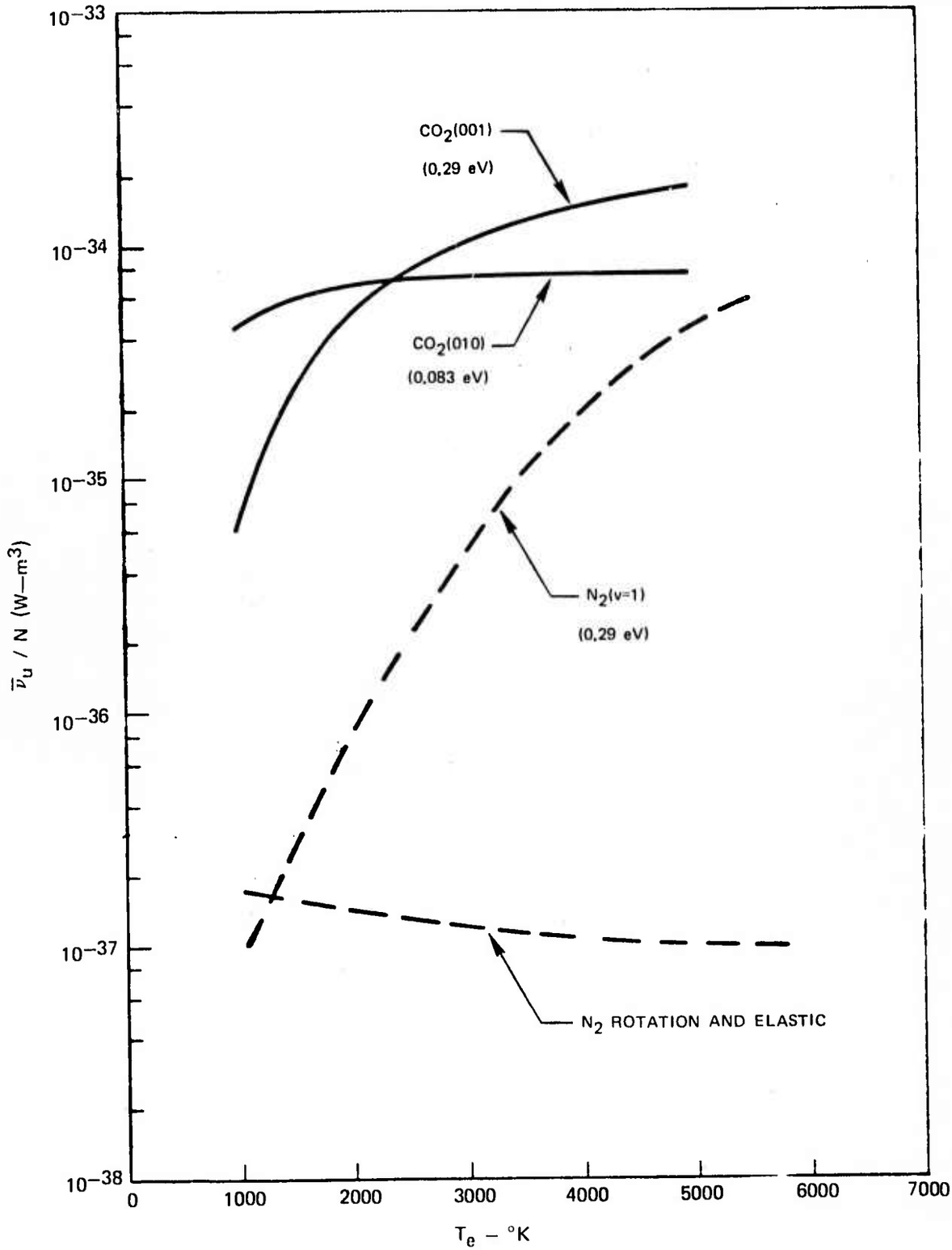

FIG. 4

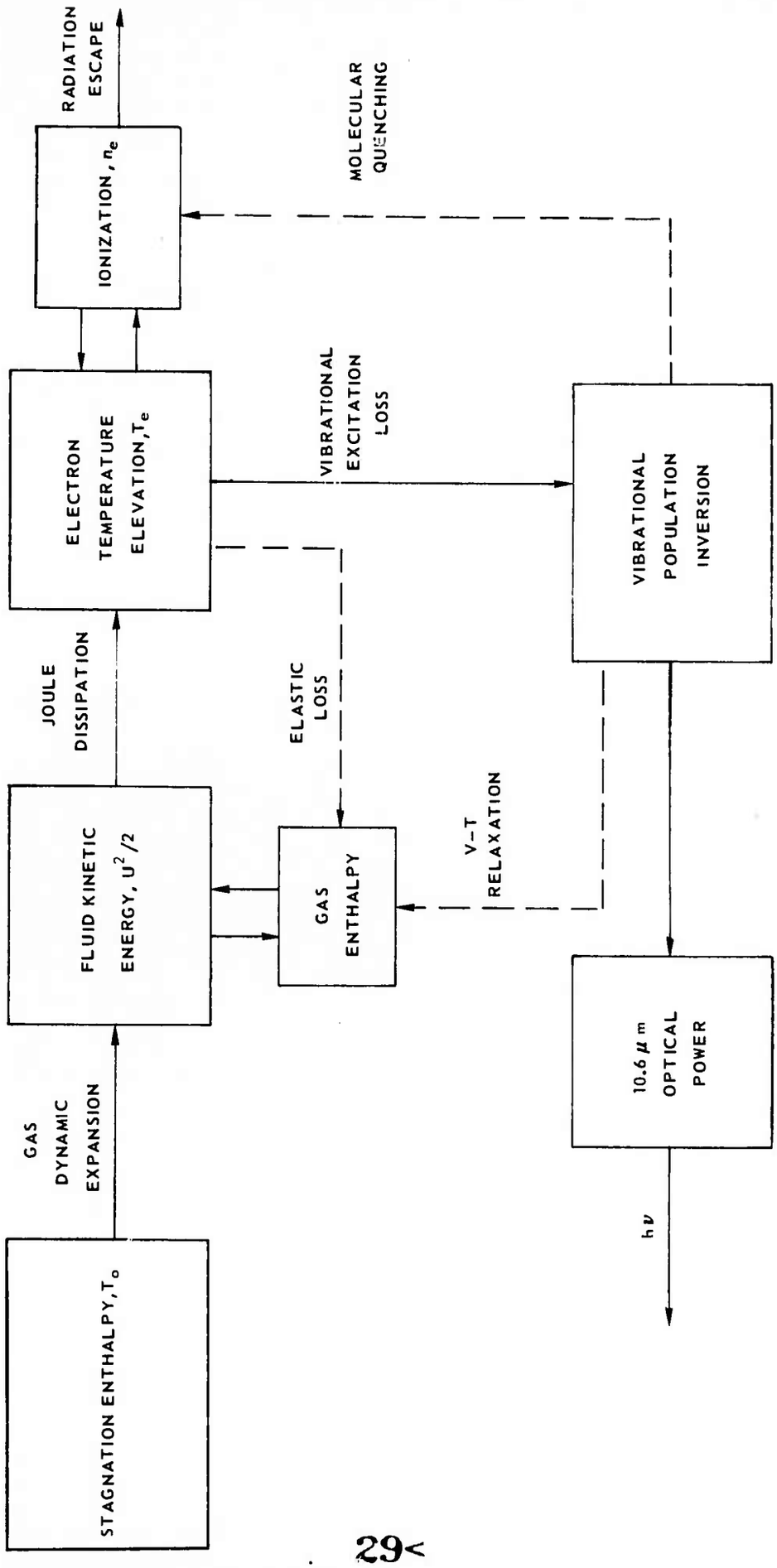
DIAGRAM OF ANALYTIC MODEL
RADIATION ESCAPE
IONIZATION, n_e
MOLECULAR QUENCHING
ELECTRON TEMPERATURE ELEVATION, T_e
VIBRATIONAL EXCITATION LOSS
VIBRATIONAL POPULATION INVERSION
JOULE DISSIPATION
ELASTIC LOSS
FLUID KINETIC ENERGY, $U^2/2$
GAS ENTHALPY
V–T RELAXATION
10.6 μ m OPTICAL POWER
GAS DYNAMIC EXPANSION
STAGNATION ENTHALPY, T_o
$h\nu$

FIG. 5

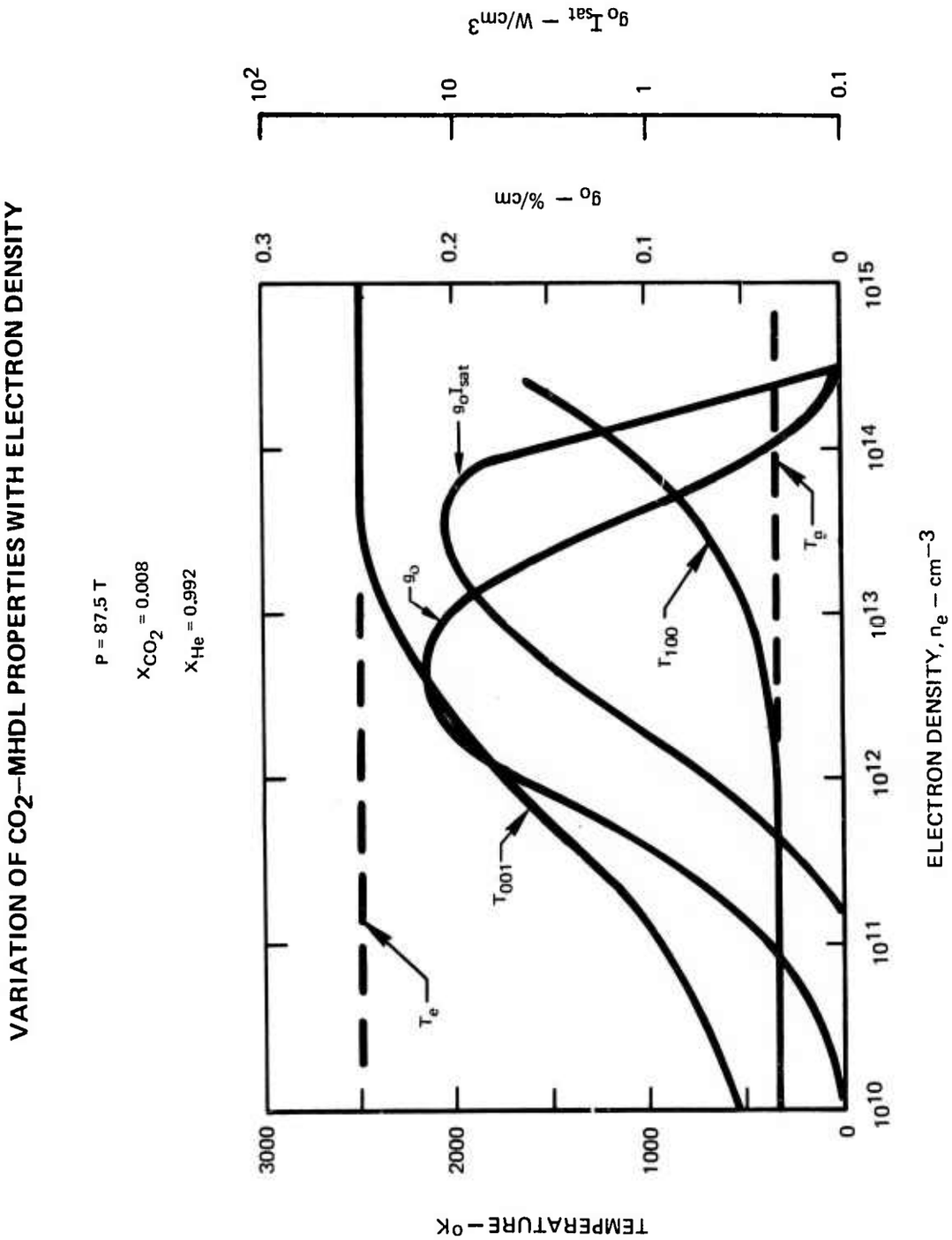
VARIATION OF CO_2–MHDL PROPERTIES WITH ELECTRON DENSITY
P = 87.5 T
X_{CO_2} = 0.008
X_{He} = 0.992
TEMPERATURE – °K
3000
2000
1000
0
T_e
T_{001}
T_{100}
T_g
q_D
$q_o I_{sat}$
q_o – %/cm
0.3
0.2
0.1
0
$q_o I_{sat}$ – W/cm^3
10^2
10
1
0.1
10^{10}
10^{11}
10^{12}
10^{13}
10^{14}
10^{15}
ELECTRON DENSITY, n_e – cm^{-3}

FIG. 6

FLOWING GAS MIXING DISCHARGE

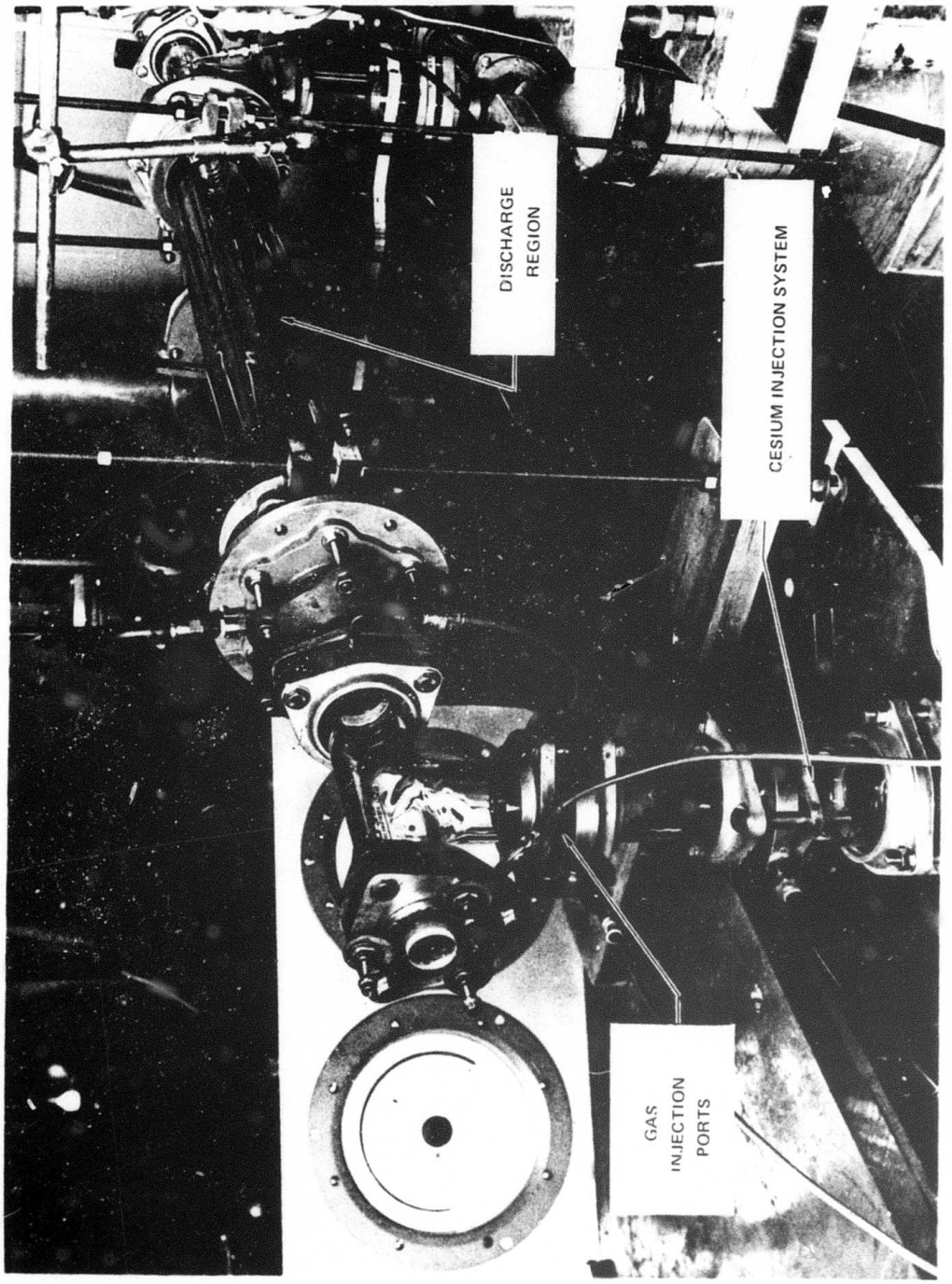

FIG. 7

COMPUTED AND MEASURED VALUES OF SMALL SIGNAL GAIN FOR MHDL SIMULATION (P = 50 TORR, 1.0% CO_2–99.0% He)

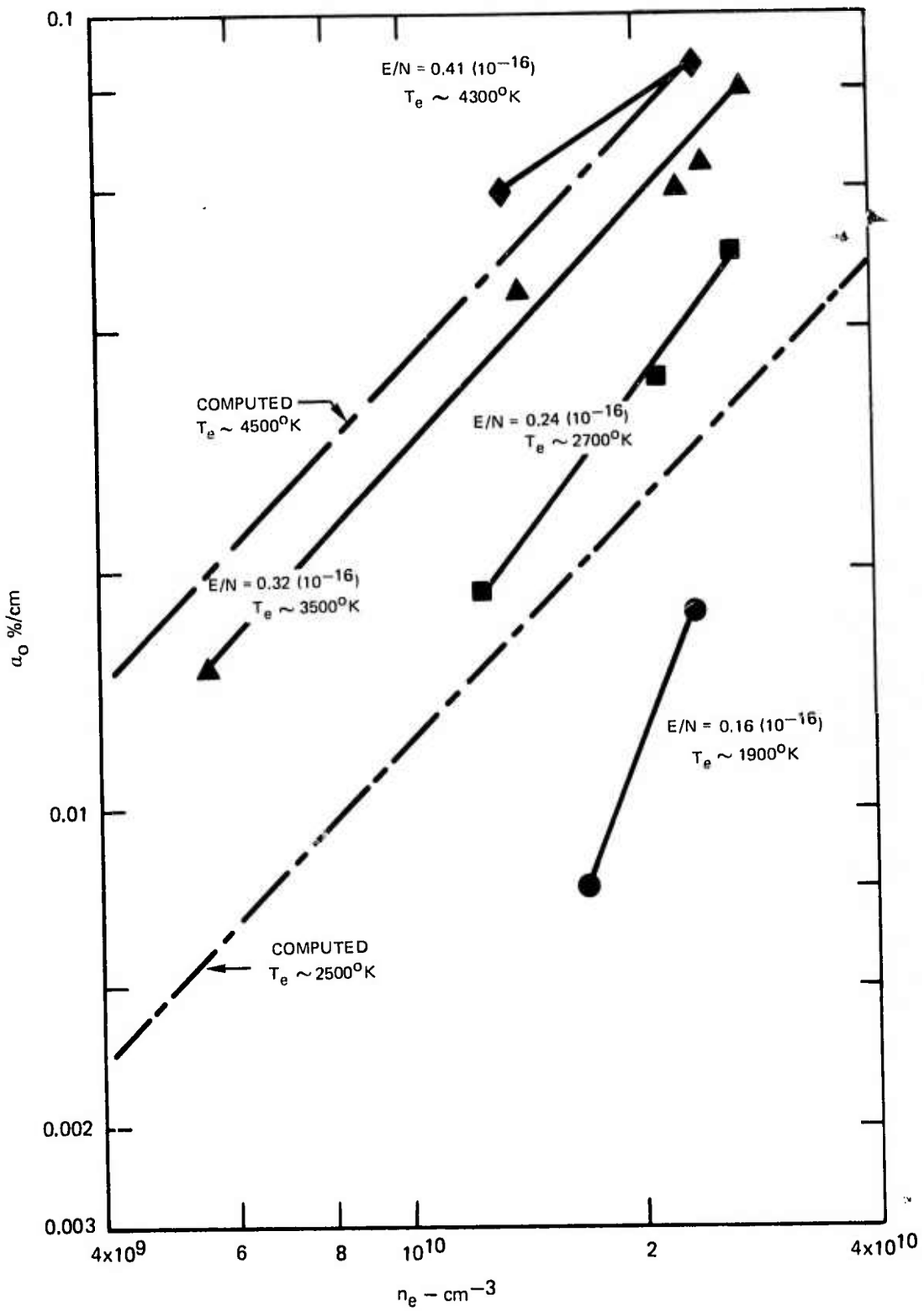

FIG. 8

CALCULATED TEMPERATURE RESPONSE PROFILES

$X_{CO_2} = 0.0175$

$X_{He} = 0.9815$

$X_{Cs} = 0.001$

$T_o = 2400^oK$

$P_o = 13.5$ atm

$M_e = 4.7$

B = 3T

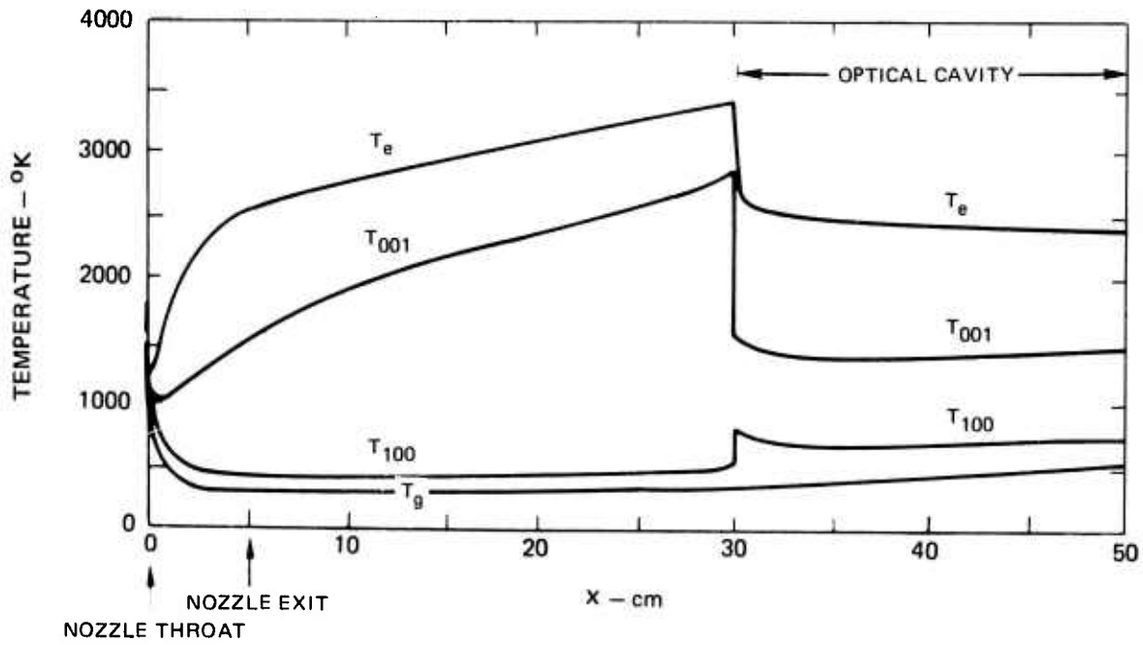

FIG. 9

THERMAL IONIZATION CALCULATION

$X_{CO_2} = 0.0175$ $\quad T_o = 2400^oK$

$X_{He} = 0.9815$ $\quad P_o = 13.5$ atm

$X_{Cs} = 0.001$ $\quad M_e = 4.7$

$B = 3$ T

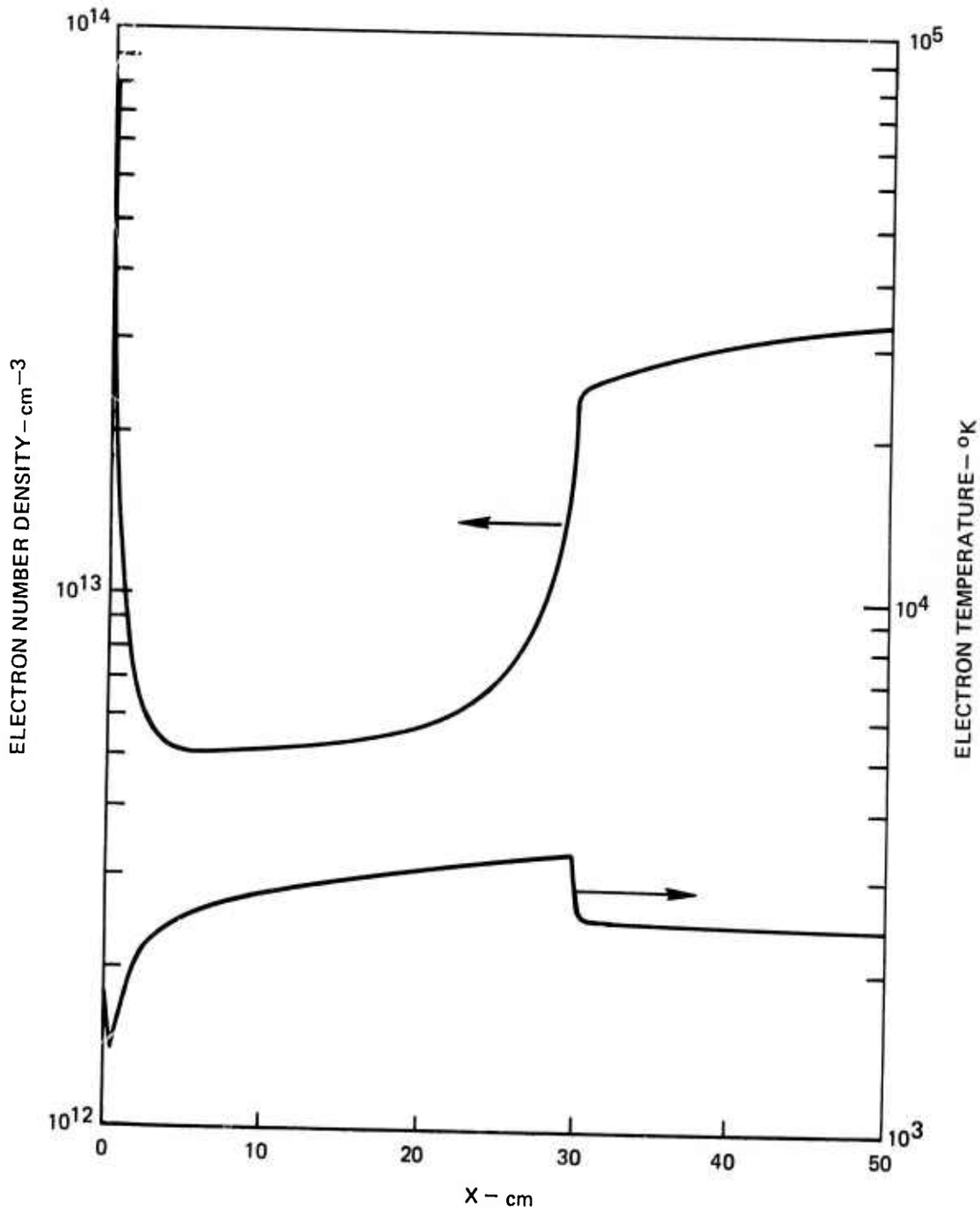

THERMAL IONIZATION CALCULATION

$X_{CO_2} = 0.0175$ $T_o = 2400^oK$

$X_{He} = 0.9815$ $P_o = 13.5$ atm

$X_{Cs} = 0.001$ $M_e = 4.7$

$B = 3$ T

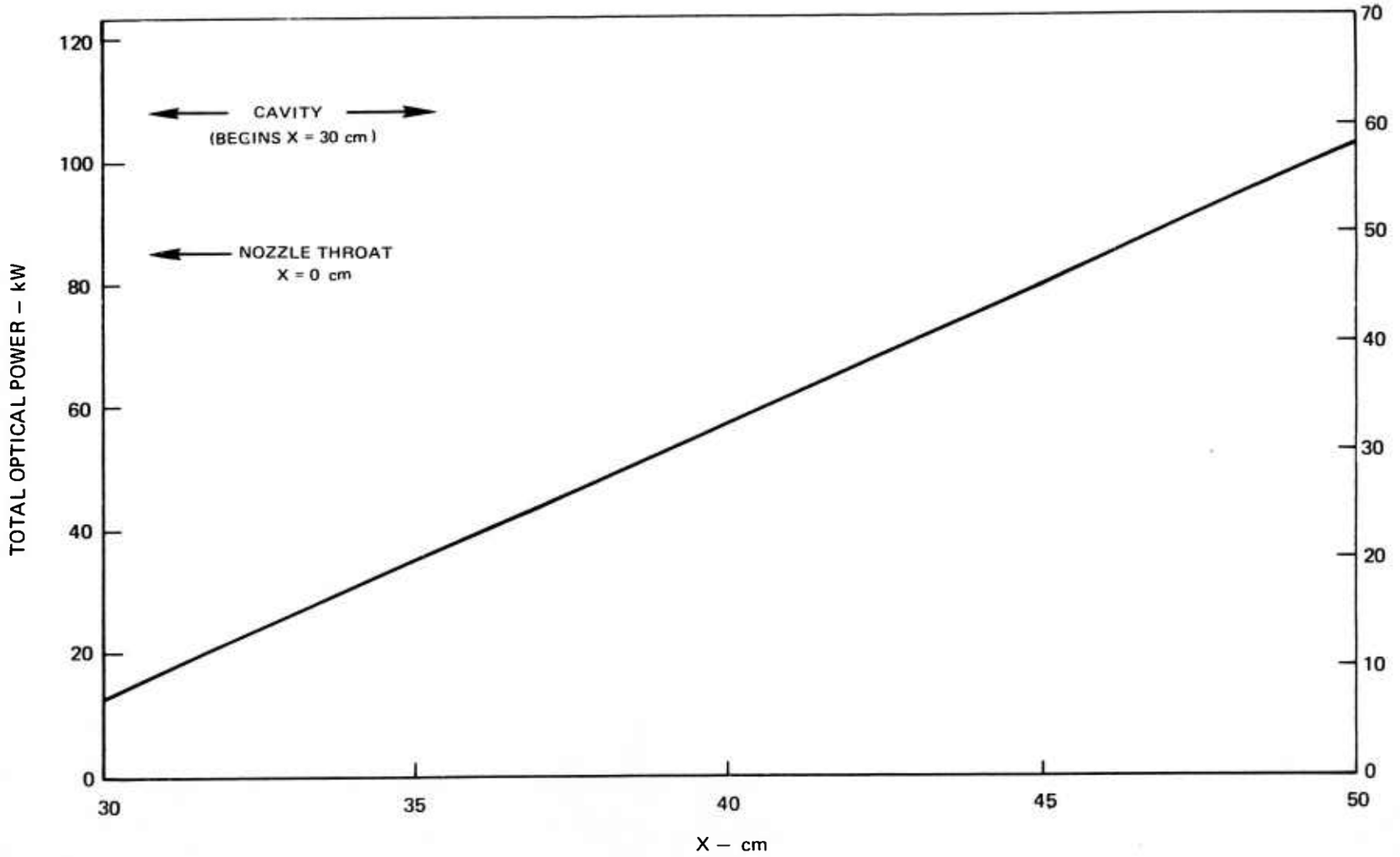

FIG. 10

FIG. 11

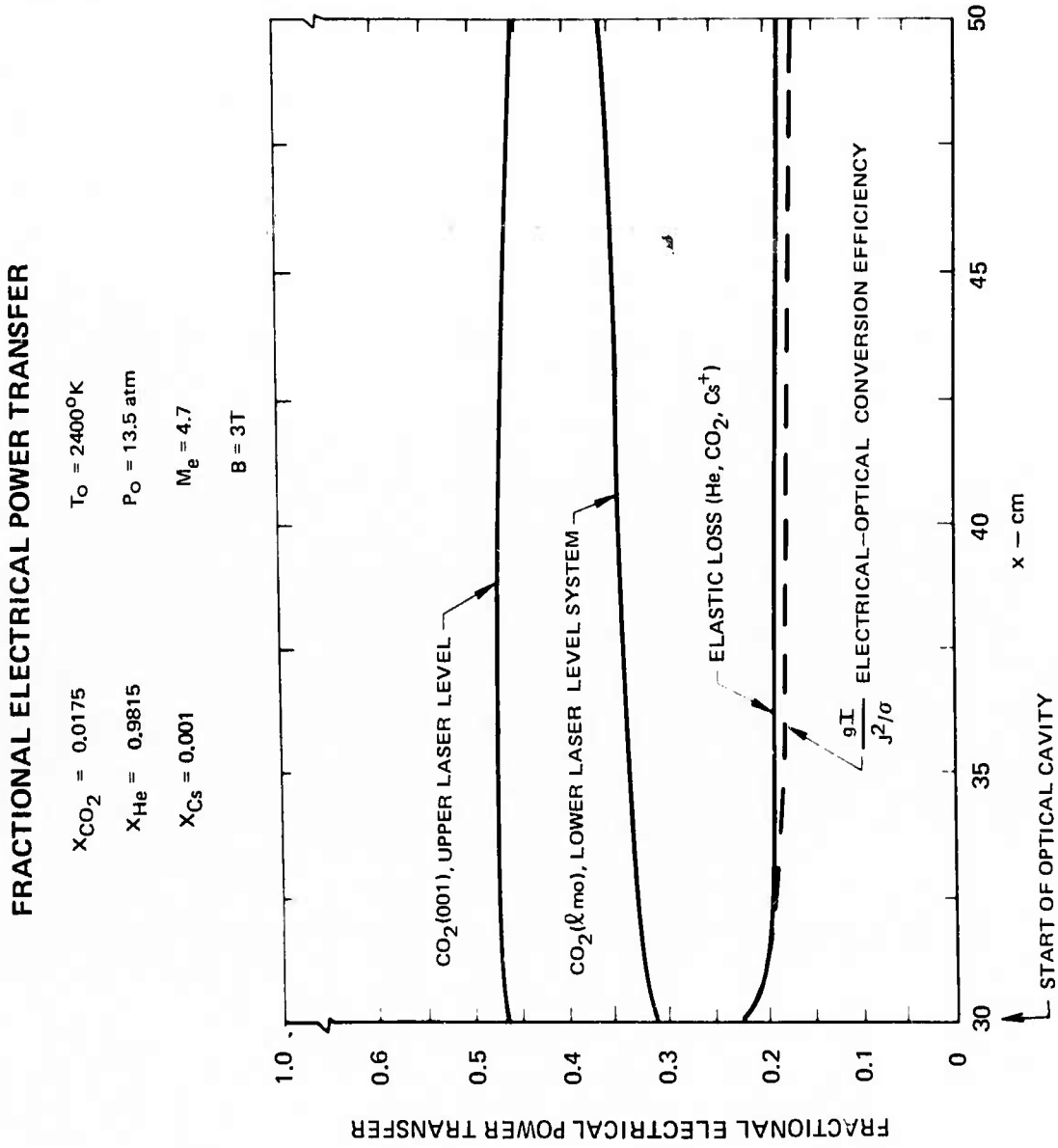
FRACTIONAL ELECTRICAL POWER TRANSFER
X_{CO_2} = 0.0175
X_{He} = 0.9815
X_{Cs} = 0.001
T_O = 2400°K
P_O = 13.5 atm
M_e = 4.7
B = 3T
CO_2(001), UPPER LASER LEVEL
CO_2(ℓmo), LOWER LASER LEVEL SYSTEM
ELASTIC LOSS (He, CO_2, Cs^+)
$\frac{gI}{J^2/\sigma}$ ELECTRICAL–OPTICAL CONVERSION EFFICIENCY
START OF OPTICAL CAVITY
x – cm
FRACTIONAL ELECTRICAL POWER TRANSFER
1.0
0.6
0.5
0.4
0.3
0.2
0.1
0
30
35
40
45
50

FIG. 12

MHDL EXPERIMENTAL APPARATUS

(MAGNET NOT SHOWN)

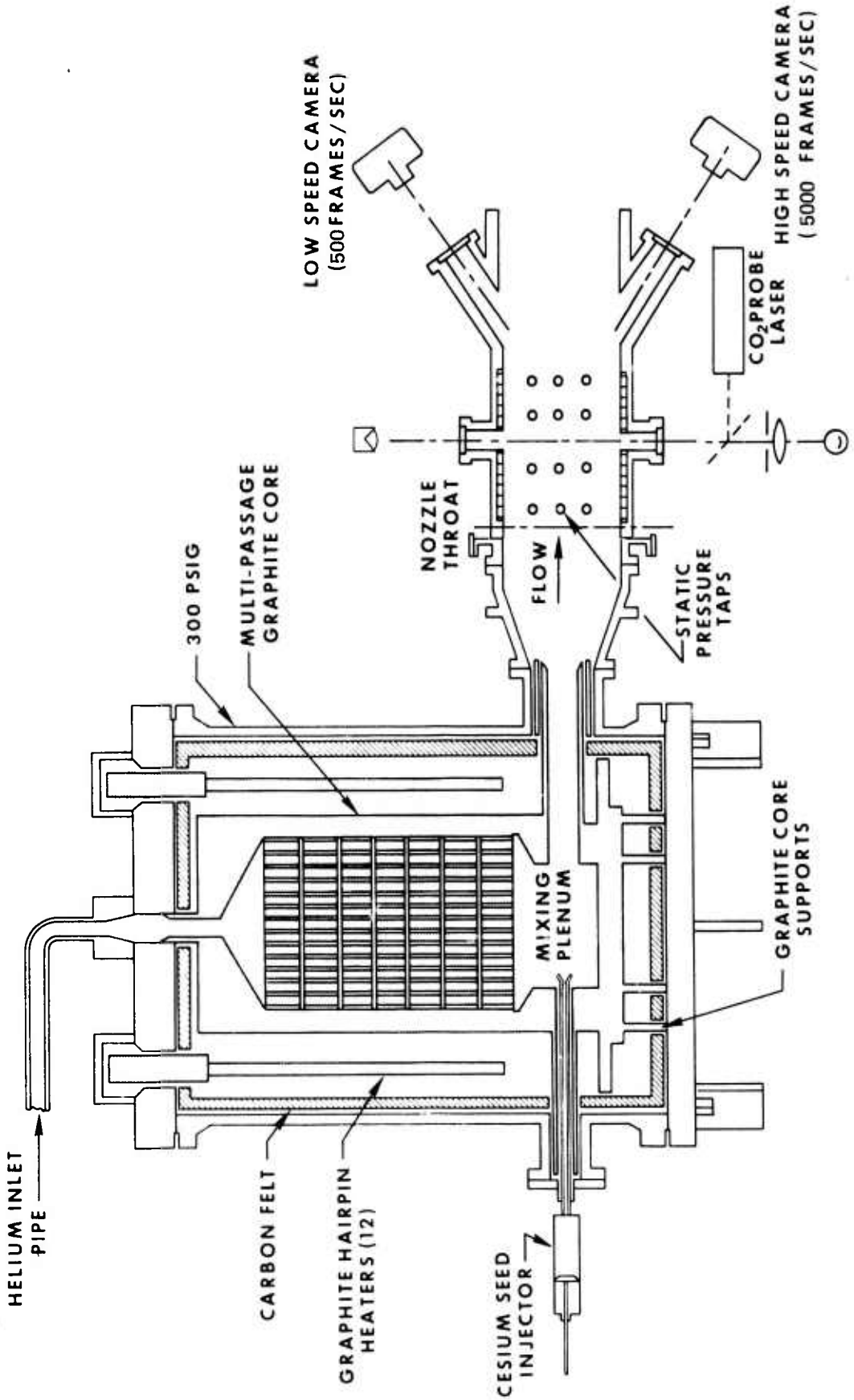

FIG. 13

MHDL NOZZLE-GENERATOR CONFIGURATION

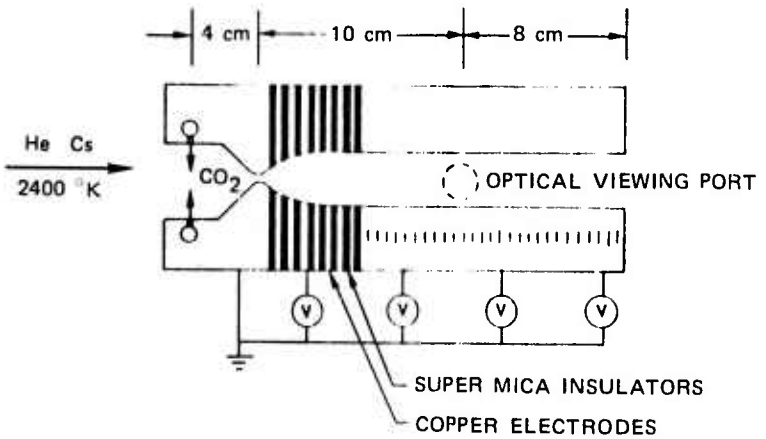

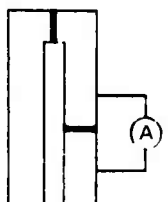

FIG. 14

LAMINATED MHDL NOZZLE–GENERATOR SECTION COMPONENTS

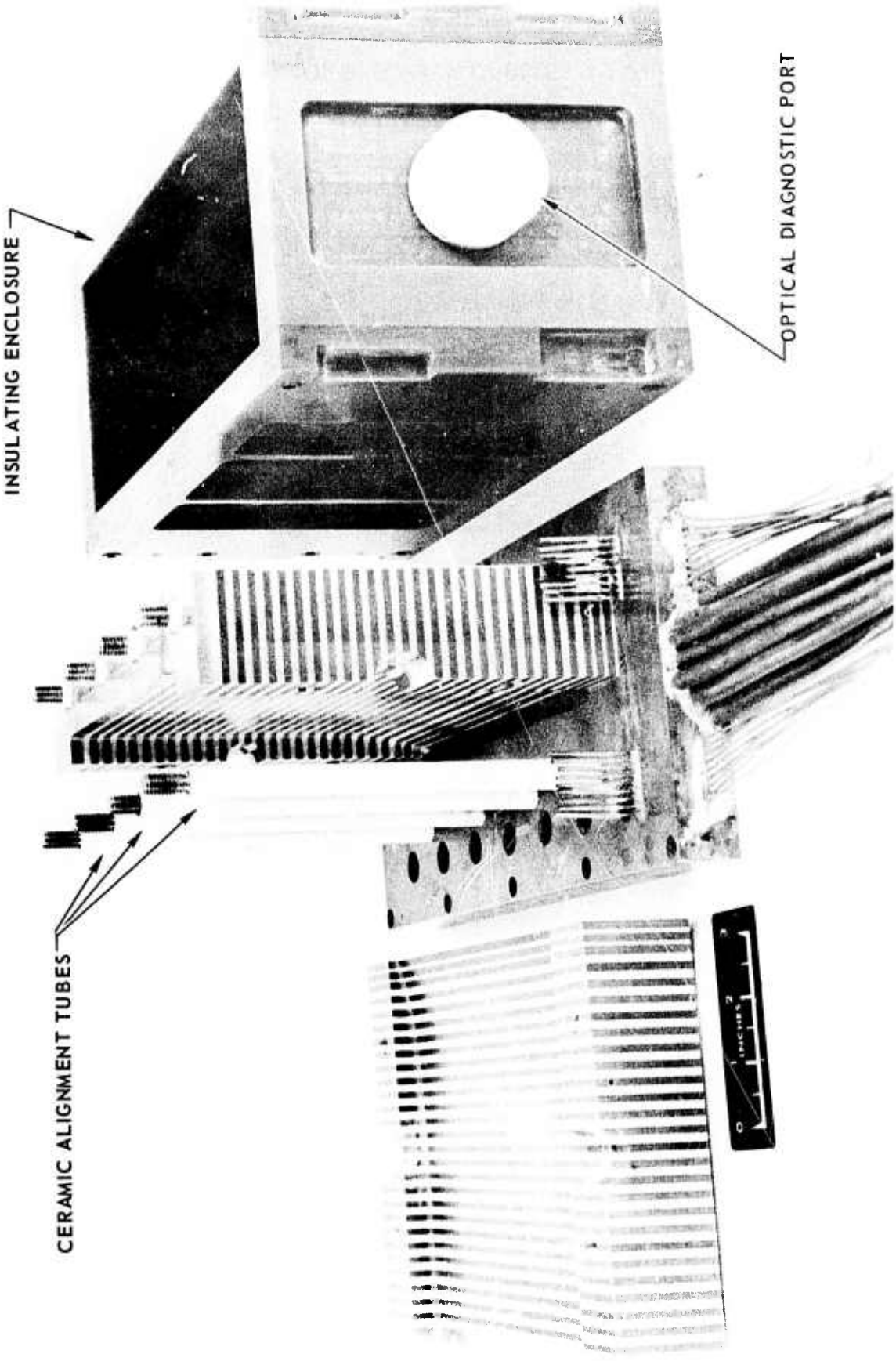

FIG. 15

CALCULATED VARIATION OF ELECTRON DENSITY WITH CO_2 CONTENT

(TYPICAL MHDL EXPERIMENTAL CONDITIONS)

$T_o = 2400^oK$

$P_o = 19.7$ atm

$B = 2.2$ T

$X_{Cs} = 0.0027$

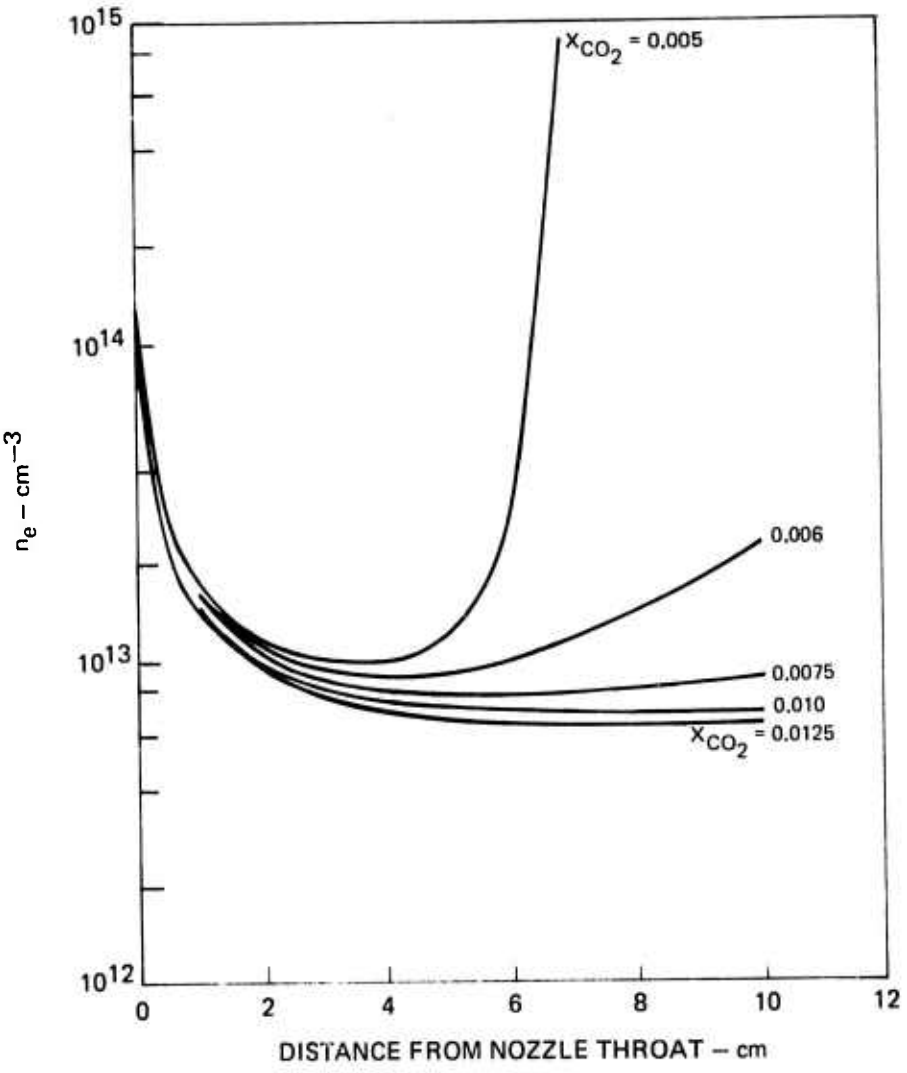

FIG. 16

MEASURED VARIATION OF ELECTRON DENSITY WITH CO_2 CONTENT

RUN 210

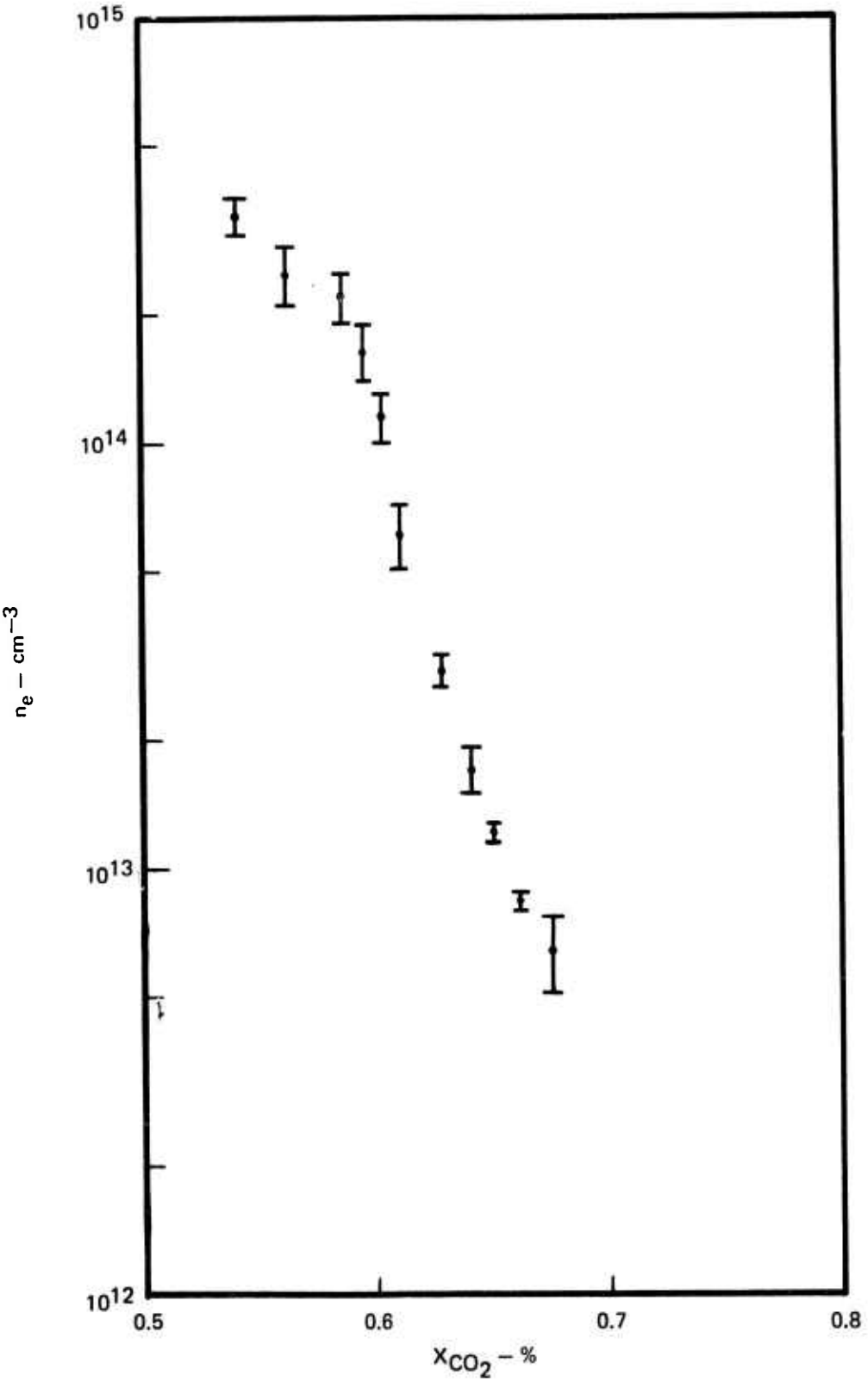

FIG. 17

CALCULATED ELECTRON TEMPERATURE VARIATION WITH CO_2 CONTENT

(MHDL EXPERIMENTAL CONDITIONS)

T_o = 2400°K

P_o = 18.7 atm

B = 2.2 T

X_{Cs} = 0.0027

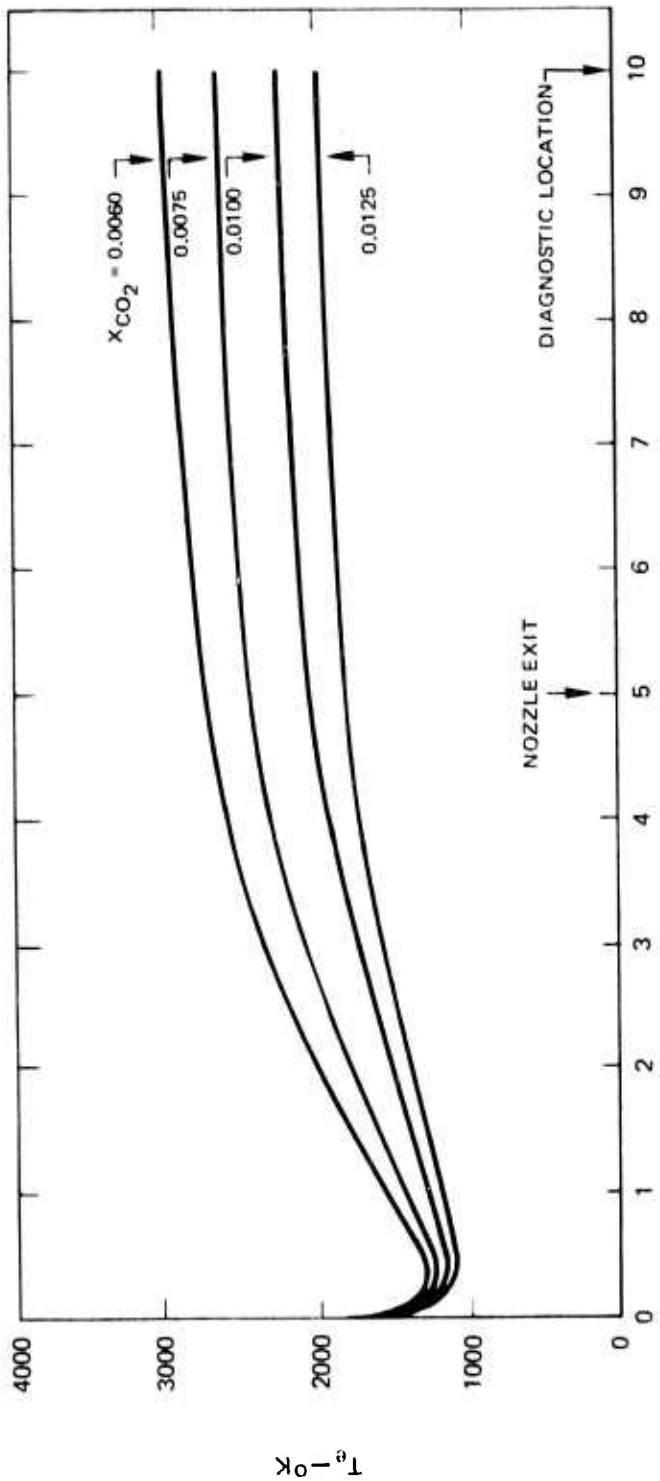

FIG. 18

MEASURED ELECTRON TEMPERATURE VARIATION WITH CO_2 CONTENT

RUN 210

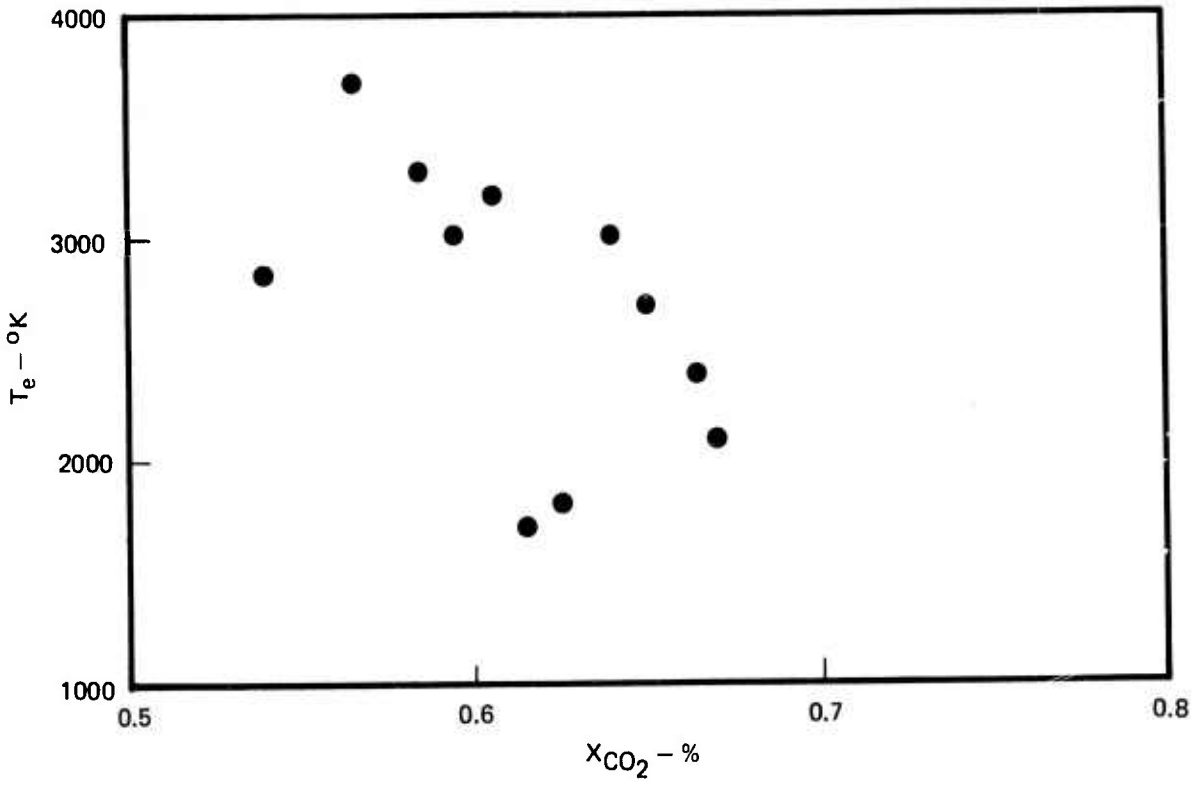

FIG. 19

SMALL SIGNAL GAIN MEASUREMENT (RUN 206)

$T_{BED} = 2490^{o}K$ $X_{CS} = 0.14\%$ $X_{CO_2} = 0.8\%$ TO 0.55%

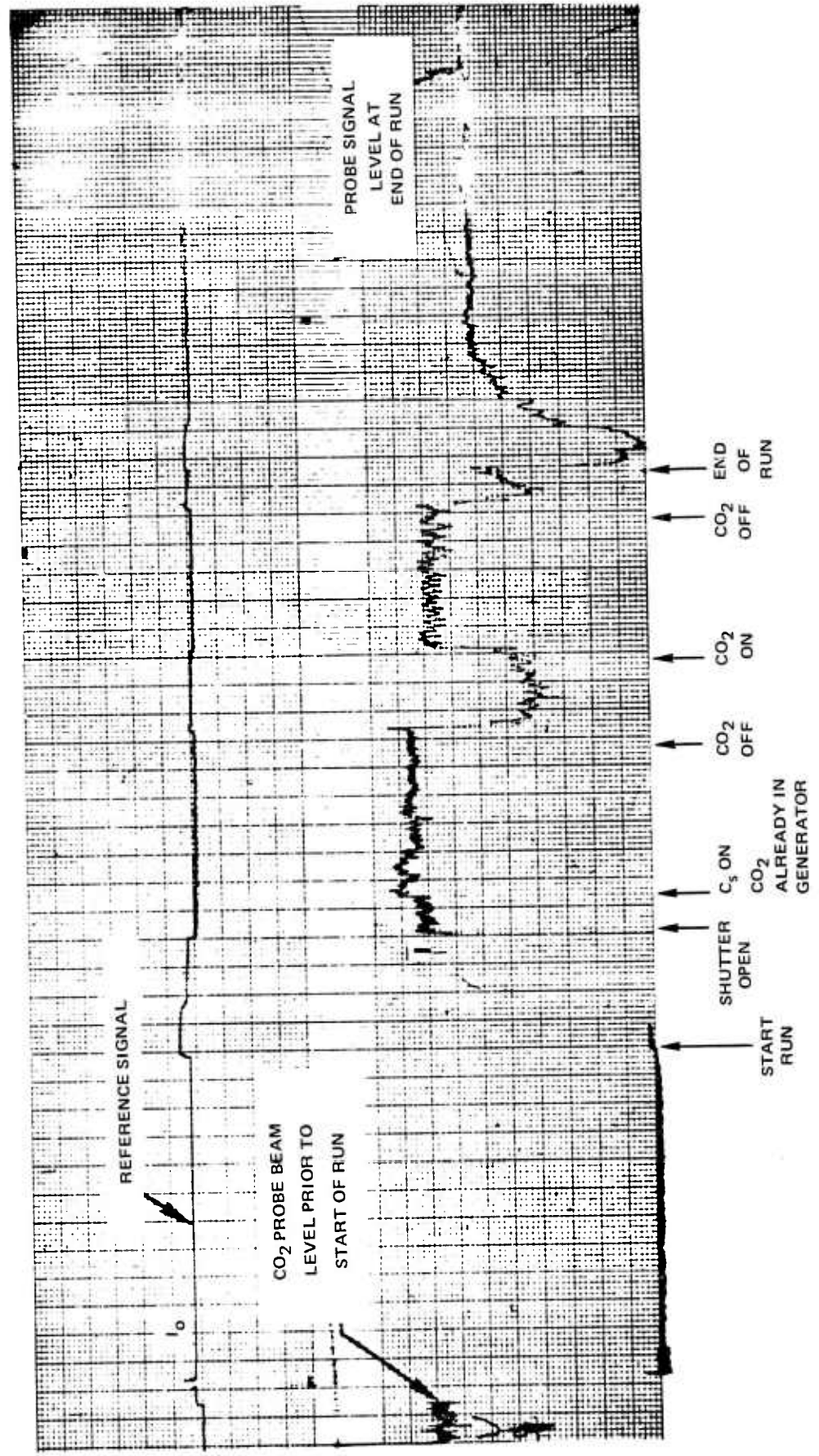

FIG. 20

HIGH SPEED MOTION PICTURES OF MHDL MEDIUM

(5000 FRAMES / SEC)

(FLOW DIRECTION)

LAMINATED GENERATOR–CAVITY

FIG. 21

RELATIVE FLUID VELOCITY PROFILES AS A FUNCTION OF WALL ROUGHNESS IN MHDL CHANNEL – 7.6 cm DOWNSTREAM OF NOZZLE THROAT

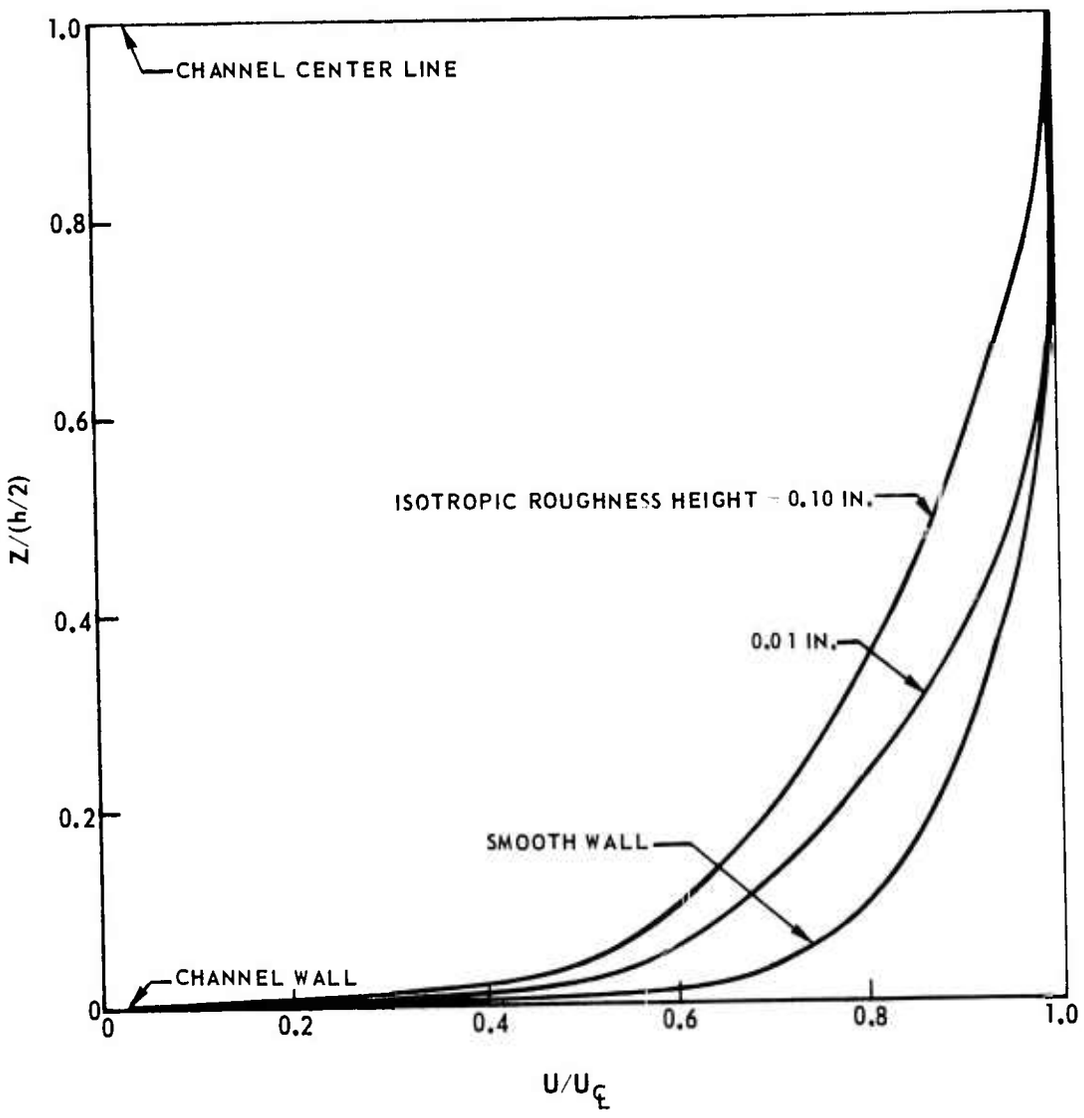

FIG. 22

VARIATION OF ELECTRON DENSITY WITH CO_2 CONCENTRATION

(SHORTED AND UNSHORTED CONDITIONS)

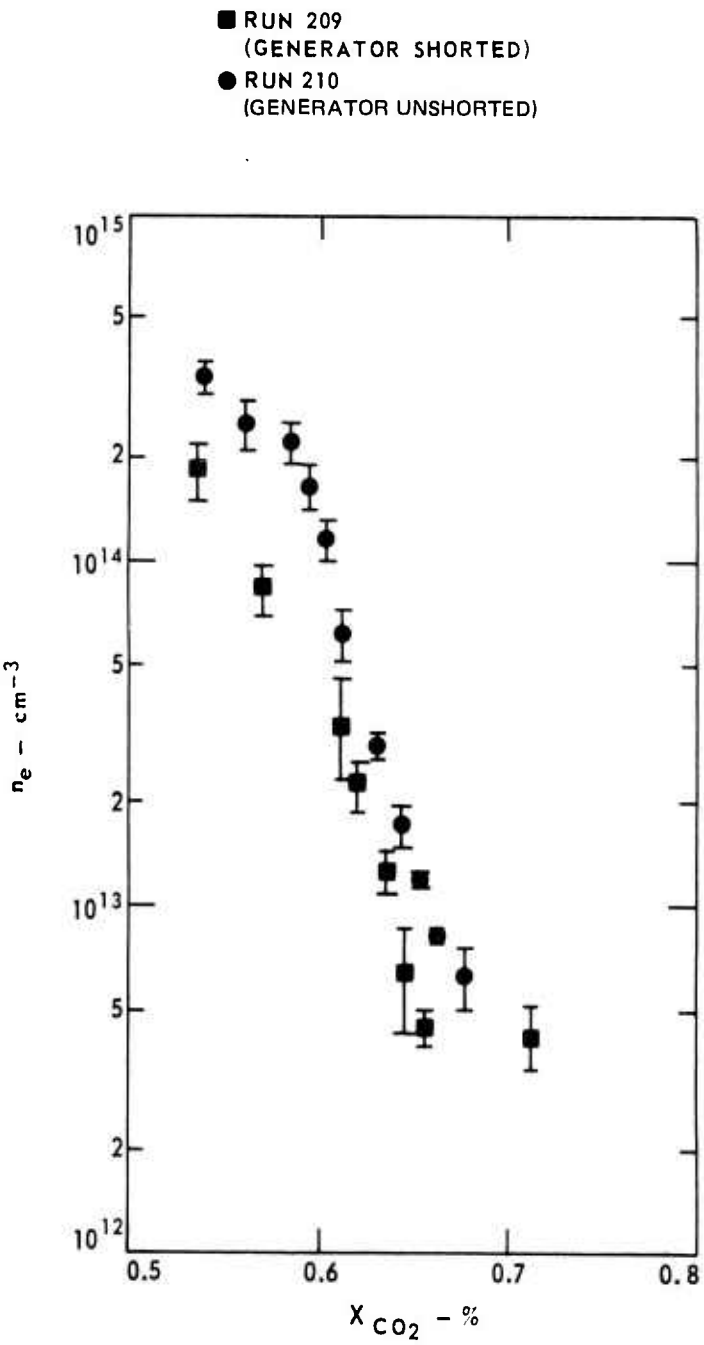

FIG. 23

SOLID COPPER GENERATOR CONFIGURATION

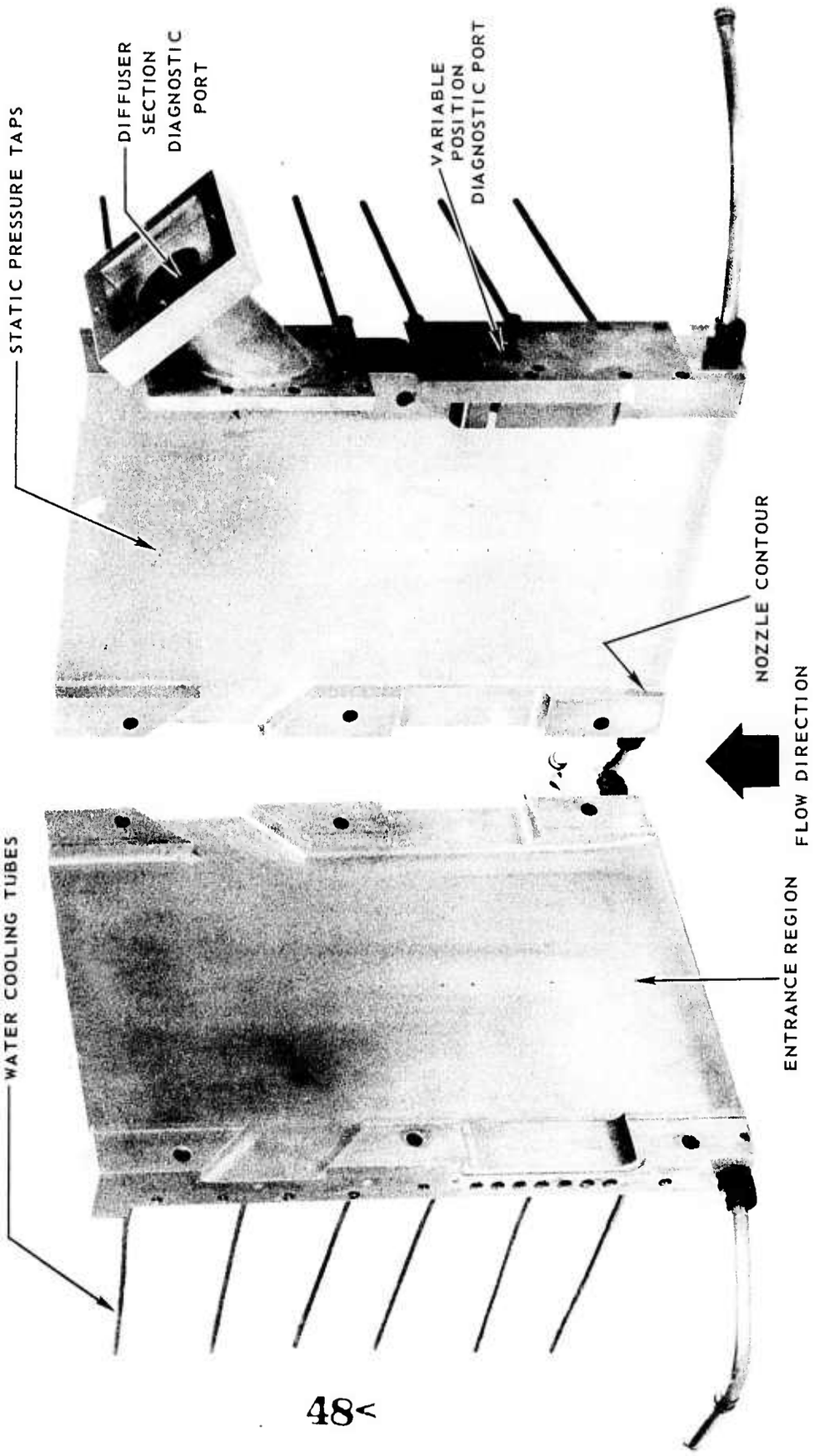

FIG. 24

HIGH SPEED MOTION PICTURES OF MHDL MEDIUM

(5000 FRAMES/SEC)

(FLOW DIRECTION)

SOLID GENERATOR–CAVITY

FIG. 25

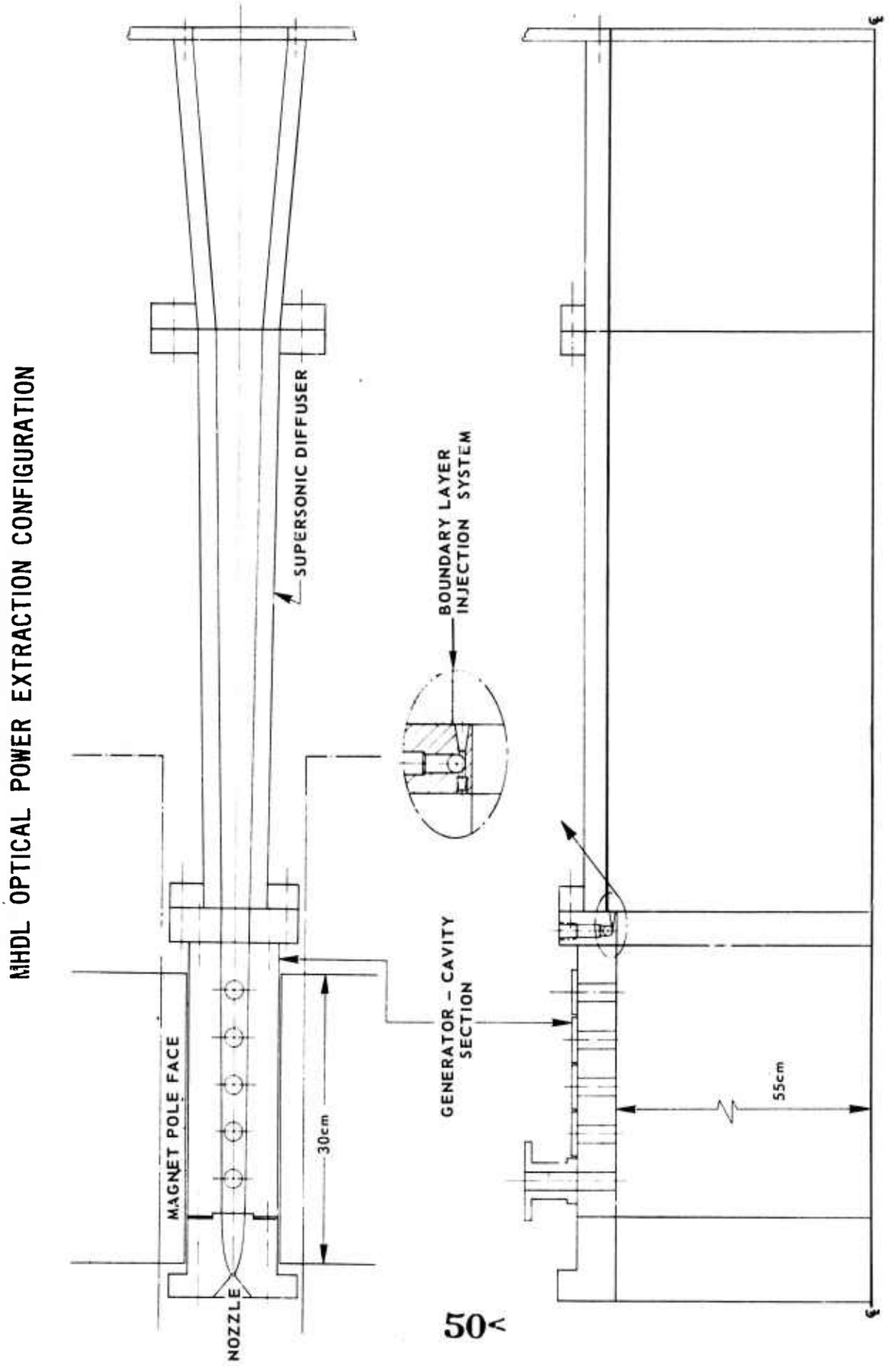
MHDL OPTICAL POWER EXTRACTION CONFIGURATION
SUPERSONIC DIFFUSER
BOUNDARY LAYER INJECTION SYSTEM
GENERATOR – CAVITY SECTION
MAGNET POLE FACE
30cm
NOZZLE
55cm
50

OPTICAL POWER EXTRACTION CONFIGURATION

(NOZZLE AND GENERATOR)

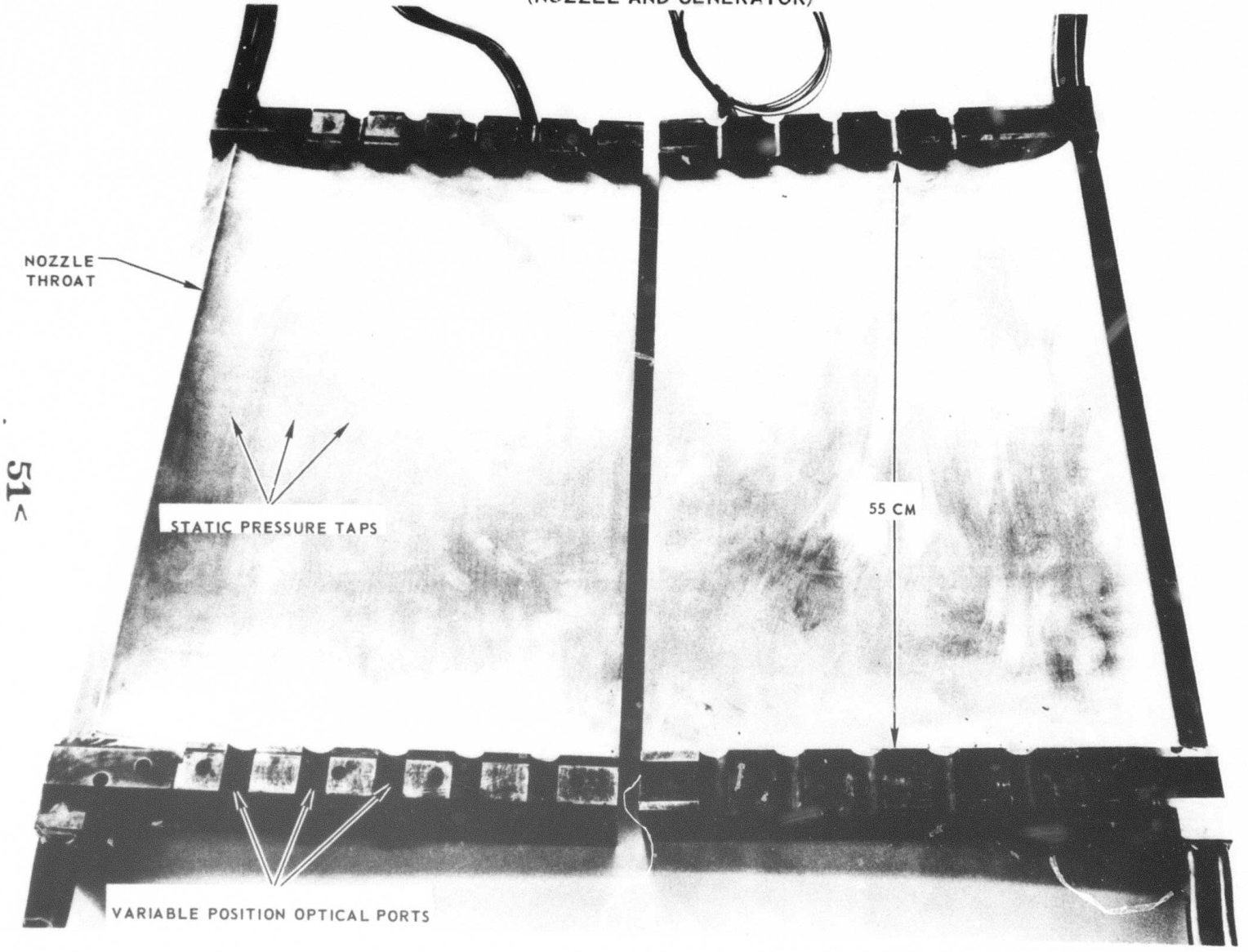

N921308-4

FIG. 26

N921308–4

FIG. 27

CO_2 INJECTION SYSTEM

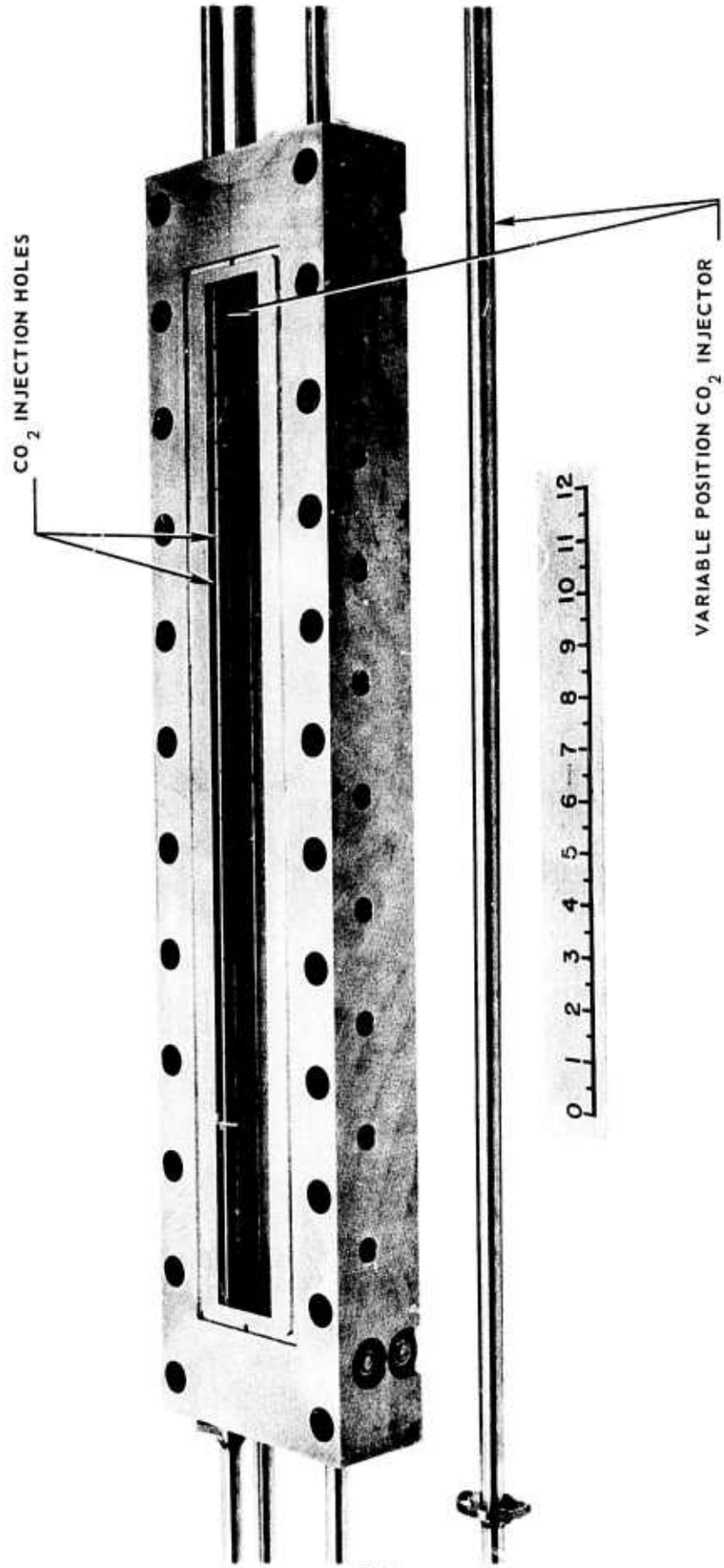

MHDL DIFFUSER SYSTEM
(55 cm CONFIGURATION)

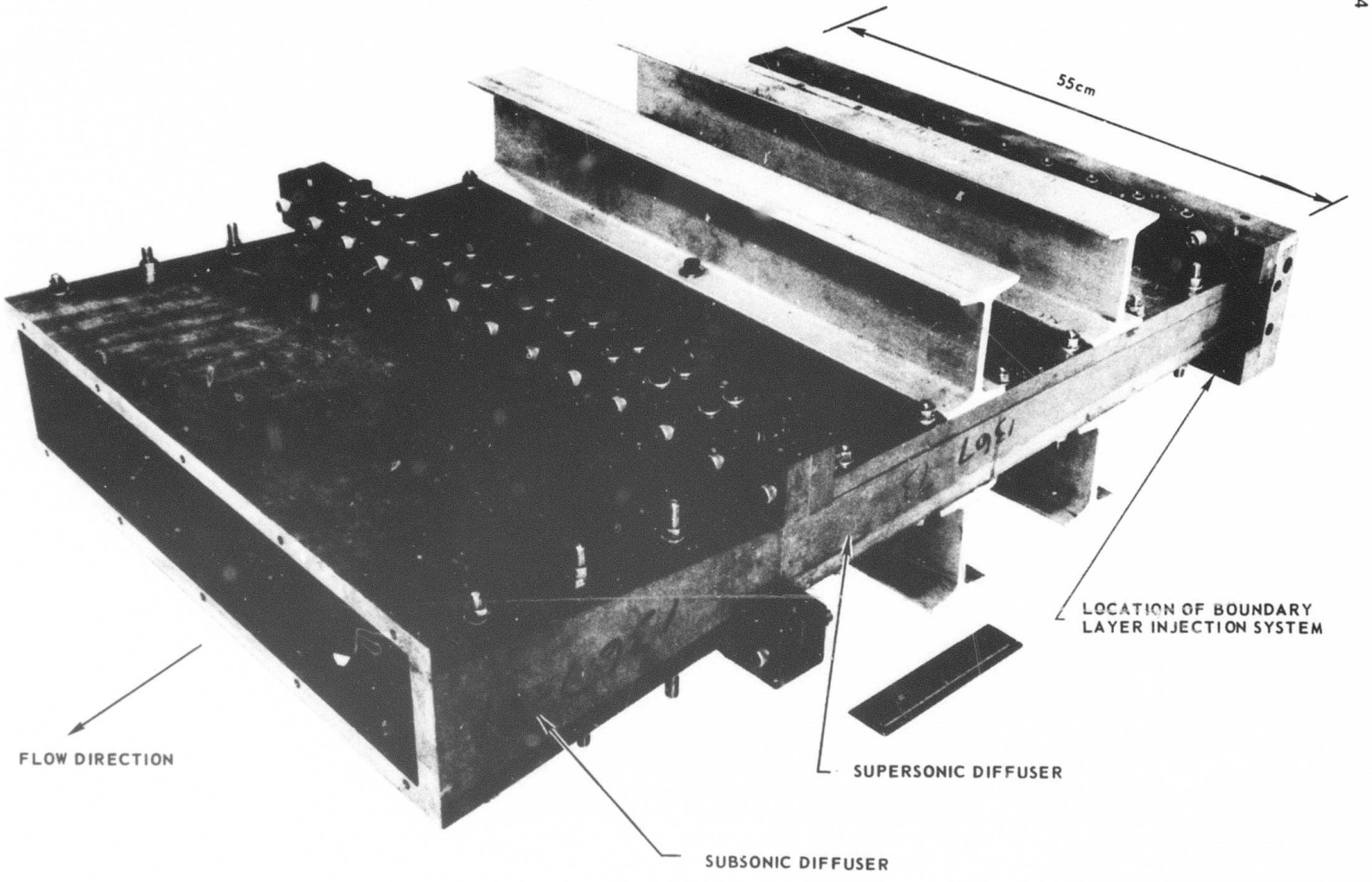

N921308-4

FIG. 28

FIG. 29

MHDL GENERATOR

(55 CM CONFIGURATION) OPTICAL POWER EXTRACTION

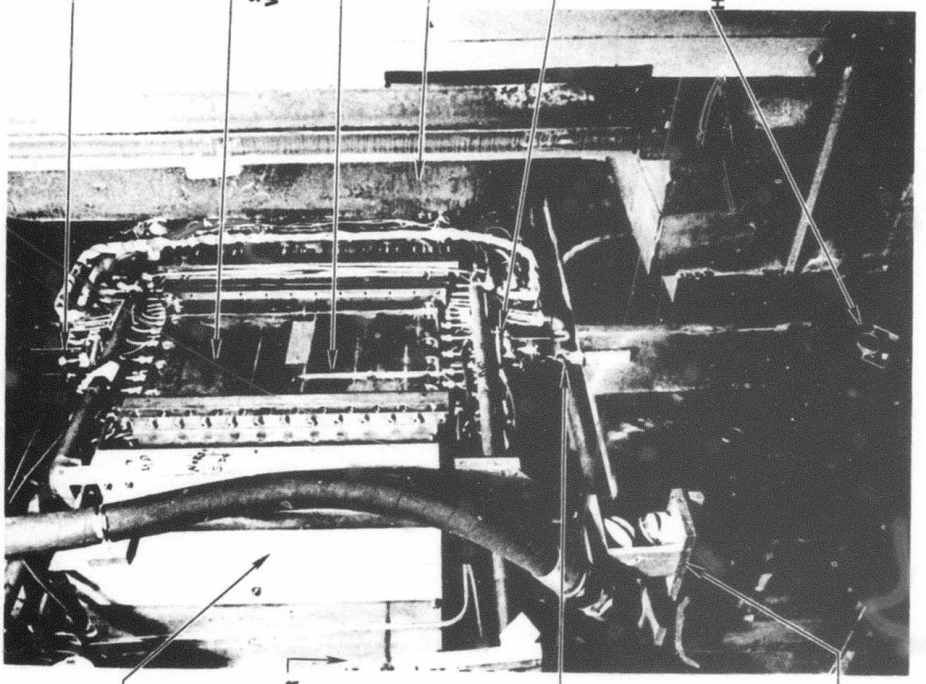

FIG. 30

MHDL DETECTION SYSTEMS

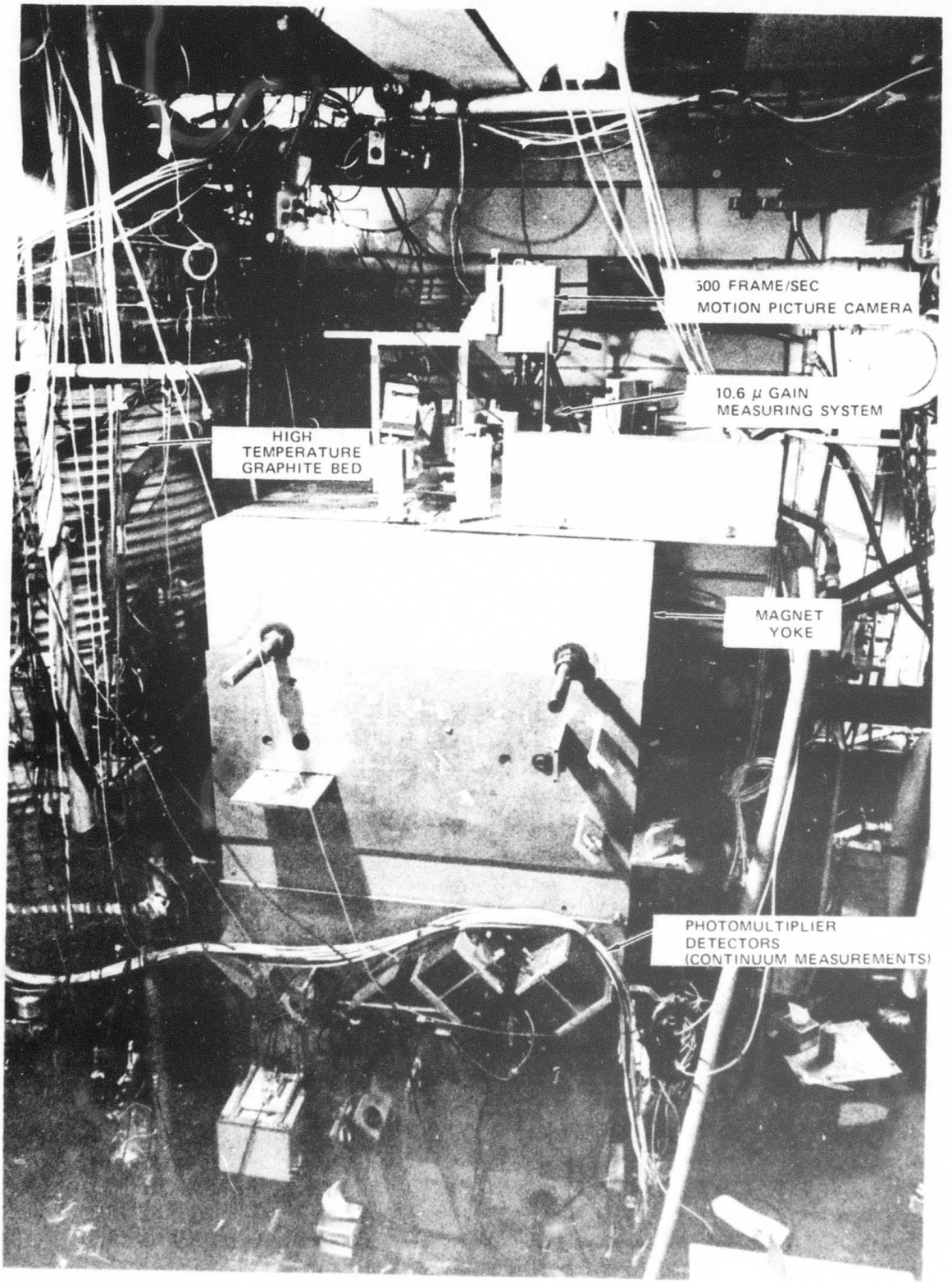

MHDL GENERATOR

N921308–4

(55 CM GAIN DETECTION CONFIGURATION)

FIG. 31

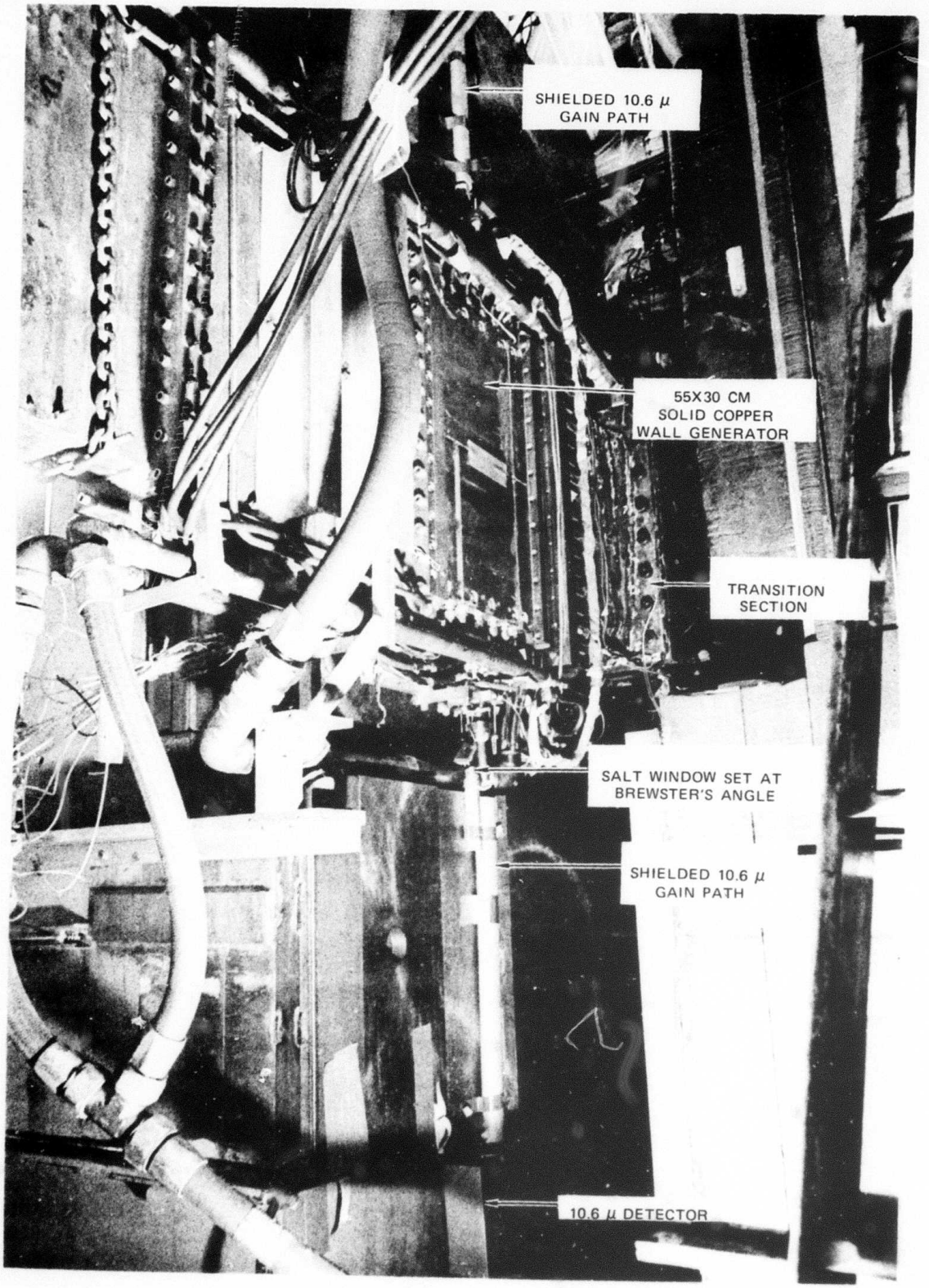

N921308—4

10.6 μm TRANSMISSION MEASUREMENTS

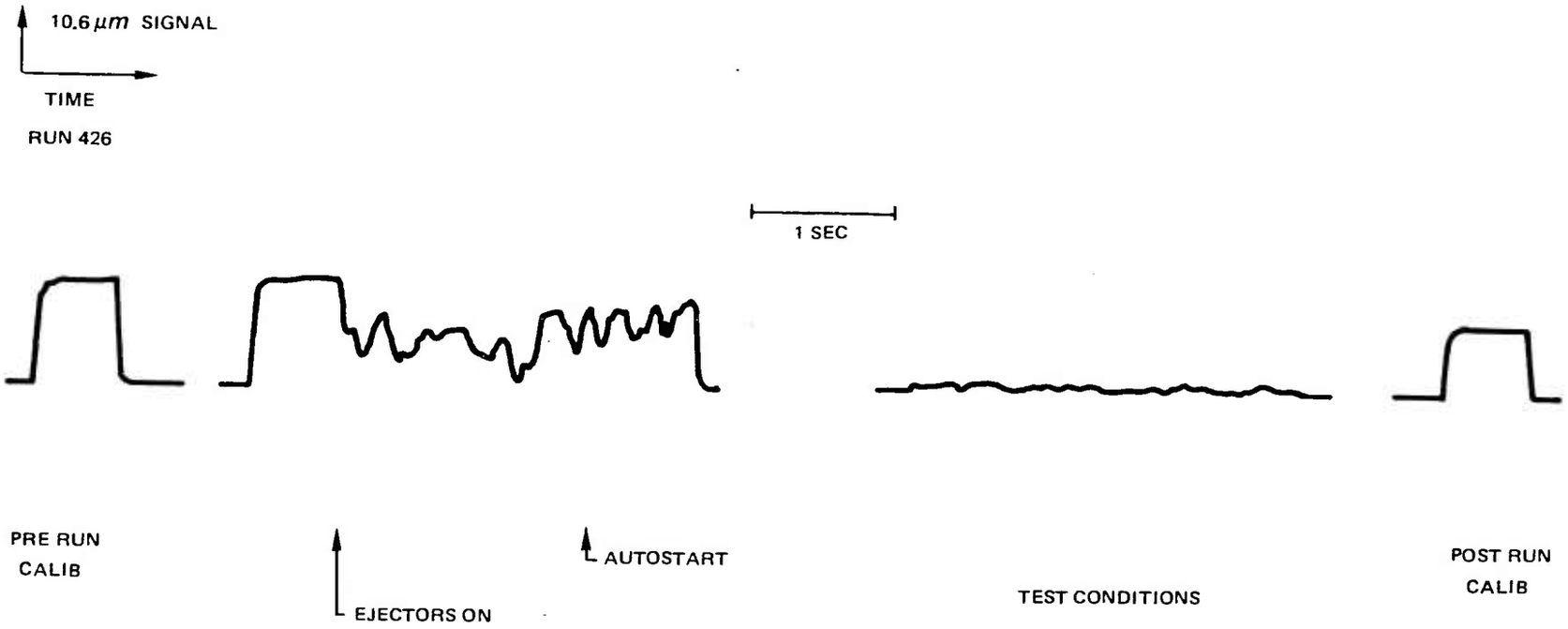

57

FIG. 32

APPENDIX I

Formulation of MHDL Analysis

FORMULATION OF MHDL ANALYSIS

An analytical model of a one-dimensional, nonequilibrium magnetohydrodynamic expansion has been developed for the purpose of establishing and evaluating conditions favorable for the development of an efficient high-power MHD laser using CO_2 as the lasing medium. Quantitative analysis of the MHDL concept, illustrated schematically in Fig. 1, requires a coupled formulation of electron and molecule kinetic processes and the fluid mechanics of a magnetohydrodynamic expansion. Figure 2 illustrates the features of the internally self-consistent analytic model, the individual elements of which are described in detail in subsequent sections.[1]

Magnetohydrodynamics

Gas Dynamics

Self-consistent evaluation of the MHDL concept requires simultaneous solution of the fluid mechanical MHD conservation equations and the microscopic electron and molecule energy transfer equations. The gas dynamic analysis used for the present study is based on the following assumptions: (a) one-dimensional, steady, inviscid, non-heat-conducting flow, (b) gas dynamic properties sensibly uniform over a channel cross section with induced magnetic fields taken to be small, and (c) transverse pressure gradients due to axial current flow (Hall current) are assumed to be insignificant. With these considerations the applicable state and conservation equations for the fluid are of the form,

STATE:
$$\frac{p}{\rho} = \tilde{R}\,(T + \alpha T_e) \quad , \qquad (1)$$

MASS:
$$\frac{1}{\rho}\frac{d\rho}{dx} + \frac{1}{U}\frac{dU}{dx} + \frac{1}{A}\frac{dA}{dx} = 0 \quad , \qquad (2)$$

MOMENTUM:
$$\rho U \frac{dU}{dx} + \frac{dp}{dx} = J_y B \quad , \qquad (3)$$

ENERGY:
$$\rho U \frac{dh}{dx} + \rho U^2 \frac{dU}{dx} = -gI + \bar{J}\cdot\bar{E} \quad , \qquad (4)$$

CALORIC EQUATION OF STATE (assuming primarily a monatomic fluid):

$$h = \frac{5}{2}\tilde{R}T + \alpha\tilde{R}\left(\frac{5}{2}T_e + T_{ion}\right) + \sum_i e_i \quad . \tag{5}$$

These expressions are the usual equations for an MHD expansion[2] with the exception of the term gI which represents the volumetric rate of energy removal from the flow by the radiation field of intensity I. Elimination of common variables in Eqs. (1-5) leads to the following expression for the rate of change of the fluid kinetic energy,

$$U\frac{d}{dx}(U^2/2) = \frac{U^2}{U^2/a_f^2 - 1}\left[\frac{U}{A}\frac{dA}{dx} - \frac{J^2/\sigma}{p} - \frac{U}{5/2\,\tilde{R}(T+\alpha T_e)}\left(\tilde{R}T_{ion}\frac{d\alpha}{dx} - \sum_i \frac{de_i}{dx}\right)\right] \quad ,$$

where

$$a_f^2 = \frac{5}{3}\tilde{R}(T+\alpha T_e) \quad . \tag{6}$$

The source terms appearing on the right-hand side of Eq. (6) are discussed in detail in subsequent sections.

Joule Dissipation

In order to evaluate the electron joule dissipation term (J^2/σ) appearing in Eq. (6) it is necessary to consider the so called "generalized" Ohm's law for an MHD plasma. The steady state-mean free path representation of Ohm's law can be written,

$$\bar{J}_e = \sigma\bar{\mathcal{E}} - \beta\bar{J}_e \times \bar{b} \quad , \tag{7}$$

where $\beta = \omega_c\tau_e$ is the Hall parameter. The generalized electric field $\bar{\mathcal{E}}$ is defined by the relations,

$$\bar{\mathcal{E}} \equiv \bar{E}' + \nabla p_e/n_e e \quad , \tag{8}$$

$$\bar{E}' \equiv \bar{E} + \bar{U}\times\bar{B} \quad .$$

The approximations inherent in the development of Eqs. (7) and (8), are discussed

in detail by Kruger, et al.[3] Ignoring electron pressure gradients in comparison with the MHD electric fields, and taking the total current $\bar{J}$ as equal to the electron current $\bar{J}_e$ (ignoring ion slip) Eq. (7) takes the form,

$$\bar{J} = \sigma \bar{E}' - \beta \bar{J} \times \bar{b} \tag{9}$$

In order to account for the effects of nonuniformities common to MHD plasmas, while retaining the simplicity of this equation, it is convenient to write an equation analogous to Eq. (9), i.e.,[4]

$$\bar{J} = \sigma_{eff} \bar{E}' - \beta_{eff} \bar{J} \times \bar{b} \tag{10}$$

The quantities σ_{eff} and β_{eff} are "bulk" plasma properties which effectively describe the reduction in the average currents and fields in the plasma due to small scale disturbances in the conductivity.[4] In a cesium seeded helium plasma, ionization instabilities are the most likely source of such small scale disturbances. The effect of ionization instabilities on the effective plasma transport properties has been studied theoretically and experimentally by several authors.[5,6] Typical theoretical results taken from Ref. 5 are shown in Fig. 3. In this figure $\langle \sigma \rangle$ and $\langle \beta \rangle$ are the microscopic values of σ and β calculated using the mean values of T_e and n_e.

Solbes shows[5] that to a good approximation σ_{eff} and β_{eff} can be written in the following form,

$$\frac{\sigma_{eff}}{\langle \sigma \rangle} = \begin{cases} 1 & , \quad \langle \beta \rangle \leq \beta_{crit} \\ \dfrac{\beta_{crit}}{\langle \beta \rangle} & , \quad \langle \beta \rangle \geq \beta_{crit} \end{cases}$$

and

$$\beta_{eff} = \begin{cases} \langle \beta \rangle & , \quad \langle \beta \rangle \leq \beta_{crit} \\ \beta_{crit} & , \quad \langle \beta \rangle \geq \beta_{crit} \end{cases} \tag{11}$$

In these expressions, β_{crit} represents a critical value of the Hall parameter above which disturbances larger than a given wavelength are amplified and grow. This minimum wavelength is the value below which electron thermal conduction and radiative

transport are effective in damping perturbations. The value of β_{crit} depends on the plasma properties, and is approximately one for cesium seeded helium. Values of $\sigma_{eff}/<\sigma>$ and β_{eff} which are being used in the present analysis are shown in Fig. 4.

For the coordinate system shown in Fig. 1, Eq. (10) can be written in component form in the following way,

$$J_x = \frac{\sigma_{eff}}{1+\beta_{eff}^2}\left[E_x - \beta_{eff} E_y'\right] \qquad J_y = \frac{\sigma_{eff}}{1+\beta_{eff}^2}\left[E_y' + \beta_{eff} E_x\right] , \quad (12)$$

where $E_x' = E_x$, $E_y' = E_y - UB$, and $J_z = 0$. By defining the quantities $\beta_{app} = |E_x/E_y'|$ and $K = |E_y/UB|$ and using Eq. (12), an expression for the joule dissipation is obtained, i.e.,

$$J^2/\sigma = \vec{J}\cdot\vec{E}' = <\sigma> U^2B^2 \underbrace{\frac{\sigma_{eff}}{<\sigma>}(1-K)^2\frac{1+\beta_{app}^2}{1+\beta_{eff}^2}}_{\zeta} , \quad (13)$$

where the quantity ζ represents the combined influence of electrical loading (K), generator effects (β_{app}), and instabilities (β_{eff}). This is the expression used by Solbes and Kerrebrock[7] to describe the electron temperature rise in an MHD plasma.

As discussed in Ref. 7, β_{app} is defined as the ratio of the average electric field in the flow direction to that in the transverse direction, in gas coordinates. Its magnitude can be influenced by the generator loading, and by electrical shorting along the boundaries, but it cannot be larger than β_{eff}. The quantity K is an effective load factor for loading in the transverse direction. In order to maximize the joule dissipation it is desirable to have $K \approx 0$ and $\beta_{app} \approx \beta_{eff}$. In principle, this can be accomplished by using segmented electrodes so as to "recover" as much of the Hall field E_x as possible, and by providing a short circuit for current flow in the "y" direction in order to maximize internal dissipation. The problem of obtaining good Hall recovery (with finite load factor K) in linear nonequilibrium generators has been studied extensively.[8] While the condition $K \approx 0$ appears to be achievable (i.e., electrode voltage drops reduced to a minimum), the condition $\beta_{app} \approx \beta_{eff}$ is more difficult to attain. However, as pointed out in Ref. 7, when $\beta_{eff} \approx 1$ the effective penalty for Hall shorting is considerably less than in the absence of instabilities. That is, the difference in J^2/σ between the situations corresponding to the conditions $\beta_{app} = \beta_{eff}$ and $\beta_{app} = 0$, is only a factor of two. However, as is well known, in the stable region where $\beta_{eff} = \beta$ there is considerable penalty associated with electrode shorting. For the purposes of the present study, the values $K = 0$ and $\beta_{app} = 0.5$ (i.e., $\beta_{app} = 0.5\,\beta_{eff}$) have been used.

Electron Kinetics

Energy Conservation

The one-dimensional electron energy conservation equation for a CO_2 loaded MHD plasma may be expressed in the form,

$$\frac{1}{A}\frac{d}{dx}\left(5/2\, UAn_e kT_e\right) - U\frac{d}{dx}\left(n_e kT_e\right) = J^2/\sigma - n_e \sum_j 2\delta_j \frac{m}{M_j} N_j \nu_{ej}\, 3/2\, k\,(T_e - T)$$

$$- n_e N_{CO_2} \epsilon_3 \nu_{e3} \frac{(1-x_2^2)(1-x_2)^2}{(1-x_3)} \left[1 - \exp\left[-\frac{\epsilon_3}{k}\left(\frac{1}{T_3} - \frac{1}{T_e}\right)\right]\right] \qquad (14)$$

$$- n_e N_{CO_2} \epsilon_2 \nu_{e2} \frac{(1-x_3)}{(1-x_2)} \left[1 - \exp\left[-\frac{\epsilon_2}{k}\left(\frac{1}{T_2} - \frac{1}{T_e}\right)\right]\right] - \dot{n}_e \epsilon_{ion} .$$

In the development leading to Eq. (14) it has been assumed that electron energy transport due to electron heat conduction and diffusion is negligible, and that radiation losses (i.e., electronic excitation) are insignificant. The convection, joule dissipation, and elastic-rotational energy transfer terms in Eq. (14) have the usual form for an MHD plasma expansion.[3] The third and fourth terms on the right-hand side represent the net effects of e-CO_2 collisions resulting in energy transfer to the asymmetric stretch vibrations and the coupled bending and symmetric stretch vibrations, respectively. The effects of nonequilibrium ionization of the Cs seed are accounted for by the term $\dot{n}_e \epsilon_{ion}$.

Electron Collision Rates

Self-consistent solution of Eq. (14) in connection with the molecular kinetic and gas dynamic equations requires knowledge of the electron temperature dependent CO_2 vibrational excitation rates ν_{e2} and ν_{e3} and the momentum transfer collision rates ν_{ej}. These rates are averages over the Maxwellian electron energy distribution function and may be expressed,

$$\nu_{ei} = (2e/m)^{1/2} (kT_e/e)^{-3/2} \frac{4}{3\sqrt{\pi}} \int_0^\infty u Q_{ei}(u)\, e^{-eu/kT_e}\, du$$

$$\nu_{ej} = (2e/m)^{1/2} (kT_e/e)^{-5/2} \frac{4}{3\sqrt{\pi}} \int_0^\infty u^2 Q_{mj}(u)\, e^{-eu/kT_e}\, du \qquad (15)$$

where $Q_{ei}(u)$ and $Q_{mj}(u)$ are the electron molecule cross sections for vibrational excitation and momentum transfer, respectively. For cesium seed concentrations below approximately 0.1 percent, CO_2 concentrations below 10 percent, and values of fractional ionization below 3×10^{-5}, electron collisions with helium atoms dominate momentum transfer in the 2000 - 4000°K electron temperature range. The electron-momentum transfer cross section for He is nearly constant[9] at low energy with a value of approximately 6×10^{-16} cm^2, and therefore ν_{mj} is easily evaluated as a function of electron temperature. The low energy cross sections $Q_{ei}(u)$ for vibrational excitation of CO_2 by electron impact[10] are shown in Fig. 5 which indicates that in the 0 - 2 eV range excitation of the CO_2 010 and 001 levels dominates. Also shown in Fig. 5 are the energy loss factors for each mode of vibration. It is important to recognize that the influence of electron-molecule energy exchange processes depends effectively on the cross section-energy loss product. Thus, near 0.5 eV where $Q_{ei}(010) \approx Q_{ei}(001)$, energy transfer to the asymmetric stretch vibration is approximately 3.5 times greater than energy transfer to the bending mode. Electron cross sections for excitation of higher levels (020, 002, etc.) are estimated to be very much smaller than those for the 010 and 001 levels, as is also the case for all levels of the symmetric stretch vibration for electron energy below 2 eV.[11] The precise details of low energy electron excitation of CO_2 are discussed by Claydon, Segal, and Taylor.[11]

Using the cross section data of Fig. 5 with Eq. (15), CO_2 vibrational excitation rates were evaluated. These data are shown in Fig. 6 along with similar results for molecular species common to CO_2 laser mixtures. Clearly the rates for CO_2 vibrational excitation are relatively large in the 2000 - 4000°K range when compared with those of typical diatomic molecules such as N_2 and H_2. Further, the electron temperature dependence of the $CO_2(001)$ rate is fairly strong favoring operation at T_e values of 3000°K and above. Although water vapor is an attractive additive for lower laser level relaxation in other laser systems, the data of Fig. 6 show that if present in quantity comparable to CO_2, parasitic energy loss to vibrational excitation of H_2O is likely to be excessive. On the other hand, the relatively low vibrational excitation rate of H_2 ($\sim 1/30$ that of $CO_2(001)$ at 3000°K), and its effectiveness as a lower laser level relaxant suggest the possible usefulness of H_2 as an additive in MHD lasers.

Ionization Kinetics

In order to determine the electron density and evaluate the effects of charged particle production on electron energy conservation, the electron continuity equation must be solved simultaneously with the electron energy equation. The one-dimensional electron continuity equation may be written in the form,

$$\frac{d}{dx}(n_e U A) = \dot{n}_e A \qquad (16)$$

The present discussion will consider the effects of various collisional and radiative processes on the net charged particle production rate $\dot{n}_e$ which may be expressed,

$$\dot{n}_e = n_e N_{Cs} \hat{S}(n_e, T_e, \epsilon_R) - \gamma(T_e) n_e^3 \quad . \tag{17}$$

McGregor, et al.[12] have calculated the effective cesium ionization rate $\hat{S}$ in the presence of radiation escape and have shown that $\hat{S}$ can be determined as a function of n_e and T_e once the resonance radiation escape parameter ϵ_R is specified. Shaw[13] has shown that the predominant effect of resonance radiation escape is depression of the population of the first excited state of cesium which in turn tends to depress the high energy portion of the electron energy distribution. The following empirical expression for $\hat{S}$ is found to fit the McGregor results within approximately a factor of two for $n_e \geq 5 \times 10^{11}$ cm^{-3} and $0 \leq \epsilon_R \leq 1$;

$$\hat{S} = \frac{S(T_e)\gamma(T_e)}{1 + \frac{2\times10^{13}}{n_e} + \frac{10^{35}\epsilon_R}{n_e^{5/2}}} \quad , \tag{18}$$

where $S(T_e)$ is the Saha function and $\gamma(T_e)$ is the Hinnov-Hirschberg[14] recombination coefficient given by,[4]

$$\gamma(T_e) = 3.4 \times 10^{-22} (T_e/10^3)^{-9/2} \quad . \tag{19}$$

The quantity ϵ_R in Eq. (18) is the radiation escape parameter, which will be discussed in more detail below.

Mnatsakanyan[15] has recently shown that quenching of electronically excited alkali levels by collision with molecules plays a role similar in effect to that of radiation escape. By considering the rate equation for the first excited level of cesium, it can be shown that molecular quenching collisions can be included in the expression for $\hat{S}$, is an approximate way, by defining an "effective escape parameter" $\hat{\epsilon}$. The resulting expression for $\hat{\epsilon}$ is,[15]

$$\hat{\epsilon} = \frac{\epsilon_R + \sum_j \frac{N_j k_{jcs}}{A_{10}} \left[1 - \exp\left[-\frac{\epsilon_{01}}{k}\left(\frac{1}{T_{vj}} - \frac{1}{T_e}\right)\right]\right]}{1 + \sum_j \frac{N_j k_{jcs}}{n_e k_{ecs}} \exp\left[-\frac{\epsilon_{01}}{k}\left(\frac{1}{T_{vj}} - \frac{1}{T_e}\right)\right]} \quad , \tag{20}$$

which for conditions typical of the present application can be simply approximated by the expression,

$$\hat{\epsilon} = \epsilon_R + \sum_j \frac{N_j k_{jcs}}{A_{10}} \tag{21}$$

Thus, it can be seen that molecular quenching plays a role exactly analogous to radiation escape in reducing the ionization coefficient $\hat{S}$. In fact, for conditions typical of this investigation the second term on the right-hand side of Eq. (21) dominates.

Based on the previous discussions, it is possible to define an effective ionization time $\tau_I = (N_{Cs}\,\hat{S})^{-1}$ and an effective recombination time $\tau_R = (\gamma\, n_e{}^2)^{-1}$. With these definitions it is then possible to determine an ionization length $\ell_I = U\tau_I$ and a recombination length $\ell_R = U\tau_R$. The ionization (recombination) length may be interpreted as the length scale (or distance down the channel) over which ionization (recombination) proceeds to its equilibrium value at a given T_e and N_{Cs}. Both ℓ_I and ℓ_R are strong functions of T_e and for $n_e \leq 10^{13}$ cm^{-3}, these quantities also depend on n_{e_o}. Values of ℓ_I and ℓ_R for typical MHD plasma conditions are shown in Figs. 7 and 8.

Molecular Kinetics

Kinetic Model

The heavy particle kinetic model required for this investigation considers three basic collisional processes. These include:

$$\begin{aligned} &\text{I} && CO_2(\nu_3) + M \rightarrow CO_2(\nu_1\nu_2) + M \\ &\text{II} && CO_2(\nu_2) + M \rightarrow CO_2 + M \\ &\text{III} && CO_2(\nu_1) + M \rightleftharpoons CO_2(2\nu_2) + M \end{aligned} \tag{22}$$

where the symbol M refers to electrons, He, CO_2, and/or other species, and ν_1, ν_2, and ν_3 denote the symmetric stretch, bending, and asymmetric stretch vibrational modes of CO_2, respectively.

Vibrational degrees of freedom are represented by harmonic oscillators while internal equilibrium within a mode is assumed to be achieved on a time scale short in comparison to time constants characterizing processes (I) and (II), making

possible the assumption of distinct vibrational temperatures. The total vibrational partition function for CO_2 is written as the product of partition functions for each vibrational degree of freedom, i.e.,

$$Q = Q_1(T_1)\, Q_2(T_2)\, Q_3(T_3)$$

where

$$Q_i(T_i) = (1 - x_i)^{-d_1} \tag{23}$$

and

$$x_i = \exp(-\epsilon_i / kT_i) \qquad d_1 = d_3 = 1, \; d_2 = 2$$

Spontaneous radiative decay processes are known to be slow and are therefore ignored in the present analysis.[16] Collisions of type III coupling the bending and symmetric stretching levels are very effective,[17] and therefore these modes are assumed to be in mutual equilibrium. The equilibrium condition

$$\frac{N_{020}}{N_{100}} = \frac{d_1}{d_2} \exp(-\Delta E / kT) \tag{24}$$

yields the following relationship between the vibrational temperatures of the bending and symmetric stretch vibrations,

$$\frac{T_1}{T_2} = \frac{\epsilon_1}{2\epsilon_2 - (2\epsilon_2 - \epsilon_1)\frac{T_2}{T_1}} \tag{25}$$

Reported values of the time constants for processes (I) and (II) are presented as functions of gas translational temperature for several species in Figs. 9 and 10. Mixture rate constants are calculated from these data using the relation,

$$pK_i = p \sum_j \frac{X_j}{(p\tau)_{ij}} \tag{26}$$

It should be noted that for both H_2 and He at room temperature the deactivation of the bending mode (lower laser level) proceeds about an order of magnitude faster than the parasitic decay of the upper laser level.

Energy Transfer Equations

The assumption of a harmonic oscillator and the use of Hermite polynomial

recursion relationships yields macroscopic vibrational rate equations similar in form to the Landau-Teller equation.[18,19] For a multiple quantum process such as (I) the resulting expression is complex, but reduces to the exponential Landau-Teller form when the vibrational temperature of the bending mode is close to the gas translational temperature, a necessary condition for maintenance of the population inversion. Further low energy electron excitation of CO_2 vibrational modes proceeds by way of a dipole interaction[11] and consequently the macroscopic rate equations for V-T_e processes are analogous to those for the V-T processes. Based on these considerations the complete set of vibrational rate equations, with terms for optical power extraction, is of the form,

$$\frac{De_3}{Dt} = pK_{3j}\left[e_3(T) - e_3(T_3)\right] + n_e K_{e3}\left[e_3(T_e) - e_3(T_3)\right] - \frac{1}{\rho}\frac{\epsilon_3}{\epsilon_3 - \epsilon_1}\, gI \quad ,$$

$$\frac{D(e_1+e_2)}{Dt} = pK_{2j}\left[e_2(T) - e_2(T_2)\right] + n_e K_{e2}\left[e_2(T_e) - e_2(T_2)\right] + \frac{1}{\rho}\frac{\epsilon_1}{\epsilon_3 - \epsilon_1}\, gI \quad ,$$

where

$$e_i = \frac{X_{CO_2}}{\tilde{M}}\,\epsilon_i x_i (1 - x_i)^{-1} \quad . \tag{27}$$

The electron rate constants K_{ei} for the V-T_e processes are related to the electron collision rates ν_{ei} (Eq. 15, Fig. 6) by the relation,

$$K_{ei} = \nu_{ei} \exp(\epsilon_i/kT_e)(1 - \exp(-\epsilon_i/kT_e)) \quad . \tag{28}$$

It is apparent from the form of Eq. (27) that the production of a CO_2 vibrational population inversion in a nonequilibrium MHD generator will depend upon the competition between electron excitation and heavy particle de-excitation of the CO_2 lasing levels. Comparison of the electron and heavy particle rate constants of Figs. 6 and 9 reveals that electron excitation of the 001 level will not become competitive with parasitic deactivation until the fractional ionization $\alpha = n_e/N$ reaches a value of approximately 10^{-6}. If the fractional ionization is raised much more than an order to magnitude beyond this value, helium collisions

alone will be insufficient to relax the bending mode, and significant excitation (and population of the 100 level) will occur. Thus, maintenance of the population inversion between the 001 and 100 states requires that the fractional ionization be maintained in the 10^{-6} - 10^{-5} range. For electron temperature in the range 2000 - 3000°K and generator static conditions of 0.1 atm and 300°K, this range of fractional ionization corresponds to electron density values in the range 3×10^{12} - 3×10^{13} cm^{-3}. The addition of H_2, which relaxes both lasing levels more rapidly than He, will shift this operating region slightly upward, depending on the amount added.

Gain Coefficient

The local value of the gain coefficient for the 10.6 micron laser transition is calculated directly from the populations of rotational states belonging to the 001 and 100 levels, viz:[20]

$$g(j) = \frac{\lambda^2}{8\pi\tau\Delta\nu_L}\left[N_{001}F(j) - \left(\frac{2j+1}{2j+3}\right) N_{100}F(j+1)\right] ,$$

with $$N_{001} = N_{CO_2}Q^{-1}x_3 \quad N_{100} = N_{CO_2}Q^{-1}x_1 , \qquad (29)$$

and $$F(j) = (2j+1)\frac{\theta_{ROT}}{T}\exp\left(-j\,(j+1)\frac{\theta_{ROT}}{T}\right) .$$

The CO_2 rotational state factors, F(j), are assumed to follow a Boltzmann distribution at the heavy particle translational temperature. This assumption is justified by the fast ($\sim 10^{-10}$ sec ATM) rotational relaxation times for CO_2[21] and the relatively small (10^{-6} - 10^{-5}) mole fraction of electrons. Electron excitation of CO_2 rotational levels should not be competitive with heavy particle relaxation.

Under typical generator static conditions, p ~ 0.1 ATM and T ~ 300°K, the transition lineshape should be essentially Lorentzian, with an optical broadening frequency given by:

$$\Delta\nu_L = \frac{2}{\pi}\sum_i N_i \sigma_{CO_2\text{-}i}\sqrt{\frac{2\pi RT}{\mu_{CO_2\text{-}i}}} , \qquad (30)$$

where the summation i is over all colliding species.

Examination of Eqs. (29) and (30) shows that the density (pressure) dependence cancels out of the gain expression in the pressure-broadened region.

The relative magnitudes of the optical broadening cross sections are those reported by Patty[22] and are summarized below:

b	$\sigma_{CO_2\text{-}b}/\sigma_{CO_2\text{-}CO_2}$
CO_2	1.000
He	0.240
H_2	0.342
Ar	0.583
N_2	0.660

The optical broadening cross section $\sigma_{CO_2\text{-}CO_2}$ is calculated from reported values of the spontaneous radiative lifetime $\tau \sim 4.7$ sec and the pure CO_2 absorption coefficient of 1.81×10^{-3} cm^{-1} (STP).[23]

Optical Power Extraction

The analysis of optical power extraction is appropriate to an optical resonator with planar mirrors aligned transverse to the flow. The energy transfer equations (Eq. (27)) are solved for the optical field intensity in the cavity in which the loaded gain of the medium just balances cavity loss. Effects of diffraction and cavity mode structure are not treated.

Following Rigrod,[24] the optical field intensity at a given point "x" in the cavity is written in terms of plane waves propagating in the "y" directions;

$$I = I^+ + I^- \quad , \tag{31}$$

with the equation of radiative transfer expressed as:

$$\frac{1}{I^+}\frac{\partial I^+}{\partial y} = -\frac{1}{I^-}\frac{\partial I^-}{\partial y} = g \tag{32}$$

Integration of Eq. (32) yields,

$$I = I^+(0)\exp\left(\int_0^y g\,dy\right) + I^-(W)\exp\left(-\int_W^y g\,dy\right) \tag{33}$$

Adding the mirror reflectance conditions,

$$\frac{I^+(W)}{I^-(W)}\,r_2 = \frac{I^-(0)}{I^+(0)}\,r_1 \quad , \tag{34}$$

leads to the relation,

$$2\int_0^W g\,dy = -\ln(r_1 r_2) \tag{35}$$

Further algebraic manipulation with Eqs. (33) - (35) shows that the ratio of minimum to maximum total intensity at a given position in the cavity is given by,

$$\frac{I_{min}}{I_{max}} = \frac{2\sqrt{r}}{1+r} \quad , \tag{36}$$

where r is the smaller of r_1, r_2. For values of r down to .70, I_{max} and I_{min} will be identical to within one percent, and the total intensity (and loaded gain) will be independent of the "y" coordinate, viz:

$$g_{osc} = -\frac{1}{2W}\ln(r_1 r_2) \tag{37}$$

At the leading edge of the cavity the gain of the medium will adjust from its free stream value to the steady-state oscillation value defined by Eq. (37). The constraint $dg/dx = 0$ is then used to solve Eqs. (27) for I(x) and the cumulative optical power at any point "x" is computed from the relation,

$$P(x) = \int_0^x \left[(1-r_1)\,I^-(0)+(1-r_2)\,I^+(W)\right] dx \tag{38}$$

REFERENCES

1. In the interest of preserving continuity in the text, symbols are defined only in the list of symbols which appears after the list of references.

2. G. Sutton and A. Sherman, Engineering Magnetohydrodynamics, McGraw-Hill, New York (1965).

3. C. H. Kruger, M. Mitchner, and U. Daybelge, "Transport Properties of MHD Generator Plasmas," AIAA Journal 6, 1712 (1968).

4. R. J. Rosa, Magnetohydrodynamic Energy Conversion, McGraw-Hill, New York (1968).

5. A. Solbes, "Quasi-Linear Plane Wave Study of Electrothermal Instabilities," Proc. Int. Symp. MHD Electr. Power Gen., Warsaw 1, 499 (1968).

6. W. Riedmüller, "Experimental Investigation of Instabilities in Potassium Seeded Argon Plasma in Crossed Electric and Magnetic Fields," Proc. Int. Symp. MHD Electr. Power Gen., Warsaw 1, 519 (1968).

7. A. Solbes and J. Kerrebrock, "Effect of Nonuniformities on the Performance of Nonequilibrium MHD Generators," Proc. Ninth Symp. on Engrg. Aspects of MHD, Tullahoma, Tenn., 160 (1968).

8. R. Decher and J. Kerrebrock, "Electrode Wall-End Loop Shorting in a Non-equilibrium MHD Generator," Proc. Ninth Symp. on Engrg. Aspects of MHD, Tullahoma, Tenn., 142 (1968).

9. L. S. Frost and A. V. Phelps, "Momentum-Transfer Cross Sectrons for Slow Electrons in He, Ar, Kr, and Xe," Phys. Rev. 136, A1538 (1964).

10. W. L. Nighan, "Electron Energy Distribution Functions and Collision Rates in Electrically Excited N_2, CO, and CO_2," Phys. Rev. A2, 1989(1970).

11. C. R. Claydon, G. A. Segal, and H. S. Taylor, J. Chem. Phys. 52, 3387 (1970).

12. D. McGregor, M. Mitchner, and J. Shaw, "Ionization Rate Calculations for Pre-Ionizers," Proc. Tenth Symposium on Engrg. Aspects of MHD, Cambridge, Mass., pp. 95-99 (1969).

REFERENCES (Contd.)

13. J. Shaw, "Effects of Nonelastic Collisions on Partially Ionized Gases," SUIPR Report No. 254, Stanford Univ., Stanford, Calif. (1968).

14. E. Hinnov and J. G. Hirschberg, "Electron-Ion Recombination in Dense Plasmas," Phys. Rev. 125, 795 (1962).

15. A. Mnatsakanyan, "Electron Energy Balance in Inert Gas-Alkali Metal-Nitrogen Mixtures," High Temperature 7, 353 (May 1969).

16. D. F. Eggers and B. L. Crawford, "Vibrational Intensities III. Carbon Dioxide and Nitrous Oxide," Journal of Chemical Physics, 19, 1554 (1951).

17. C. Rhodes, M. Kelley, and A. Javan, "Collisional Relaxation of the 100 and 020 Levels in CO_2," Meeting of American Physical Society, Washington, D. C., April 22-25, 1968.

18. W. G. Vincenti and C. H. Kruger, Physical Gas Dynamics, pp. 198-206, J. Wiley, New York, 1965.

19. R. N. Schwarz, Z. I. Slawsky, and K. F. Herzfeld, "Calculation of Vibrational Relaxation Times in Gases," Journal of Chemical Physics, 20, 1591 (1952).

20. E. T. Gerry and D. A. Leonard, "Measurement of 10.6μm CO_2 Laser Transition Probability and Optical Broadening Cross Sections," Applied Physics Letters, 8, 227 (1966).

21. F. O. Carroll and S. Marcus, "A Direct Measurement of Rotational Relaxation Time in CO_2," Physics Letters, 27A, 590 (1968).

22. R. R. Patty, E. R. Manning, and J. A. Gardner, "Determination of Self-Broadening Coefficients of CO_2, Using CO_2 Laser Radiation at 10.6μm ," Applied Optics, 7, 2241 (1968).

23. C. Rossetti, R. Farrenq, and P. Barchewitz, "Lasers Moleculaires a Excitation Haute Frequence; Coefficient d'Amplification et d'Absorption dans le Gaz Excites Vibrationnellement," Journal de Chimie Physique, Vol. 64, 93 (1967).

24. W. W. Rigrod, J. Appl. Phys. 36, 2487 (1965).

LIST OF SYMBOIS

a - mirror absorptivity

a_f - gas sonic speed

A - channel cross sectional area

A_{10} - Einstein coefficient for spontaneous decay of first excited state of Cs

B - applied magnetic field

$\bar{b}$ - unit vector in direction of magnetic field, $\bar{b} \equiv \bar{B}/B$

c_p - gas specific heat at constant pressure

d_i - degeneracy of the i'th state or mode of CO_2

e - electronic charge

e_i - vibrational energy of the i'th mode of CO_2

E - electric field

$F(j)$ - Boltzmann population factor for j'th rotational level in CO_2

g - optical gain coefficient

h - gas enthalpy

H - total thermal energy input per unit mass

I - optical field intensity

j - rotational quantum number

J - current density

k - Boltzmann constant

k_{eCs} - electron-Cs de-excitation coefficient

k_{jCs} - effective de-excitation coefficient for the j'th molecular species

L - MHD generator length in flow direction

$\ell_{I(R)}$ - effective ionization (recombination) length for Cs

$\dot{m}$ - mass flow rate

M_j - mass of the j'th heavy particle

$\tilde{M}$ - average molecular weight of the gas mixture

N_j - number density of the j'th species

n_e - electron number density

n_{e_o} - inlet electron number density

$\dot{n}_e$ - net electron production rate

p - gas static pressure

p_e - electron pressure

P - cumulative optical power

Q_i - vibrational partition function of the i'th vibrational mode of CO_2

Q_{ei} - electron cross section for vibrational excitation of the first level of the i'th mode of CO_2

Q_{ej} - electron momentum transfer cross section for the j'th species

r - mirror reflectivity

R - universal gas constant

$\tilde{R}$ - gas constant for the mixture, $R/\tilde{M}$

ΔT_g - temperature difference corresponding to flow enthalpy of the gas

T - heavy particle translational-rotational temperature

T_i - vibrational temperature of the i'th mode of CO_2

T_e - electron temperature

T_{ion} - temperature equivalent of Cs ionization energy

$\hat{S}$ - effective cesium ionization rate

$S(T_e)$ - Saha function, $(2\pi mk\, T_e/h^2)^{3/2} \exp(-\epsilon_{ion}/kT_e)$

u - electron energy

U - gas flow speed

V - channel volume

W - channel width in the $\bar{J} \times \bar{B}$ (optical flux) direction

X_j - fractional concentration of species j, N_j/N

x_i - $\exp(-\epsilon_i/kT_i)$

x - coordinate in flow direction

y - coordinate in $\bar{U} \times \bar{B}$ and beam propagation direction

z - coordinate in direction of magnetic field

α - degree of ionization, n_e/N

β - Hall parameter

β_{eff} - effective Hall parameter

β_{app} - apparent Hall parameter

$<\beta>$ - spatial average of microscopic Hall parameter

γ - effective three-body recombination rate for cesium

δ_j - effective energy loss parameter for the j'th species ($\delta = 1$ for atoms)

ϵ_i - characteristic energy of the i'th vibrational mode of CO_2

ϵ_{01} - energy of the first excited state of cesium

ϵ_{ion} - cesium ionization energy

ϵ_R - radiation escape parameter for cesium

ϵ' - effective radiation escape parameter in the presence of molecules

ζ - effective joule dissipation factor

θ_{rot} - characteristic temperature of CO_2 rotation

λ - wavelength of CO_2 laser transition

ν_i - fundamental frequency of the i'th vibrational mode

ν_{ei} - normalized electron collision frequency for vibrational excitation of the first level of the i'th mode of CO_2

ν_{ej} - normalized electron momentum transfer collision frequency for the j'th species

$\Delta\nu_L$ - optical broadening frequency

ρ - gas density

σ - electrical conductivity

$<\sigma>$ - spatial average of microscopic electrical conductivity

σ_{eff} - effective electrical conductivity

σ_{opt} - optical broadening cross section

τ - spontaneous lifetime of CO_2 laser transition

τ_e - effective electron momentum transfer collision time

$\tau_{I(R)}$ - effective ionization (recombination) time

ω_c - electron cyclotron frequency, eB/m

FIG. 1

LASER EXCITATION USING SHORT–CIRCUITED MHD GENERATOR

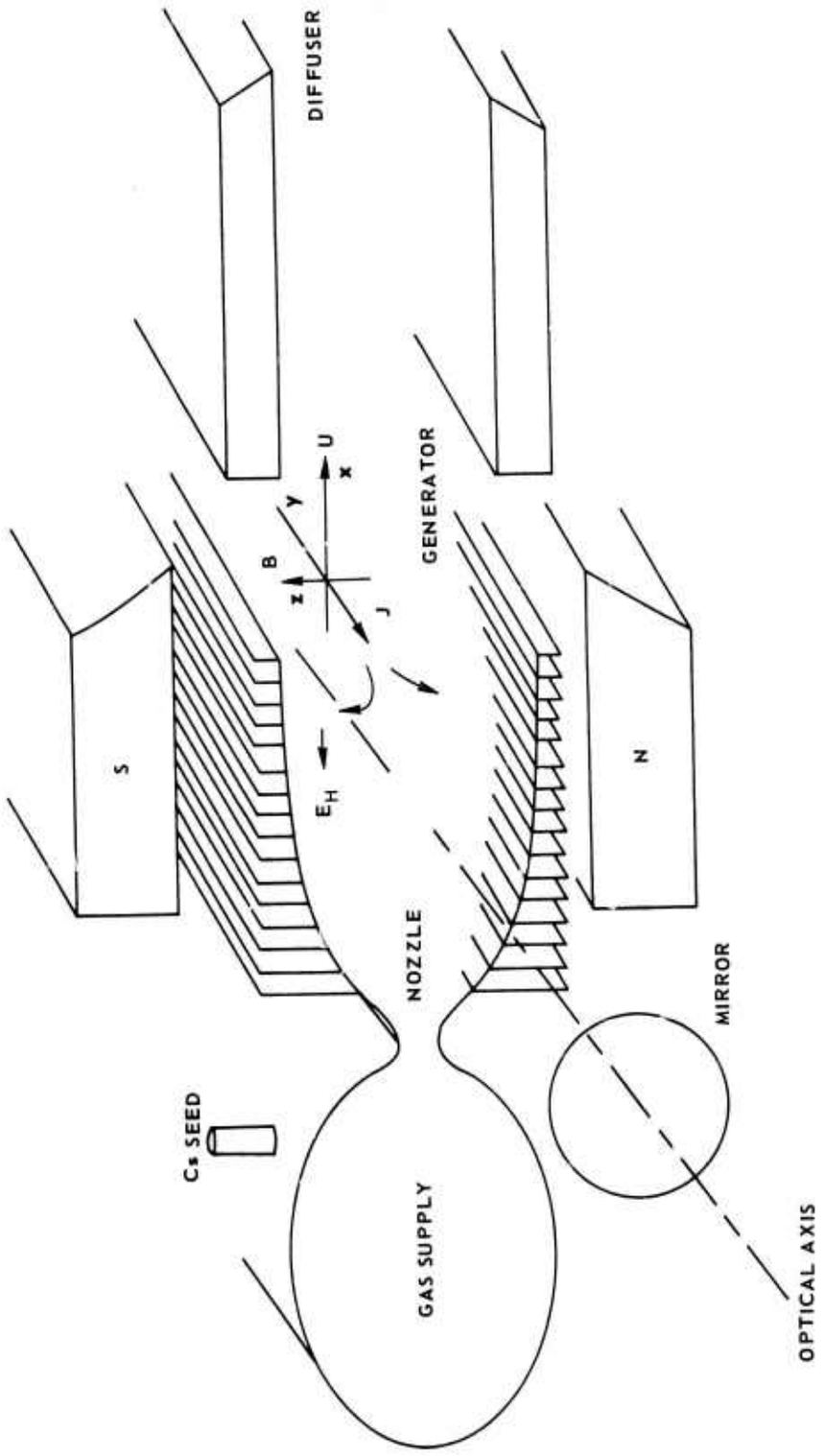

N921308–4

FIG. 2

DIAGRAM OF ANALYTIC MODEL

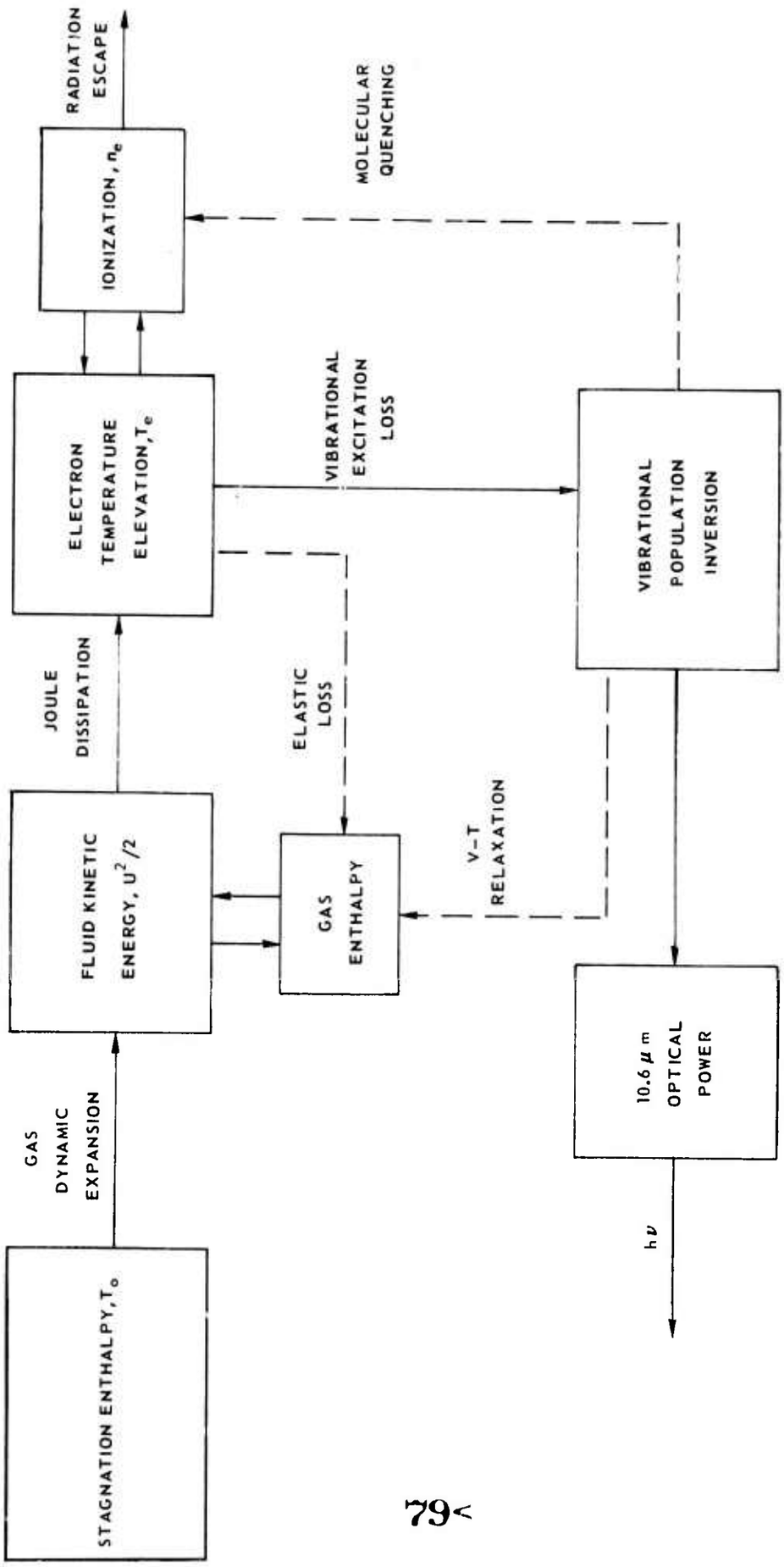

FIG. 3

CALCULATED VARIATION OF σ_{eff} AND β_{eff} WITH $<\beta>$

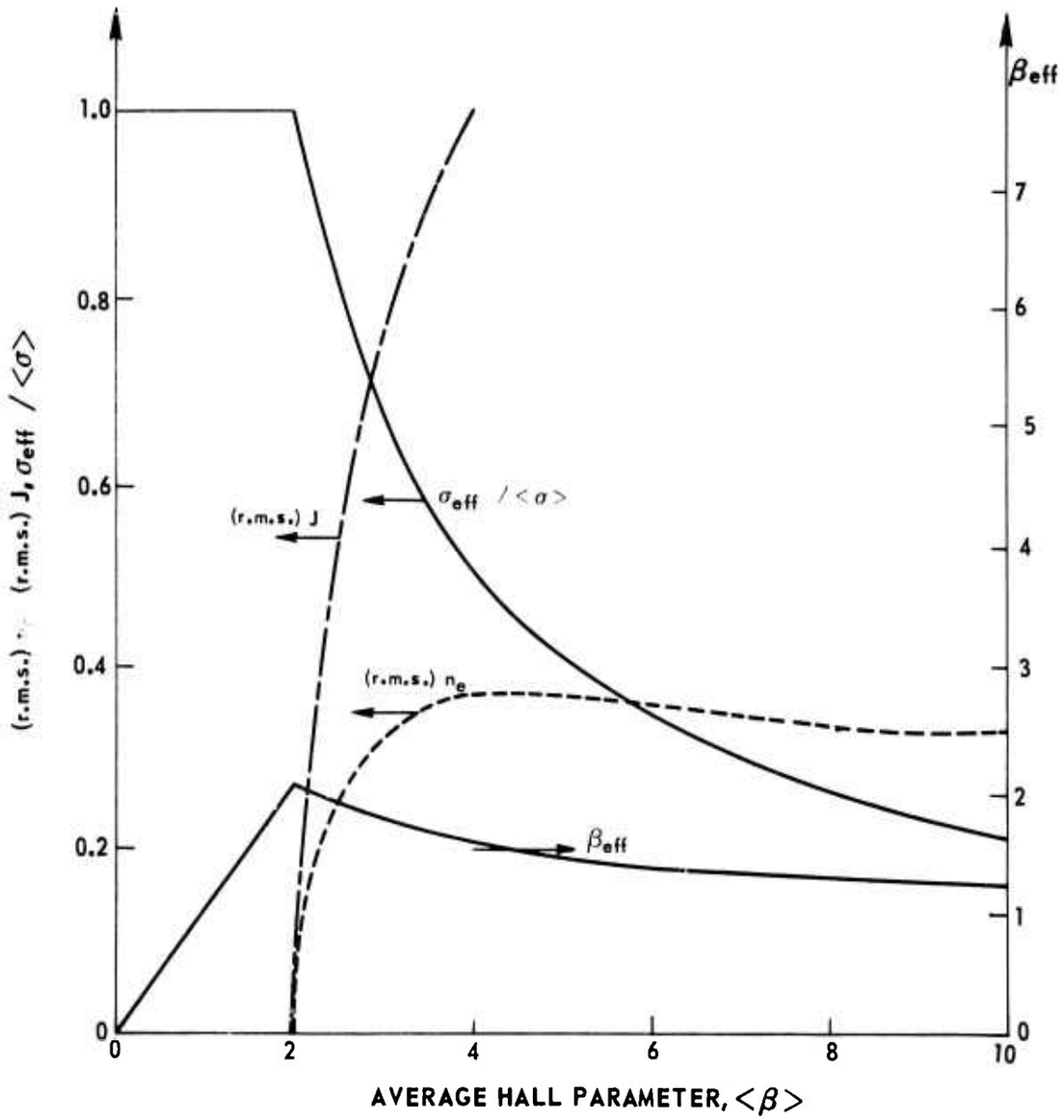

FIG. 4

FUNCTIONAL FORM OF σ_{eff} /$<\sigma>$ AND β_{eff} USED IN THE PRESENT STUDY

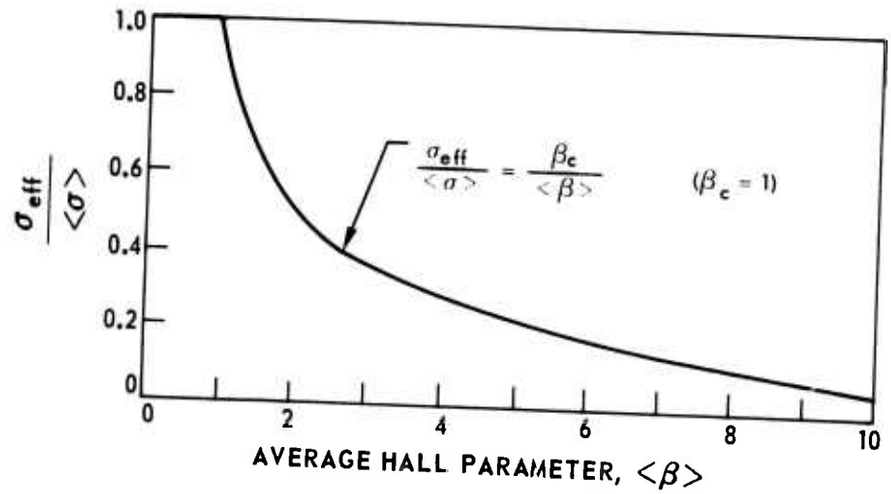

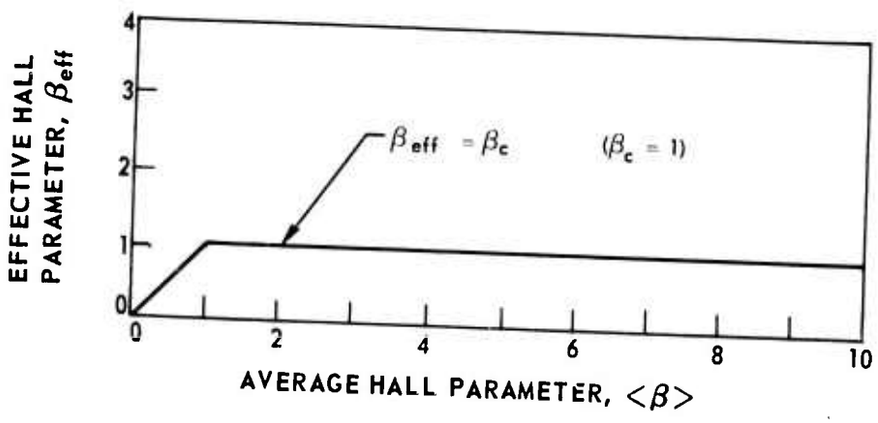

FIG. 5

CROSS SECTIONS FOR VIBRATIONAL EXCITATION OF CO_2 BY ELECTRONS

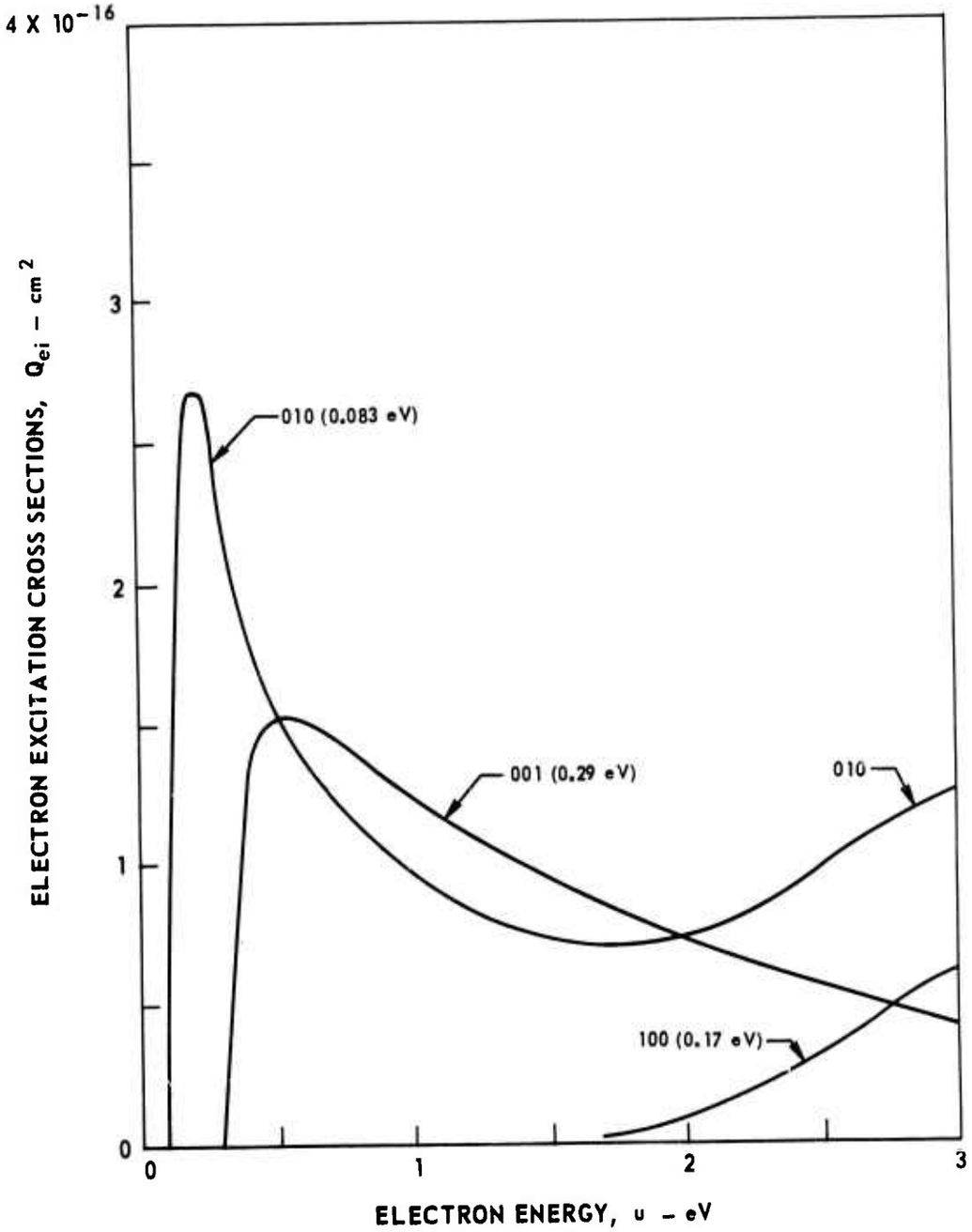

FIG. 6

ELECTRON-MOLECULE VIBRATIONAL EXCITATION RATES

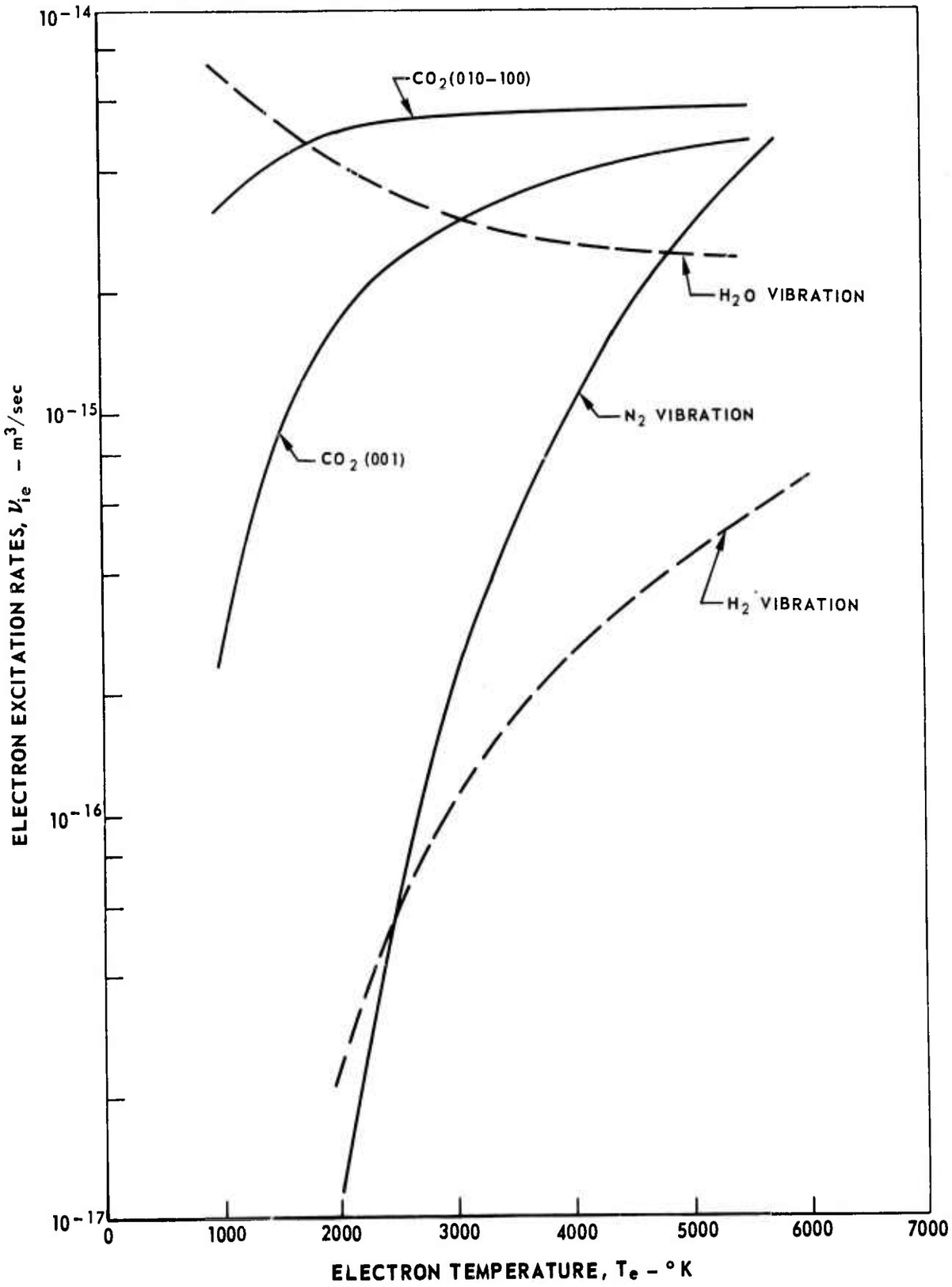

FIG. 7

VARIATION OF IONIZATION LENGTH WITH PLASMA CONDITIONS

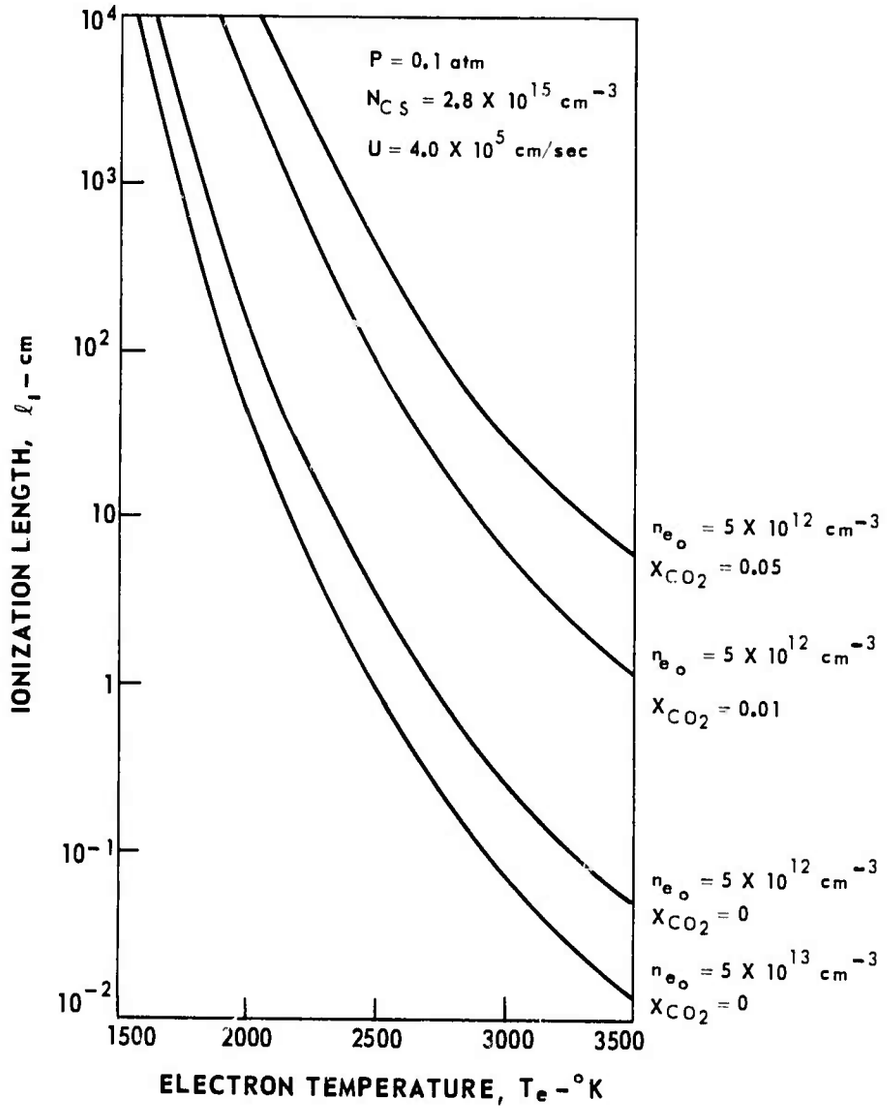

FIG. 8

VARIATION OF RECOMBINATION LENGTH WITH PLASMA CONDITIONS
(SAME AS IN FIG. 7)

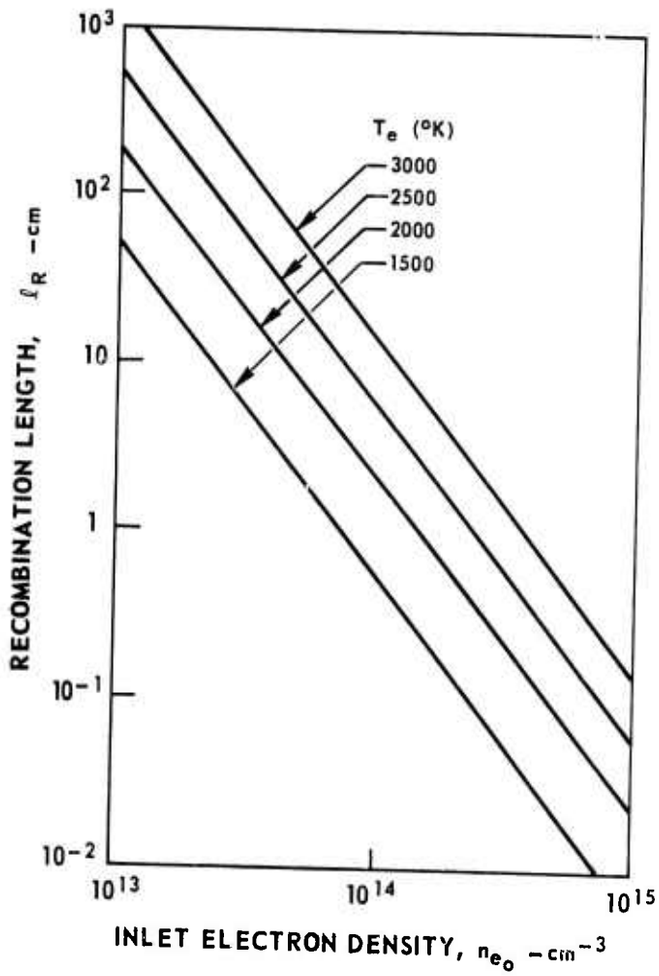

N921308–4

FIG. 9

TIME CONSTANTS FOR DEACTIVATION OF UPPER LASER LEVEL

$$CO_2\ (\nu_3) + M \rightleftharpoons CO_2\ (\nu_1 \nu_2) + M$$

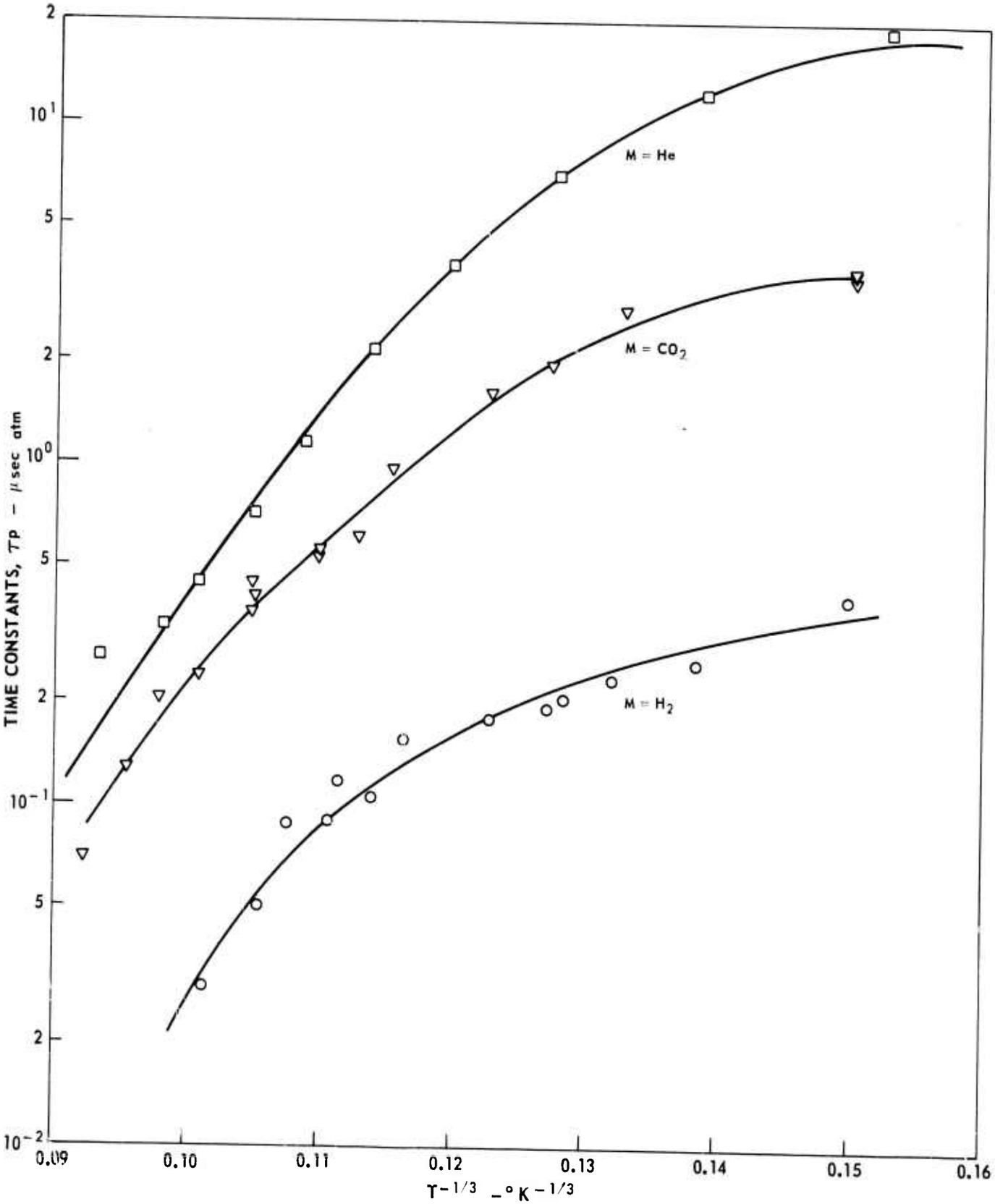

N921308–4

FIG. 10

TIME CONSTANTS FOR DEACTIVATION OF LOWER LASER LEVEL

$$CO_2\ (\nu_2) + M \rightleftharpoons CO_2 + M$$